



HAL
open science

Study of the interaction between the musician and the instrument. Application to the playability of the cello

Timothy Wofford

► **To cite this version:**

Timothy Wofford. Study of the interaction between the musician and the instrument. Application to the playability of the cello. Acoustics [physics.class-ph]. Sorbonne Université, 2018. English. NNT : 2018SORUS336 . tel-02864778

HAL Id: tel-02864778

<https://theses.hal.science/tel-02864778>

Submitted on 11 Jun 2020

HAL is a multi-disciplinary open access archive for the deposit and dissemination of scientific research documents, whether they are published or not. The documents may come from teaching and research institutions in France or abroad, or from public or private research centers.

L'archive ouverte pluridisciplinaire **HAL**, est destinée au dépôt et à la diffusion de documents scientifiques de niveau recherche, publiés ou non, émanant des établissements d'enseignement et de recherche français ou étrangers, des laboratoires publics ou privés.



THÈSE DE DOCTORAT DE
SORBONNE UNIVERSITÉ

Présentée par :

Timothy Wofford

Pour obtenir le grade de
DOCTEUR DE SORBONNE UNIVERSITÉ

Spécialité :
Acoustique

Sujet de la thèse :

STUDY OF THE INTERACTION BETWEEN THE MUSICIAN AND THE
INSTRUMENT. APPLICATION TO THE PLAYABILITY OF THE CELLO.

Soutenue le : 6 décembre 2018

devant le jury composé de :

Marcelo Wanderley	McGill University, Schulich School of Music	Rapporteur
Jim Woodhouse	Cambridge University, Engineering Department	Rapporteur
Sølvi Ystad	CNRS, PRISM	Examineur
Frédéric Ablitzer	Laboratoire d'Acoustique de l'Université du Mans	Examineur
Joël Pouget	Sorbonne Université, Institut Jean Le Rond d'Alembert	Examineur
Benoît Fabre	Sorbonne Université, Institut Jean Le Rond d'Alembert	Directeur de thèse
Claudia Fritz	Sorbonne Université, Institut Jean Le Rond d'Alembert	Co-Directrice de thèse
Jean-Marc Chauvel	Sorbonne Université, Institut de Recherche en Musicologie	Co-Directeur de thèse
Paul Noulet	Luthier à Limoges	Invité

Abstract

Little is known about the relationship between the physical properties (materials, geometry, vibrational modes) of bowed string instruments and their perceptual properties (quality, sound, playability).

Bissinger measured physical properties of several violins, but failed to find any correlations with their supposed quality ratings, possibly due to overly simplified quality characterizations. Fritz and Saitis investigated how players subjectively evaluate instruments. They found that musicians provide self-consistent ratings but disagree with other musicians, not only in terms of subjective preferences, but more surprisingly, in terms of what could be considered as more objective criteria. The disagreement is hypothesized to be due to differences in playing techniques. That musicians use control parameters differently from one another, even when playing the same music, has indeed been demonstrated by Chudy.

Guettler identified meaningful control parameters for attacks and used a listening test to find the duration of acceptable attacks for the violin. Schelleng looked at the set of steady state gestures which support the string motions associated with normal cello playing and identified upper and lower force limits for a given note and bow speed. Woodhouse improved on Schelleng's estimate of the lower force limit and connected it to the wolf note. He further proposed the bridge mobility as a physical mechanism which could explain the perception of playability. Zhang tested this hypothesis in the context of the wolf note and found good correspondence between the bridge mobility and the perceived severity of the wolf note.

In this thesis we attempt to further validate the link between the bridge mobility and the perception of playability by observing whether the musician perceives differences in Schelleng's upper and lower limits for notes other than the wolf note. We also look for other factors which are relevant to the musician's perception of playability by studying the interactions between the player and the instrument during an evaluation and performance task. Unlike previous approaches, we observe all parts of the playability feedback loop, including the control parameters, some vibro-acoustical measurements taken with an impact hammer, the response of the instrument to the control parameters, and the musician's comments about perceptual properties.

We use a camera-based motion capture system to follow the movements of the cello and bow as a professional musician evaluates each of two cellos. Piezoelectric sensors in the bridge under each string record the vibrations of individual strings. The motion capture data along with the string motions and calibration data are used to estimate the musician's control parameters: applied bow force, bow speed, bow position, bow angles, and string length. The bridge mobility is used to estimate bow force limits for comparisons with the observed control parameters. The musician's comments about perceptual properties are used to interpret the measurements.

We observed some evidence that the perceived "power" or "loudness" of a string is indeed an intrinsic property of the cello. We calculated the ratio of the RMS microphone amplitude to the RMS string vibration amplitude for each note, creating a quantity similar to the more traditional radiation transfer function. The result was greater on one cello for notes which were perceived to be more powerful on that cello. We further suggest that this intrinsic loudness property may be estimated by combining the horizontally and vertically excited radiation transfer functions in a way which takes into account all string polarizations.

We present a new diagram, similar to Schelleng's, which allows us to combine data from different control parameters, notes, strings, and cellos. The new diagram makes it easy to see, in one picture, that the musician maintains a large margin from Schelleng's limits. More concretely, for typical bow speeds, Schelleng's upper limit is usually much larger than what the bow deformation affords the musician, while Schelleng's lower limit is much smaller than the minimum used by the musician, with the exception of wolf notes. We conclude that small variations in these limits are not likely to be perceived and that the range of forces consistent with Helmholtz motion is not likely to play a role in the evaluation of cellos.

A preferred strategy for changing the direction of bow movement on the cello is identified. The strategy produces a distribution of attack times on the cello. While about 50% of attacks had acceptable transient durations by Guettler's criterion (with many perfect attacks), the musician did not complain about the quality of any attack specifically, or of attacks in general, and seemed content with recordings which include transients which never achieved Helmholtz motion. This emphasizes that the acceptability of an attack transient is not solely dependent on its duration and that Guettler's criterion is not an absolute threshold. It is sometimes suggested that a string on which the musician produces longer transients on average should be perceived negatively. We did not find this to be the case. Instead, we found that greater bow forces lead to shorter transient durations. In one case, a string was described negatively as [soft] and the musician used less force, resulting in longer transients. But in another case, a string was described negatively as having a poor timbre and the musician used more force, resulting in shorter transients.

Geometric features of the cello set-up (in particular, the bridge curvature) may lead the musician to use less force than usual in order to avoid accidentally touching adjacent strings. This results in longer transients and different timbres, which are perceived in ways that are not related to geometry or control parameters. Sometimes unconscious adaptations to the geometry affect the sounds produced and the subsequent perception of the instrument. A conscious effort is needed to overcome these natural behaviors in order to compensate for set-up geometry and arrive at a stable evaluation. Thus if any reliable link between perceived properties and physical properties is to be found, we must ensure that each musician evaluating the instrument has sufficient cause to try to overcome any unsatisfactory perceptions.

Résumé

Les relations entre les propriétés physiques (matériaux, géométrie, modes de vibration) des instruments à cordes frottées et leurs propriétés perceptives (qualité, son, jouabilité) sont encore peu connues.

Bissinger a mesuré les propriétés physiques de plusieurs violons, mais n'a pas trouvé de corrélation avec les évaluations de qualité de ces violons, probablement parce que celles-ci étaient trop simplifiées. Fritz et Saitis ont enquêté sur la manière dont les violonistes évaluent subjectivement les instruments. Ils ont constaté que les musiciens fournissent des évaluations cohérentes mais ne sont pas d'accord avec les autres musiciens, non seulement en termes de préférences subjectives, mais plus surprenant en termes de critères que l'on pourrait considérer comme plus objectifs. Ce désaccord est certainement dû aux différences dans les techniques de jeu. Ainsi, Chudy a montré que les musiciens utilisent les paramètres de contrôle différemment les uns des autres, même lorsqu'ils jouent le même extrait musical.

Guettler a identifié des paramètres de contrôle pertinents pour les attaques et, grâce à un test d'écoute, pu déterminer la durée des attaques acceptables pour le violon. Schelleng a étudié l'ensemble des paramètres de contrôle en régime stationnaire qui permettent la vibration des cordes en jeu normal (mouvement dit de Helmholtz) et a identifié les limites de force supérieure et inférieure pour une note et une vitesse d'archet données. Woodhouse a amélioré l'estimation de Schelleng concernant la limite de force inférieure et l'a reliée à la note de loup. Il a en outre proposé la mobilité au chevalet comme mécanisme physique pouvant expliquer la perception de la jouabilité. Zhang a testé cette hypothèse dans le contexte de la note de loup et a trouvé une bonne correspondance entre la mobilité au chevalet et la sévérité perçue de la note de loup.

Dans cette thèse, nous essayons d'explorer davantage le lien entre la mobilité au chevalet et la perception de la jouabilité en observant si le musicien perçoit des différences dans les limites supérieure et inférieure de Schelleng, pour les notes autres que la note de loup. Nous recherchons également d'autres facteurs pertinents pour la perception de la jouabilité par le musicien en étudiant les interactions entre le musicien et l'instrument lors d'une tâche d'évaluation et d'interprétation. Contrairement aux approches précédentes, nous observons toutes les parties de la boucle de rétroaction qui pourraient être impliqués dans la jouabilité, à savoir les paramètres de contrôle, les réponses vibratoires et acoustiques de l'instrument mesurés avec une excitation contrôlée (marteau d'impact), la réponse de l'instrument en situation de jeu et les commentaires du musicien sur les qualités de cet instrument.

Nous utilisons un système de capture de mouvement basé sur des caméras infrarouges pour suivre les mouvements relatifs du violoncelle et de l'archet, tandis qu'un musicien professionnel évalue deux violoncelles. Des capteurs piézoélectriques dans le chevalet sous chaque corde enregistrent les vibrations de chaque corde. Les données de capture de mouvement, ainsi que les mouvements des cordes et les données de calibrage, sont utilisés pour estimer les paramètres de contrôle du musicien: la force d'archet appliquée, la vitesse de l'archet, la position de l'archet, les angles de l'archet et la longueur de la corde vibrante. La mobilité du chevalet est utilisée pour estimer les limites de force d'archet qui sont comparées aux paramètres de contrôle mesurés. Les commentaires de qualité du musicien servent à interpréter les mesures.

Nos observations semblent montrer que la « puissance » d'une corde est une propriété intrinsèque du violoncelle. Nous avons calculé le rapport entre l'amplitude RMS du microphone et l'amplitude RMS des vibrations de corde pour chaque note, créant ainsi une quantité similaire à la fonction de transfert de rayonnement traditionnelle. Cette quantité était plus grande sur le violoncelle pour lequel les notes étaient perçues comme plus puissantes. Nous suggérons en outre que cette propriété intrinsèque de puissance pourrait être estimée en combinant les fonctions de transfert de rayonnement obtenues par excitations horizontale et verticale de manière à prendre en compte toutes les polarisations possibles de la corde.

Nous présentons un nouveau diagramme, similaire à celui de Schelleng, qui nous permet de combiner les données de différents paramètres de contrôle, notes, cordes et violoncelles. Le nouveau diagramme permet de voir facilement, dans une image, que le musicien conserve une marge importante par rapport aux limites de Schelleng. Plus concrètement, pour des vitesses d'archet typiques, la limite supérieure de Schelleng est généralement beaucoup plus grande que celle offerte au musicien par la déformation de l'archet, tandis que la limite inférieure de Schelleng est bien inférieure au minimum utilisé par le musicien, à l'exception des notes de loup. Nous concluons que de petites variations dans ces limites ne seront probablement pas perçues et que la gamme des forces compatibles avec le mouvement de Helmholtz n'est pas susceptible de jouer un rôle dans l'évaluation des violoncelles.

Une stratégie préférée pour changer la direction du mouvement de l'archet sur le violoncelle est identifiée ; elle produit une distribution des temps d'attaque. Bien qu'environ 50% des attaques aient des durées transitoires acceptables selon le critère de Guettler (avec de nombreuses attaques parfaites), le musicien ne s'est pas plaint de la qualité d'une attaque en particulier, ni des attaques en général, et semble se contenter d'enregistrements incluant des transitoires qui n'ont jamais atteint le mouvement de Helmholtz. Cela souligne que l'acceptabilité d'un transitoire d'attaque ne dépend pas uniquement de sa durée et que le critère de Guettler n'est pas un seuil absolu. Il est parfois suggéré qu'une corde sur laquelle le musicien produit des transitoires plus longs en moyenne devrait être perçue négativement. Nous n'avons pas observé un tel effet. Au lieu de cela, nous avons constaté que des forces d'archet supérieures entraînaient des durées de transitoires plus courtes. Dans un cas, une corde était décrite négativement comme "molle" et le musicien utilisait moins de force, ce qui entraînait des transitoires plus longs. Mais dans un autre cas, une corde était décrite négativement comme ayant un timbre médiocre et le musicien utilisait plus de force, ce qui réduisait les transitoires.

Les caractéristiques géométriques de la structure du violoncelle (en particulier la courbure du chevalet) peuvent amener le musicien à utiliser moins de force que d'habitude afin d'éviter de toucher accidentellement des cordes adjacentes. Cela entraîne des transitoires plus longs et des timbres différents, qui sont perçus d'une manière non liée à la géométrie ou aux paramètres de contrôle. Parfois, des adaptations inconscientes de la géométrie affectent les sons produits et la perception ultérieure de l'instrument. Un effort conscient est nécessaire pour surmonter ces comportements naturels afin de compenser la géométrie de la configuration et d'arriver à une évaluation stable. Ainsi, si un lien fiable doit être trouvé entre les propriétés perçues et les propriétés physiques, nous devons nous assurer que chaque musicien évaluant l'instrument dispose de suffisamment de raisons pour tenter de surmonter les perceptions non satisfaisantes.

Acknowledgements

This project would not have been possible if it weren't for the opportunity and funding provided by Sorbonne Université (previously the Université Pierre et Marie Curie). The cellos, bow, and motion capture equipment were funded through additional grants from Sorbonne Université. I enjoyed some additional training during a Short Term Scientific Mission funded by WoodMusICK COST Action FP1302. The Universidad Nacional Autónoma de México provided office space (with great weather and a beautiful view of the ocean) while I finished the manuscript.

I would like to thank my advisors Benoît Fabre, Jean-Marc Chauvel, and especially Claudia Fritz for their support, encouragement, and patience throughout this project.

Further thanks to everyone from the Lutheries - Acoustique - Musique team of the Institut Jean le Rond d'Alembert, for exposing me to their research projects, for discussing cultural differences and political issues, and for sharing their musical talents.

I thank Laurent Quartier for his support in the workshop, including laser cutting the plastic supports for the bridge sensor, and Hélène Moingeon for making the circuitry for the bridge sensor. I acknowledge the efforts of the interns who worked with me, especially Élodie Guillet and Maxime Bachoffer for helping me take measurements and explore models.

Thanks go to instrument makers Paul Noulet and George Stoppani for hosting me at their homes and workshops. Paul helped us purchase and set-up the cellos, made adjustments to them, and prepared the bridges. George gave me experience taking measurements and performing modal analysis using the software he developed.

I would like to thank the ten amateur and professional cellists that I observed and who provided me with feedback at Violoncelle En Seine, our lab, or in other venues. I am grateful to Augustin Ernault, Adam Cheminet, and Xavier Gagnepain for their help as we developed the measurement system and experimental protocol.

I had stimulating conversations at conferences or via email with many researchers outside of our lab. Their comments were helpful and their interest was motivating. I thank Jim Woodhouse, Colin Gough, Murray Campbell, Esteban Maestre, Quim Llimona, Alfonso Pérez-Carillo, Charlotte Desvages, Frédéric Ablitzer, Robert Mores, and Jean Kergomard.

I cannot separate the experience of working on this project from the experience of living in France. I thank my wife Aïda for bringing me here, my new friends Aude Secheret, Eugénie de Mey, and Jean-Christophe Brizard for making life outside of work interesting, and my son Maxwell for bringing me joy.

Contents

Abstract	ii
Résumé	iii
Acknowledgements	v
1 Introduction	1
1.1 Playability	2
1.2 Research questions	3
1.3 Thesis outline	3
2 Background material	5
2.1 Introduction to the cello	5
2.1.1 The cello	5
2.1.2 Right hand controls bowing parameters	7
2.1.3 Left hand controls string length	9
2.2 Physical characterization of the cello	10
2.3 Helmholtz motion	13
2.4 Schelleng's diagram	19
2.5 Guettler diagram	22
2.6 Playability of bowed string instruments	25
2.7 Mental maps between music descriptors and control parameters	25
2.8 Measuring control parameters	26
2.8.1 Bow kinematics	26
2.8.2 Bow force	31
2.8.3 String length	33
2.8.4 Other measurements	34
3 Musician's control parameters	35
3.1 Effective string length	35
3.1.1 String model	35
3.1.2 Finger model	37
3.1.3 Stopped string length estimation	37
3.1.4 Discussion of string modeling	39
3.2 Bow kinematics	40
3.2.1 Orientation of the bow	40
3.2.2 Position and speed of the bow	42
3.3 Bow force	43
3.3.1 String compliance	44
3.3.2 Hair compliance	46
3.3.3 Bow force model	52

4	Experimental equipment	55
4.1	Microphone	55
4.2	Bridge sensor	55
4.2.1	Design	56
4.2.2	Calibration	59
	Measurement procedure	59
	Parameter estimation	61
	Interpretation of calibration coefficients	62
4.3	Motion capture	64
4.3.1	Using rigid body models to find landmarks	68
4.3.2	Force transducer markers and reference frame	70
4.3.3	Cello markers and reference frames	72
4.3.4	Bow markers and reference frames	75
4.4	Discussion of errors	78
5	Experiment	81
5.1	Prior observations	82
5.2	The musicians	82
5.3	The two cellos	83
5.4	The bow	83
5.5	Repertoire selection	84
5.6	Framing the experiment	87
5.7	Eliciting comments	87
5.8	Discussion	89
6	Data processing and exploration	91
6.1	Data pre-processing	91
6.1.1	Fundamental frequencies.	91
6.1.2	Open string tension	92
6.1.3	Stopped string length, stopping point, and stopped string tension.	92
6.1.4	Rigid body models.	92
6.1.5	Landmark estimation.	92
6.1.6	Orientation of reference frames.	92
6.1.7	Kinematic control parameters.	93
6.1.8	Bow force model.	93
6.1.9	Piezo calibration.	93
6.1.10	Schelleng's Limits.	94
6.2	Data segmentation	94
6.2.1	Segmentation based on the inclination angle	94
6.2.2	Segmentation based on the piezo amplitudes	96
6.2.3	Segmentation based on the bow force or total depth	97
6.2.4	Segmentation using the score, pitch, and control parameters	98
6.3	Statistics of control parameters	99
6.3.1	Extreme values	99
6.3.2	Typical values	100

7	General results	103
7.1	On the perception of Schelleng's bow force limits	103
7.1.1	The normalized Schelleng diagram	103
7.1.2	Results.	105
7.1.3	Interpretation.	106
7.2	On the interpretation of Guettler diagrams	107
8	Comparison between cellos	111
8.1	Signs of adaptation	111
8.1.1	Influence of cello and string on force	111
8.1.2	Influence of cello and string on absolute bow speed	112
8.1.3	Influence of cello and string on bridge-to-bow distance	113
8.1.4	Influence of cello and string on tilt	114
8.1.5	Influence of cello and string on absolute skew	115
8.2	Normalized Schelleng diagrams for both cellos	116
8.3	Transients	118
8.4	Perception of bridge curvature	120
8.5	Richness comment	121
8.6	Piezo to microphone ratio and radiation	123
9	Conclusion	127
9.1	Contributions in experiment design	127
9.2	Summary of results	128
9.3	Schelleng's limits	129
9.4	Guettler's diagram	132
9.5	Limitations and Perspectives	132
A	Circuit for bridge sensors	135
B	Skew Projection	137
C	Bridge Sensor Calibration Coefficients	141
D	Recording session outline	143
E	Texts, questions, and sheet music presented to the musician	145
	Bibliography	149

Chapter 1

Introduction

Context. There are very few, if any, studies on the extent to which the perceived quality of a bowed-string instrument is affected by the choice of interactions used to evaluate it. Yet it is precisely these interactions which define musical instruments as tools rather than as simple objects. The quality of a tool lies in its capacity to be manipulated by the user to achieve his purpose for using it. Certainly the physical properties of an instrument are relevant to evaluating its quality, but the way the instrument is played as well as the musician's intended purpose must also be taken into account.

Complication. There has been a lot of research which treats instruments as objects. Instrument makers and scientists have studied the materials, geometry, construction, and vibrational behavior of bowed string instruments with the hopes of predicting their quality as perceived by musicians. The result of this research is that we have very good models of how the instruments work and are making in-roads on how we can control their vibrational behavior through modifying materials and geometry. Unfortunately, we still don't fully understand the relationships between our physical measurements and the reported quality ratings of the instruments.

Observations. Having not found a satisfactory correspondence between physical measurements and reported quality ratings, researchers questioned the relevance of the measurements and the accuracy of the quality ratings. While some researchers started looking for new ways of visualizing and analyzing physical measurements, others began a series of experiments to better understand how musicians establish quality ratings. These studies have shown that (1) neither age nor monetary value of instruments are reliable indicators of quality ratings, implying that previous research which assumed quality ratings based on these indicators should be revisited; (2) individual musicians have consistent perceptions, which validates the assumption that the comments of musicians give us meaningful information about the instrument; but (3) musicians do not agree with each other when sorting instruments based on perceptual properties, which brings into question the existence of universally accepted overall quality ratings.

Hypothesis. While physical properties of the instrument may be inferred from very different measurement methods, apparently the same cannot be said about perceptual properties. Each musician has his own unique way of interacting with the instrument. Thus, they receive different stimuli when playing the same instrument which leads them to disagree about that instrument's quality rating. The next step is to investigate the role that musician-instrument interactions play in rating an instrument's perceptual properties, and later, to research the role of various perceptual properties in forming an overall quality rating. This thesis, focusing on the perceived playability of cellos, is the first study to take steps along these lines of research.

1.1 Playability

General definition. Playability is a perceptual property that we attribute to the instrument which is related to the interactions between the musician and the instrument. It encompasses the control parameters (fingering and bowing) applied to the instrument, the aural and haptic feedback produced by the instrument according to its physical properties, and the sensation, perception, and interpretation of this feedback by the musician.

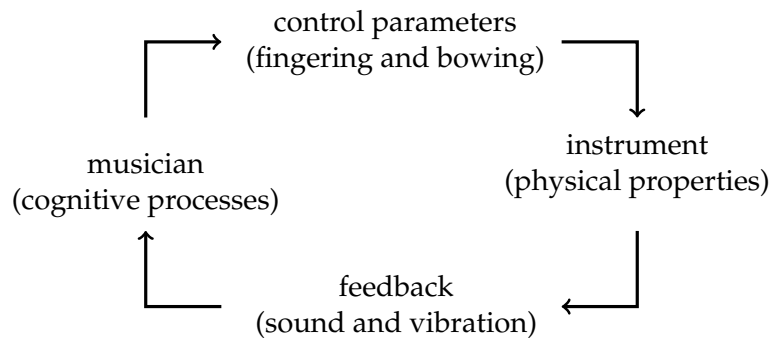


FIGURE 1.1: A complete understanding of playability requires studying each of the four parts of the interaction feedback loop between the musician and the instrument.

Working definition. The notion of playability as described above is pretty vague, so researchers have adopted a more quantitative definition in the context of bowed-string instruments: the ability to reliably and quickly initiate and sustain a desired string motion. This working definition is clearly relevant to some aspects of playability, after all it is motivated by the researchers' personal experiences as musicians. It also conveniently suggests several physical and perceptual studies. Researchers have studied the combinations of control parameters which permit various sustained periodic string motions (Schelleng, 1973). They have studied what happens to sustained motions when perturbations are introduced (Woodhouse, 1994). They have looked at the duration of transients for various sets of control parameters (Guettler, 2002). And they have studied how these transient durations are affected by initial conditions (Demoucron, 2015).

Musician's definition. While researchers have adopted the working definition above, they recognize that it is only one facet of what the musician perceives as playability. Unfortunately not all facets of playability have been well characterized. To do so, we would need to listen to how musicians talk about instruments in general and playability in particular. We could then identify different facets of playability and the phrases used to talk about each facet. Finally, we would then hope to align their statements with physical measurements. The difficulty of this challenge can be seen with an example. When the musician says "harder to play," some possible meanings are that the instrument requires (1) larger physical forces applied to the string to control its vibrations, (2) more physical work done on the instrument to radiate at a sufficiently loud volume, (3) greater perceived muscular effort due to (a) applying larger forces to the instrument, (b) doing more work on the instrument, or (c) eccentric activation of opposing muscles, or (4) greater perceived mental effort due to (a) more sensitive feedback or (b) unfamiliar feedback. For the simple phrase "harder to play" we have hypothesized seven possible alignments to investigate, none of which have easily accessible

physical measurements. Clearly completely characterizing the musician's definition of playability by aligning their statements with physical measurements is no small task.

1.2 Research questions

- What are typical values and ranges of control parameters on the cello?
- Are musicians sensitive to changes in Schelleng's upper and lower bow force limits?
- How often do cellists have perfect or acceptable transients by Guettler's criterion?
- What strategies do musicians use to perform bow changes?

There is a widespread assumption that musicians are sensitive to the physical properties of their instruments and adapt their control parameters accordingly.

- How do control parameters vary between cellos?
- How do control parameters vary between strings?
- What links exist between the control parameters, instrument properties, instrument response, and musician's perceptions?

1.3 Thesis outline

This thesis is conceived in two parts. Chapters 2-4 provide the background knowledge needed to understand the place of the thesis among the existing literature and the technical details of data acquisition. Chapters 5-9 describe the experiment, analysis of results, and conclusions. It may be helpful to read the introduction to Chapter 5 to get an overview of what was done and why before diving into the details in Chapters 2-4. Section 6.1 gives a step-by-step outline of the calculations developed in Chapters 3-4 for readers who prefer such an organization.

Chapter 2 reviews a small fraction of the literature related to measuring bowed string instrument control parameters, string vibrations, and instrument properties as well as some relevant perceptual studies.

Chapter 3 defines control parameters and the models used to extract them from assumed available measurements. Original contributions in this chapter are explicit algebraic equations for each of the kinematic bowing parameters and an approach to bow force estimation which takes into account the compliance of the string.

Chapter 4 describes the equipment used for collecting raw data as well as the pre-processing necessary to obtain the measurements assumed in Chapter 3. Original contributions include a sensor design which is more robust than previous generations, a new analysis of the calibration coefficients for the sensor, and discussions about minimizing systematic errors in infrared camera-based motion capture systems.

Chapter 5 describes early field observations and the subsequent development of the experimental protocol.

Chapter 6 describes the pre-processing pipeline for the data collected during the experiment, a few strategies for segmenting data, and some initial analysis of the data. Notably we present statistics for extreme and typical values of control parameters which are useful for considering the results of simulations found in the literature.

Chapter 7 describes the results concerning the Schelleng and Guettler diagrams. Original contributions include a modified Schelleng diagram which allows us to plot gestures of different pitches, bow speeds, and bridge mobilities in the same figure, allowing us to answer questions about the role of Schelleng's limits in the perception of playability. We also present statistics of transient durations for the cello, similar to those collected by Guettler for the violin.

Chapter 8 describes the results of comparing the two cellos. In particular we look at how the musician adapted her gestures to accommodate the individual properties of each cello, and how the control parameters and instrument behavior are related to the musician's perceptions of the instrument. We also present some original contributions to the discussion of how radiation measurements may be used to compare cellos.

Chapter 9 contains a summary of the experiments, results, and conclusions. I then discuss the implications of these results and point to possible directions for future research.

Chapter 2

Background material

In Section 2.1, we present some background information about the cello for readers who are unfamiliar with the instrument, describing its construction, how it is played, and some typical measurements used to characterize its behavior. In Section 2.3, we review some basic theory of bowed string motions and ways to measure it. In Sections 2.4 and 2.5, we review some previous studies of bowed strings which have framed the discussion of playability from a physical point of view. The discussion is rather limited, focusing on those parts which are of immediate relevance to this thesis. Section 2.6 points at a recent study which attempted to relate physical differences between cellos to the perceptions of the players. Section 2.7 reviews a study which gives some insight into the cognitive aspects of how cellists play the instrument. Finally, in Section 2.8 we review many techniques that have been used for measuring the control parameters applied to bowed string instruments.

2.1 Introduction to the cello

This section is a very brief introduction to the cello highlighting the specific knowledge about its construction, function, and use that I assume the reader is familiar with in the rest of the thesis. Section 2.1.1 describes the construction, tuning, and principles of operation of the cello. Section 2.1.2 describes the construction and use of the bow, listing the bowing parameters that we will measure. Typical maximum forces that the bow can apply to the string are presented to bridge the gap between the cellist's qualitative experience and the measurements that are discussed in the literature. Section 2.1.3 addresses some common questions I've been asked about how the musician changes the pitch of the string, including vibrato. For the purposes of this thesis, this section serves to point out the string length as a control parameter and to define the vocabulary term "stopping point."

2.1.1 The cello

The cello is a bowed-string instrument with four strings tuned in fifths with a range from C_2 (65.4 Hz) to higher than C_6 (1046.5 Hz). Table 2.1 gives the tuning and Figure 2.1 shows the construction of the cello. Missing from the diagram are the strings; they are attached to the tailpiece and pass over the bridge, above the fingerboard, and over the nut before wrapping around the tuning pegs in the pegbox. The bridge stands on the front plate between the f-holes and is held in place by the tension of the strings. The front plate and back plates are glued to the ribs and a sound-post is friction-fit between the front and back plates near the treble foot of the bridge.

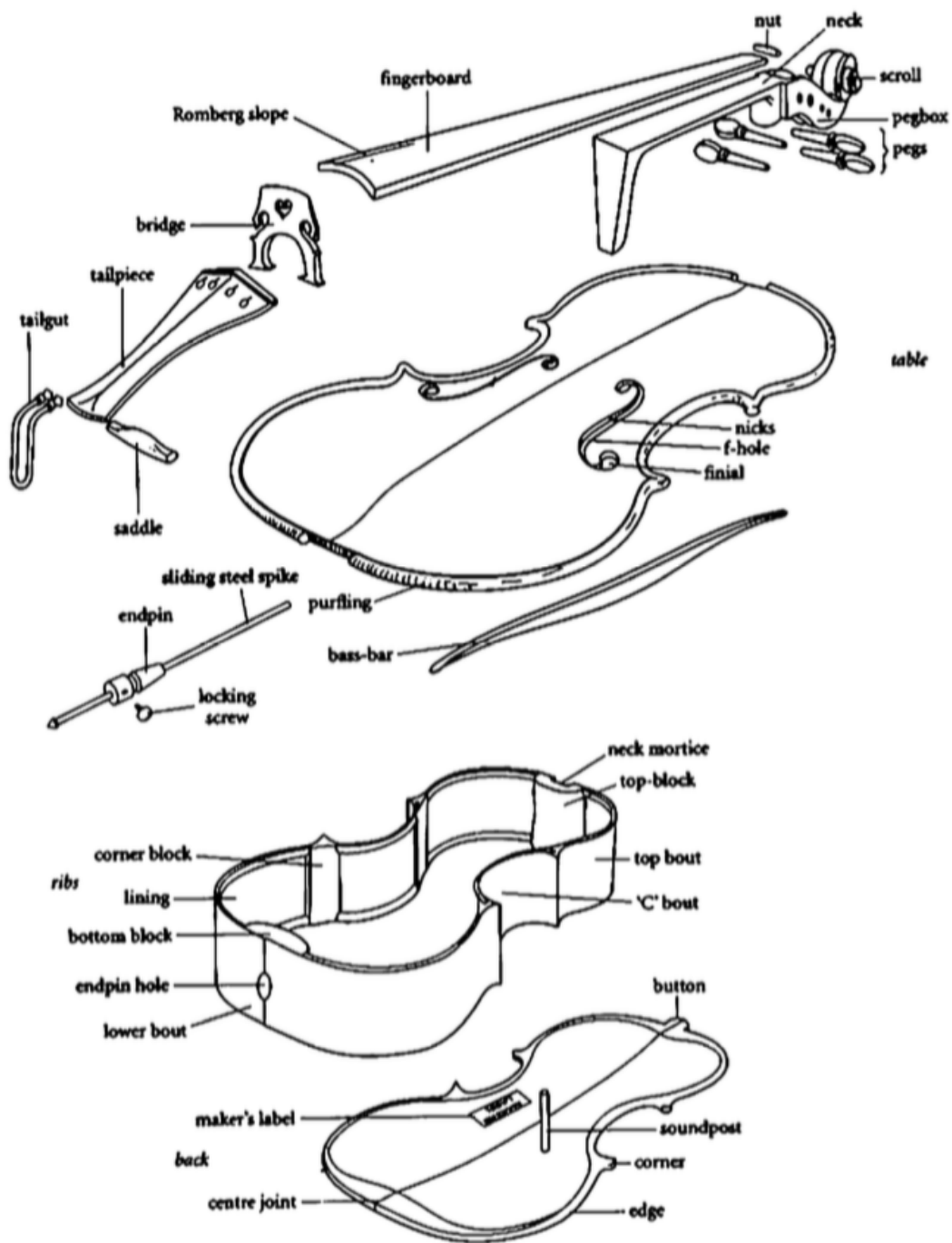


FIGURE 2.1: An exploded view of the cello construction, from Rossing et al., 2010.

String #	Solmization	Pitch	Frequency
I	La	A_3	220 Hz
II	Re	D_3	147 Hz
III	Sol	G_2	98.0 Hz
IV	Do	C_2	65.4 Hz

TABLE 2.1: Reading across the rows gives the correspondence between the string number, fixed-do solmization, pitch, and nominal fundamental frequency of each open string in equal temperament tuning using the A_4 440 Hz pitch standard. Note that the actual frequency of each pitch depends on the pitch standard and the tuning scheme used by the individual cellist.

The cellist usually causes the string to vibrate by rubbing it with the rosined hairs of a bow, but the string may also be struck or plucked. The strings themselves contribute very little to the amplitude (or volume) of the sound radiated as can be verified by playing a monochord. The vibrations in the string are carried through the bridge to the front plate (labeled "table" in the diagram). The vibrations of the front plate are coupled to the ribs, back plate, and the air within the box formed by the front plate, ribs, and back plate. It is the vibration of the large surfaces of this box which are responsible for sound propagating from the cello.

2.1.2 Right hand controls bowing parameters

The principal components of the bow are shown in Figure 2.2. The hair is attached at the tip and the frog. The end of the stick above the frog is hollow. This allows an adjustment screw to be inserted from the end. The top of the frog has a nut attached to it. The stick has a mortise which allows the nut to be inserted into the stick. An adjustment screw is inserted into the hollow shaft and passes through the nut, securing the frog in position. Turning the button (the exposed end of the adjustment screw) causes the frog to move closer or further from the tip, loosening or tightening the hair.

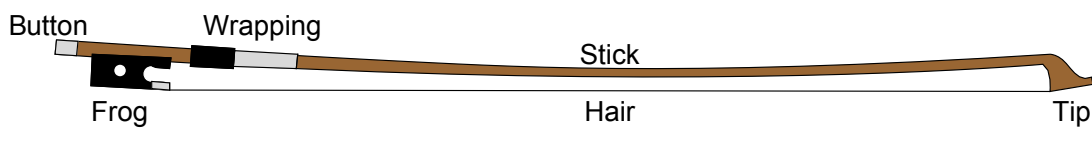


FIGURE 2.2: The parts of the bow.

The musician holds the bow with the right hand (Figure 2.3). While violinists place the little finger on top of the bow, cellists drape all four fingers over the face of the frog. The index finger presses against the wrapping. The thumb is placed between the wrapping and the frog or on the end of the frog.

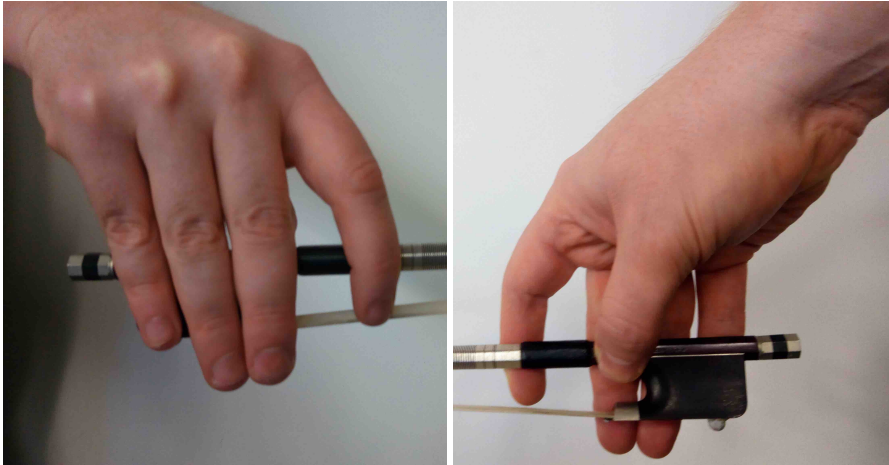


FIGURE 2.3: Holding the bow

The force of the bow on the string is a reaction to the weight of the bow and the torque applied by the index and thumb (Figure 2.4). If these forces are not in equilibrium, then the bow will either lift or press harder into the string until equilibrium is achieved. If the torques are not in equilibrium, then the bow will rotate until the player actively restores equilibrium.

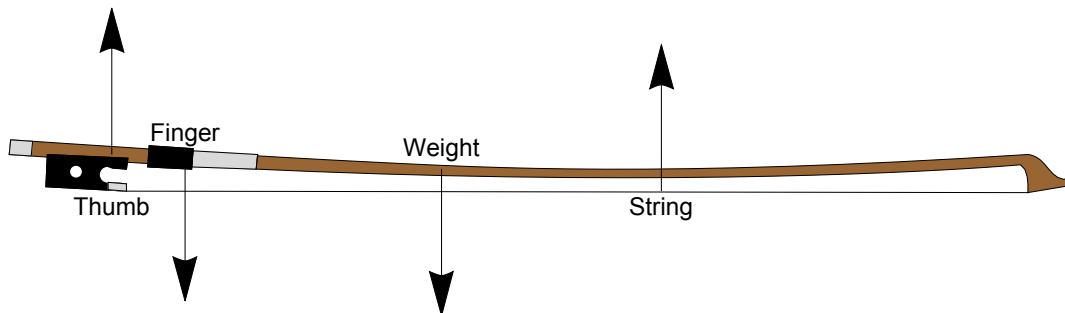


FIGURE 2.4: A free body diagram showing the vertical forces applied to the bow. The small horizontal forces of the hand and of friction with the string are not indicated.

As the bow hair is pressed against the string, the frog and tip rotate, the hair at the contact point is deflected upward, and the middle of the stick is deflected downward. An upper limit is reached when the force causes the contact point to touch the stick. By pressing the bow against a load cell (see Section 3.3.2), we observed that forces larger than 10 N can be applied underneath the wrapping. Typical maximum forces in the middle of the stick are between 5 N and 10 N depending on the tension of the hair and the compliance of the stick. It is difficult to apply more than 3 N to 6 N near the tip due to the mechanical disadvantage.

About 175-200 hairs from the tail of a horse form a ribbon of hair about 610 mm long, 10 mm wide, and 1 mm thick. As a natural material grown over time, material properties vary across the width (from hair to hair) and along the length of the hair ribbon. Models of the bow hair typically use an average homogeneous model for material

properties of the hair. Most models use a single hair approximation (e.g. Ablitzer, 2011) though finite-width hair ribbon models exist (Pitteroff and Woodhouse, 1994). The choice of hair, length of hair, and shape of the hair ribbon are determined by the bow re-hairer about once or twice a year depending on climate and use. The musician adjusts the tension of the hair and applies rosin to the hair before playing. No adjustments are made to the bow while playing.

The stick is almost exclusively made of pernambuco wood, though CITES¹ restrictions since 2007 limit this material to pre-existing stock. A market for carbon-fiber bows has grown as bow makers look for suitable alternatives to pernambuco, including other wood species and synthetic materials. The stick usually has an octagonal, circular, or elliptic cross-section. The bow is tapered; the thickness of the stick changes along the length of the stick. It is thickest near the frog and thinnest near the tip. The bow is cambered; when in a non-tensioned state, the stick is curved toward the hair, and usually touches the hair at the middle of the stick. The bow maker cambers the stick by applying heat to a local portion of the stick and bending the heated stick. The bow maker is able to set the weight, stiffness, and balance of the bow stick, which, along with the tension set by the player, contribute to its playing properties. Ablitzer (2011) has modeled the static properties of the bow, developing a method of estimating its effective material properties. Gough (2012) has modeled the dynamic properties of the bow, in an attempt to understand how measured dynamic properties may be related to the playing properties as expressed by the musician. Caussé et al. (2001) have done a perceptual study to try to relate static and dynamic properties of a bow to perceived playing properties and bow quality.

For our study, we are interested in measuring the bowing parameters: the orientation, position, and speed of the bow with respect to the cello and the normal force between the bow hairs and the cello string. Calculating the position and orientation of the bow only requires the relative position of a single point and the relative orientation of a reference frame attached to that point. Estimating the bow force will require knowing at least the position of the bow and a position-dependent compliance model. If we want to include the effects of bowing angles and finite bow width on the bow force estimation, then we will also need the orientation and a position-and-orientation-dependent compliance model.

2.1.3 Left hand controls string length

To change the pitch of the string while playing, the musician uses a finger to deform the string until it is pinned against the fingerboard at a point called the stopping point. The musician usually uses the tip of the finger (Figure 2.5a) or the fleshy part of the finger opposite the nail (Figure 2.5b). When playing beyond the neck of the cello, the side of the thumb from the knuckle to around the middle of the nail is often used (Figure 2.5c). It is sometimes necessary to use the nail of the index finger when playing in the thumb positions (Figure 2.5d).

Vibrato on the cello is initiated in the arm causing the bones of the finger to translate and rotate over the string. The finger does not slide along the string. The flesh of the fingertip deforms and rolls along the string. In addition to the amount of arm movement, the vibrato width is affected by orientation of the finger. By placing the

¹The Convention on International Trade in Endangered Species has categorized pernambuco as Category II in good faith as a result of conservation efforts made by the bow-making community. This allows finished bows to be passed across international borders without certificates, though new wood stock may not be harvested, and the movement of existing stock is restricted.

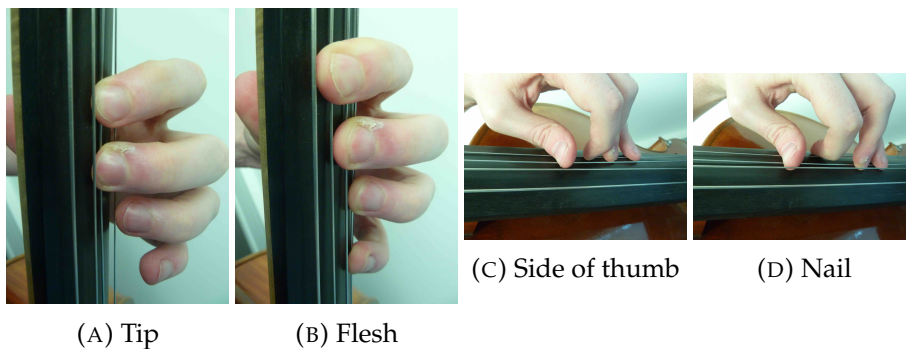


FIGURE 2.5: The parts of the finger used to stop the string.

finger at an angle with respect to the string, the effective width of the finger increases, so the portion of string which is covered and revealed during a vibrato cycle is longer, leading to more pitch variation. For a few seconds after pressing the string with the finger, an indentation can be found in the flesh of the finger which clearly indicates the portion of the finger which was in contact with the string (Figure 2.6).



FIGURE 2.6: The string leaves an impression in the fingertip.

Models of the interaction between the string and the finger have been developed for the purposes of sound synthesis by Desvages and Bilbao (2016) based on their measurements of the nonlinear and hysteretic deformation of the finger. The distributed interactions between the string and fingerboard have been modeled by Desvages and Bilbao (2016) and Issanchou et al. (2017).

One musician indicated that he was sensitive to the minimum force needed to fully stop the string. While this would be interesting to study, it would require more equipment for measuring the force, additional research to properly define fully stopped, and even more research to develop a method of distinguishing between a fully stopped and a partially stopped string. For our study, we will focus only on the stopped string length which we will be able to estimate from the frequency of the vibrating string.

2.2 Physical characterization of the cello

Several studies have aimed at shedding light on the relationship between the construction of an instrument and its perceived quality. Most of these studies have focused

on the relationship between the construction of the instrument and its vibrational behavior. (Bissinger, 2008) is a typical example of the few studies which have tried to find a relationship between the vibrational behavior of the instrument and its perceived quality. Bissinger collected physical measurements—radiativity and modal analysis—of 17 violins having qualities ranging from bad to excellent, but found no convincing correlations between any of the features and the perceived quality. This may have been because the quality ratings were not reliable: they were based on either the opinion of a single player (for bad to good violins) or on reputation (for excellent violins). Saitis et al. (2012) perform a similar study while addressing the concerns about the reliability of perceptions. In that study, 13 musicians evaluated 10 instruments and ranked them according to preference. While the musicians were found to be self-consistent in their preferences, there was a significant lack of agreement between them. It is not surprising, therefore, that no links between bridge mobility and preference were found. Nonetheless, Curtin (2018) and other luthiers find radiativity and bridge mobility measurements play a useful role in the instrument making process.

The vibrational behavior of the cello is usually characterized by two sets of measurements: bridge mobility and radiation transfer functions. When a system like the cello is driven by a sinusoidal force of a certain frequency it will eventually begin to vibrate and radiate sound at that frequency. For a given amplitude driving force, the amplitude of the vibrations and radiated sound will depend on the frequency. In general, the phase of the vibrations and sound radiation will be shifted with respect to the phase of the sinusoidal driving force, with the shift also depending on the frequency. That is, the moment when the driving force reaches a maximum may not be the moment when the bridge is moving the fastest or when the radiated pressure is greatest. We can represent the relationship between the amplitudes and phases of the driving force and the resulting vibrations and sound radiation using complex numbers; the magnitude of the complex number represents the ratio of the amplitudes and the argument of the complex number represents the phase shifts.

To measure mobility or radiation transfer functions, we take advantage of the linearity of the system which allows us to simultaneously apply driving forces of every frequency and measure their separate contributions to the response of the cello. Frequency domain signals have time domain representations which can be found using Fourier transforms. We would like to use a frequency domain signal in which every frequency is present at equal levels. The time-domain representation of this signal is a delta function impulse. We can approximate a delta function impulse by quickly tapping the bridge with a hammer. The hammer is equipped with a sensor giving the force applied by the hammer as a function of time. An accelerometer or laser vibrometer is used to measure the movement of the bridge in response to the hammer tap. The bridge mobility is then calculated as the ratio of the Fourier transform of the time-domain bridge velocity to the Fourier transform of the time-domain applied force. The radiation transfer functions are calculated similarly, using a microphone to record the time-domain radiated sound pressure.

Not only do bridge mobility and radiation transfer functions depend on frequency, but also on the position and orientation of the applied force and of the accelerometer or microphone. In practice, we usually consider a complete measurement of the bridge mobility to consist of four measurements: the force is applied horizontally/vertically at a fixed location and the motion is measured horizontally/vertically at a fixed location on the bridge. Likewise we usually consider a complete measurement of the radiation transfer function to include at least two measurements: the force is applied

horizontally/vertically at a fixed location while the microphone is held at a fixed location. Some researchers prefer to collect many radiation transfer function measurements by moving the location of the microphone relative to the instrument, often followed by averaging the measurements to reduce the data to a single function of frequency.

We would like to study how the movement of the bridge in response to string motions affects those string motions. It would be ideal if we could measure the force and bridge movement at the point of contact between each of the strings and the bridge, but the accelerometer did not permit this. Instead, we chose to use an impact hammer and accelerometer as shown in Figure 2.7. An alternative procedure could have used the piezoelectric sensors underneath the string (described in Section 4.2) to measure the applied force following the method described in (Zhang and Woodhouse, 2014b).



FIGURE 2.7: Bridge mobility and radiation transfer function measurements conducted with horizontal forces (left figures) and vertical forces (right figures). The horizontal acceleration is measured with the accelerometer on the side of the bridge (top figures) while the vertical acceleration is measured with the accelerometer between the legs (bottom figures). The microphone was located 160 cm in front of the cello.

Figure 2.8 shows the amplitude of the radiativity measurements and Figures 2.9 and 2.10 show the amplitude of the mobility measurements for our two cellos as measured in the space where the experiment of this thesis was performed. The axes are logarithmic which closely corresponds to how we perceive loudness and pitch. The frequencies are indicated above the figures and the corresponding pitches are indicated below. The horizontal lines have 2 dB spacing, corresponding to typical just noticeable differences in sound amplitudes. The vertical lines mark off typical vibrato widths of 28 cents centered on each chromatic note. Thick colored vertical lines indicate the nominal pitch of the open strings of the cello. The colored dots indicate the harmonics of those open strings. The cello repertoire does not often require notes above C_6 (1047 Hz), which is marked with a line.

There is a reciprocity argument that states that when the motion is measured at the point where the force is applied, then the component of the mobility measurement corresponding to a horizontal force and a vertical motion should equal the component corresponding to a vertical force and a horizontal motion. That is, the yellow line should be the same as the green line in Figure 2.9 as well as in Figure 2.10. If the bridge were constrained to move only by translations, then our measurements would show this reciprocity, but this is not the case. The bridge rotates as each of its feet is raised and lowered by different amounts. The center of rotation depends on the

driving frequency as studied in (Zhang, Woodhouse, and Stoppani, 2016). Whenever the accelerometer is close to the center of rotation, it will record a smaller acceleration; farther from the center of rotation, a larger acceleration is measured.

Later on, we will follow common practice and use these measurements to approximate the mobilities at each of the string notches. The results will be used to estimate a theoretical lower bow force limit which we compare with observed bow forces. We do not expect that the errors in these estimated limits will be large enough to affect the conclusions that we draw.

2.3 Helmholtz motion

The string motion associated with the normal sound of a violin was first reported by Helmholtz in 1877 (Helmholtz, 1954). Helmholtz used a vibration microscope to observe the displacement of a point on the string as it was bowed. His observations were consistent with a model of alternating phases of sticking and slipping between the string and bow hair.

Ideal motions. In idealized Helmholtz motion, the velocity of the string switches instantaneously between two constant values (Figure 2.12). The transverse displacement of a string element then takes on an asymmetric triangle waveform. The asymmetry depends on the longitudinal position of the element along the string. By comparing the displacement waveforms at several points along the string, and applying his knowledge of solutions to the equations of motion of an ideal string, Helmholtz was able to infer that the string itself takes the form of two straight lines joined by a corner (the Helmholtz corner), and that the corner travels from bridge to nut and back with a constant longitudinal speed while tracing out a parabolic envelope (Figure 2.11). At any given moment, the transverse force applied to the bridge is equal to the transverse component of the tension vector of the string element at the bridge. For the ideal Helmholtz motion, the force is described by a sawtooth waveform (Figure 2.12).

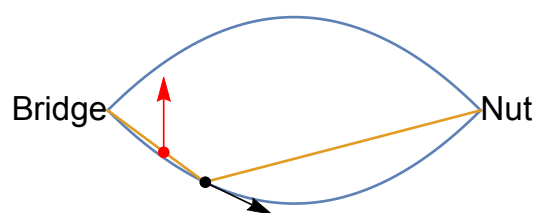


FIGURE 2.11: The state of the string shortly after the sticking phase begins. The contact point (red) is sticking to the hair and traveling at the speed of the bow. The string forms two straight line segments (orange) joined by the Helmholtz corner (black). The Helmholtz corner is propagating toward the nut at the wave speed of the string. The Helmholtz corner traces out a parabolic envelope as it moves from bridge to nut and back.

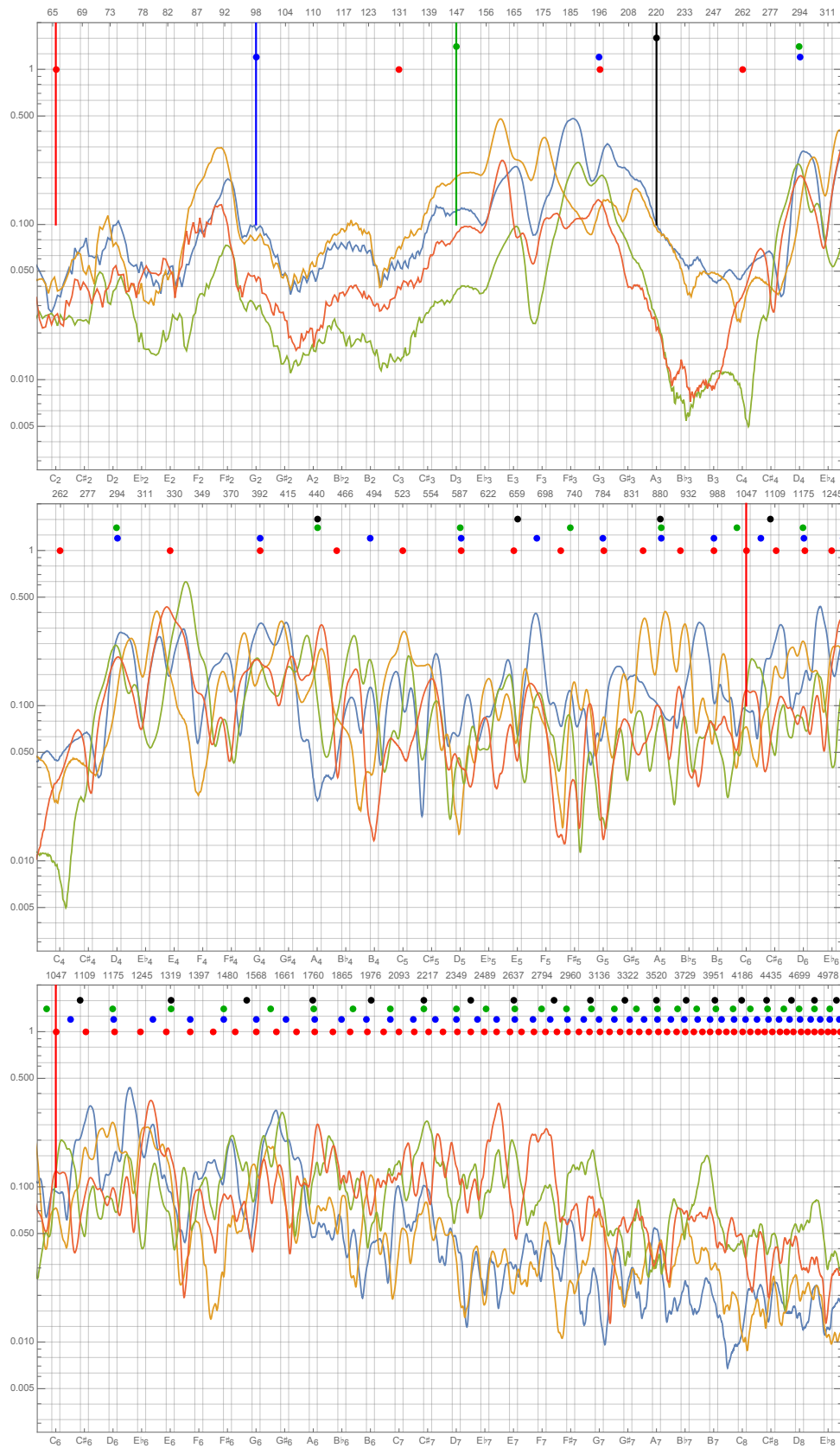


FIGURE 2.8: Radiativity measurements (in $\frac{Pa}{N}$) of the two cellos used in this thesis measured at 160 cm in front of the cello. Cello A, horizontal (yellow) and vertical force (red); Cello B, horizontal (blue) and vertical force (green).



FIGURE 2.9: Mobility measurements (in $\frac{m/s}{N}$) of Cello A. Horizontal force, horizontal motion (blue), horizontal force, vertical motion (yellow); vertical force, horizontal motion (green); vertical force, vertical motion (red).

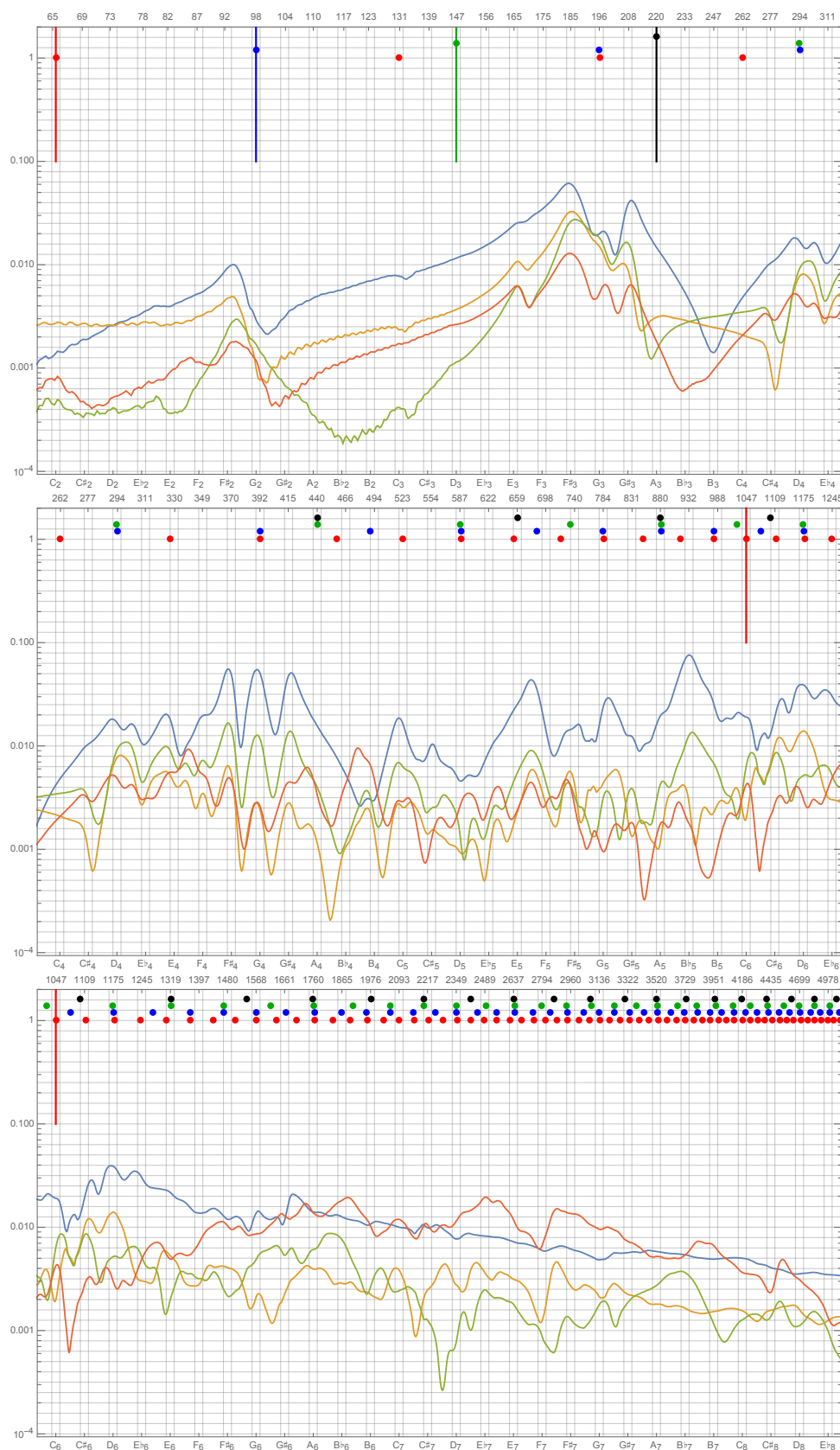


FIGURE 2.10: Mobility measurements (in $\frac{m}{N \cdot s}$) of Cello B. Horizontal force, horizontal motion (blue); horizontal force, vertical motion (yellow); vertical force, horizontal motion (green); vertical force, vertical motion (red).

Interactions. The observed motions are explained by alternating phases of sticking due to static friction and slipping due to restoring forces and inertia. During the longer sticking phase, the Helmholtz corner travels from the bow to the nut and back. As the Helmholtz corner passes underneath the bow hair, the transverse force on the corner due to tension overcomes the static friction between the string and hair, causing the string to begin slipping. During the short slipping phase, the corner continues moving toward the bridge and back to the bow again. When the corner arrives at the bow this time, the transverse force due to tension causes the contact point to accelerate back to the bow speed and static friction causes the string to stick to the bow hair again.

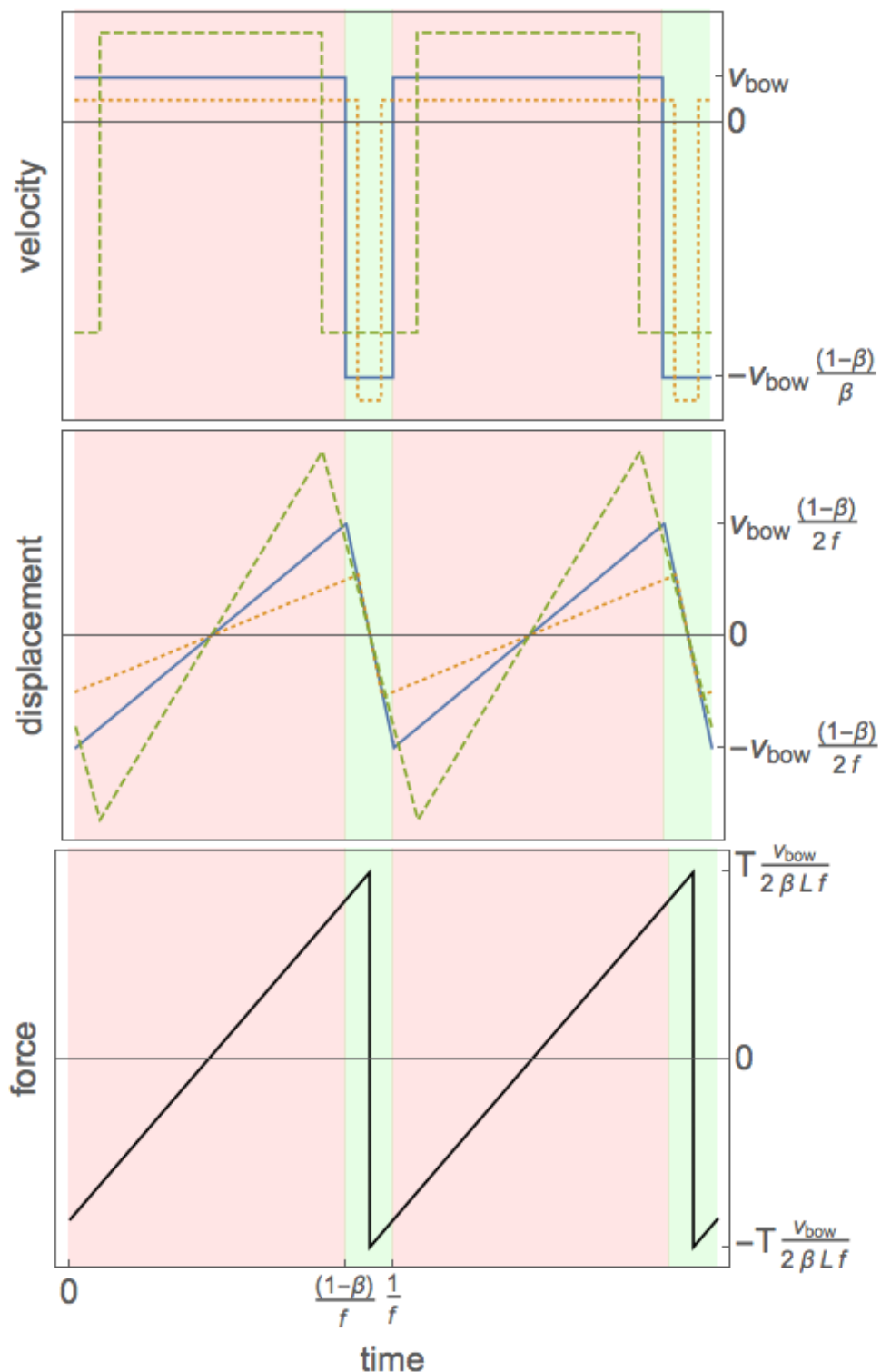


FIGURE 2.12: **Ideal Helmholtz Model** (Top) The velocity of the string at the bow contact point (solid), at an observation point closer to the bridge (dotted), and at an observation point further from the bridge (dashed). The sticking and slipping phases are highlighted in red and green respectively. (Middle) The displacement of the string at the bow contact point and two observation points. (Bottom) The transverse force at the bridge due to the tension of the vibrating string.

Measurement techniques. To observe the string motion, we can use an electromagnetic pickup (Schelleng, 1973) to measure the velocity of a string segment. We initially considered electromagnetic pickups since they are extremely common in electric guitars, and since Schelleng was able to do useful research with them. We can use an optical fork (Le Carrou et al., 2014) to measure the displacement of a string segment. The optical forks require some support for mounting them on the cello, may have issues with ambient lighting, and will prevent the player from bowing near the bridge. We can use piezoelectric elements (Zhang, 2015) to measure the force at the bridge. We chose to mount piezoelectric elements in the bridge because they give us information about the interactions at the interface between the two major components of a cello model: the string and body.

Real string motions. When observing real bowed string motions, we will see various departures from the ideal waveforms shown in Figure 2.12. We almost always observe small ripples during the sticking phase. These are caused by secondary corners being generated as the principal Helmholtz corner is partially reflected each time it encounters the bow. The stiffness of the string prevents a perfectly sharp Helmholtz corner and causes dispersion. Bridge mobility and damping at the finger affect the waves traveling on the string. It is possible to observe coupling between the two polarizations of transverse vibrations as well as torsional modes. And most evidently, we will see transient effects as the contact point, bow force, and bow speed change.

2.4 Schelleng's diagram

The diagram. Schelleng's diagram (Figure 2.13) indicates the kinds of sustained string motions associated with different regions of the steady-state control parameter space. Usually the diagram is presented with bow force on the vertical axis and distance from the bridge on the horizontal axis, both in logarithmic scales, assuming a fixed bow speed and a fixed vibration frequency. Of particular interest is the region associated with Helmholtz motion and its theoretical boundaries: the upper and lower bow force limits.

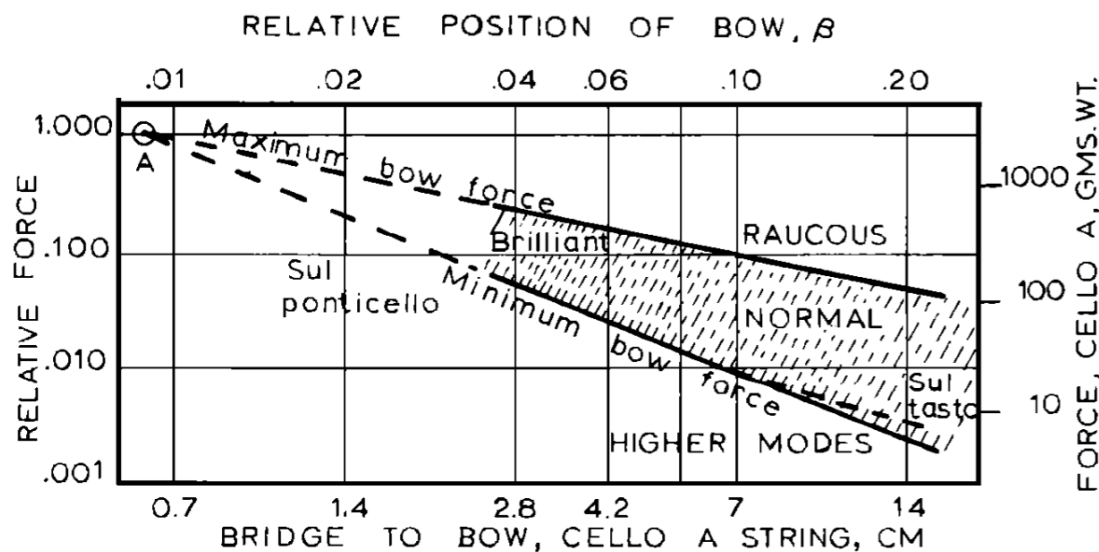


FIGURE 2.13: A typical Schelleng diagram for a cello A string bowed at 20 cm/sec. Helmholtz motion may be sustained in the region between the maximum and minimum bow force limits. The string motion may vary slightly within the Helmholtz region to produce different timbres. Gestures outside of these limits constitute special techniques, and produce aperiodic motions (raucous sound) or multiple slips (higher modes). The figure is taken from Schelleng, 1973.

Upper limit. The upper bow force limit is represented by a line with a slope of -1 on Schelleng's diagram due to an inverse linear dependence on the distance between the bridge and the bow. The vertical position of this line depends on the bow speed, the mass, tension, and length of the string, as well as the kind of rosin used, its temperature, and its distribution on the string and hair. Schelleng (1973) proposes a stick-slip friction interaction between the string and hair with a constant friction force during the slipping phase, leading to the equation for the upper bow force limit:

$$F_{max} = \frac{2Z_0 v_{bow}}{\beta(\mu_s - \mu_d)} \quad (2.1)$$

where v_{bow} is the bow speed, β is the distance between the bridge and the bow as a fraction of the string length, Z_0 is the string admittance, and μ_s and μ_d are the static and dynamic coefficients of friction between the string and the hair. While different models of sliding friction may produce slightly different dependencies on bow speed, experimental measurements (Schoonderwaldt, Guettler, and Askenfelt, 2008) are generally well described using the simple model shown here.

Our interest. Musicians sometimes make comments indicating that the instrument doesn't support playing with excessive bow force, that the musician cannot "dig in," as evidenced by a short raucous sound ("crack") associated with exceeding the upper limit. These comments may suggest that the upper limit may depend on something which is not predicted by the current models. Since our cellos have the same make and model of strings with approximately the same amount of use, and since the musician uses the same bow and rosin, we can reasonably assume that the two cellos will have the same upper bow force limit function. Thus, we don't expect the musician to feel a difference in the upper bow force limit between the cellos, but we will listen for

comments which indicate perception of the upper bow force limit to see if it plays a role in the cello evaluation. Our interest in the upper bow force limit is whether, how often, and under what circumstances the musician exceeds the upper bow force limit.

Lower limit. The theoretical lower bow force limit is a line with a slope of -2 on Schelleng's diagram due to an inverse square dependence on the distance between the bridge and the bow as observed by Raman (1918) using a mechanical bowing machine. In addition to the factors which affect the upper bow force limit, the lower bow force limit also depends on the bridge mobility. Schelleng (1973) modeled the bridge as a dashpot resistance which predicts a lower bow force limit, showing that the bridge mobility is a key ingredient of the model leading to predictions of a lower bow force limit. Woodhouse (1993) models the bridge as a system of damped harmonic oscillators and implements the model in terms of frequency dependent reflection functions. Mansour, Woodhouse, and Scavone (2017) modified the condition leading to the minimum bow force—he uses a perfect stick-slip at the bow rather than a perfect sawtooth at the bridge—to give the latest expression for the lower bow force limit as

$$F_{min} = \frac{2v_{bow}Z_0^2}{\pi^2\beta^2(\mu_s - \mu_d)} \left(\max_t \left\{ \Re \sum_{n=1}^{\infty} \frac{(-1)^{n+1}}{n^2} \zeta(n\omega_0) Y(n\omega_0) e^{in\omega_0 t} \right\} + \Re \sum_{n=1}^{\infty} \frac{\zeta(n\omega_0) Y(n\omega_0)}{n^2} \right) \quad (2.2)$$

where

$$\zeta = \frac{\sin(k\beta L)}{\sin(k\beta L) - iZ_0 Y \cos(k\beta L)},$$

$$k = \frac{\omega}{c}, \quad \text{and} \quad \omega = 2\pi f.$$

where k is the wavenumber, c is the wavespeed, ω is the wave frequency, ω_0 is the wave frequency of the fundamental, Y is the bridge mobility, and \Re indicates taking the real part of the complex number.

Our interest. Since the mobility is frequency-dependent, the lower limit differs between notes. And since the mobility of each cello has its own frequency-dependence, the lower limit differs between cellos. It has already been shown (Zhang, 2015) that excessively high lower limits are associated with problematic notes ("wolf notes") on the cello and that the musician can perceive changes in the lower limit for these notes. On the other hand, cellists may not mention a wolf note if it exists and may even accept a cello with a prominent wolf note, so its importance in the evaluation of cellos is up for debate. We are interested in whether, how often, and under what circumstances the musician drops below the lower bow force limit, whether the musician perceives differences in this limit and how these perceived differences affect her evaluation of the instrument.

Limit intersection. The upper bow force limit as a function of distance from the bridge has a slope of -1 on logarithmic axes, while the lower bow force limit has a slope of -2 . The two limits must intersect at some point near the bridge (Figure 2.14). It is not possible to sustain Helmholtz motion while playing closer to the bridge than this intersection point. If we compare two cellos which have different lower bow force limits, we may find that we can play a certain note quite close to the bridge on one cello,

but that we are obliged to play further from the bridge on the other.² We are interested in whether, how often, and under what circumstances the musician plays near the intersection point, and whether the musician perceives differences in its position.

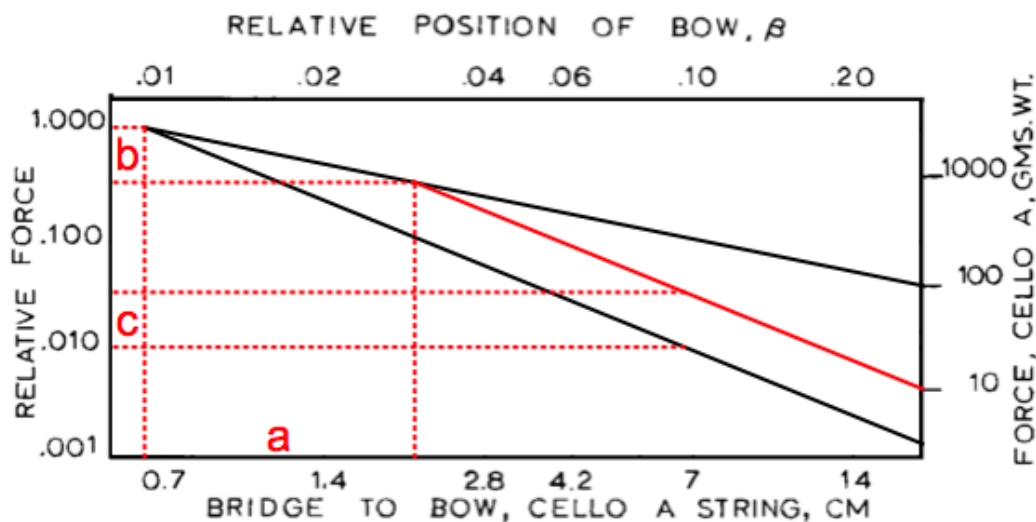


FIGURE 2.14: Comparison of Schelleng diagrams of two hypothetical cellos. A larger bridge mobility raises the lower bow force limit, moving its intersection with the upper force limit further from the bridge. (a) A portion of the string is no longer available to be played on. (b) The maximum force is reduced. (c) The range of forces available at any given point is reduced.

Range of forces. Raising the lower bow force limit has two effects on the range of forces permitting Helmholtz motion. The first effect is to move the intersection point further from the bridge, reducing the maximum force at the intersection point. The second effect is to move the lower limit up at every position along the string, reducing the range of forces available from the fixed upper limit to the greater lower limit. We are interested in whether the musician perceives differences in the range of forces available.

2.5 Guettler diagram

A Guettler diagram such as Figure 2.15 indicates the time required to achieve a sustained string motion from an initial transient. The evolution of the control parameters over time are defined by functions which include two parameters. Varying the two parameters generates a plane with each point corresponding to a slightly different gesture. At each point, the corresponding gesture is applied to the string and the time to achieve a periodic motion is measured. The point is then colored according to the observed duration.

Guettler (2002) studied different classes of attacks, from which the diagram gets its name. Galluzzo (2004) used different friction models in computer simulations and compared with experimental results produced with a robot and a perspex bow. It is

²This is a hypothesis which follows logically from the diagram; not an affirmation based on experience.

reassuring that the physical experiments with the robot were in agreement with the simulations.

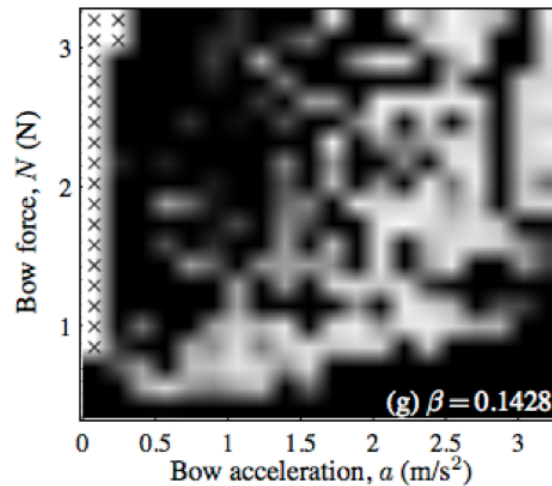


FIGURE 2.15: Guettler diagram for a certain family of initial transient gestures. The string is initially at rest. A perspex rod (the bow) applies a constant force to the string and uniformly accelerates from rest. Shades of gray indicate the number of period durations before Helmholtz motion was achieved. White pixels indicate Helmholtz motion was achieved immediately, black pixels required at least twenty period durations to achieve Helmholtz motion. The pixels marked with \times indicate failed measurements. The figure is taken from Galluzzo, 2004.

Observations. In Figure 2.15, we can see that certain combinations of force and acceleration are guaranteed to give long initial transients, as shown by large regions of black pixels in the upper left and lower right. What may be surprising is that the region in the middle is speckled with black pixels found among white pixels rather than having smoothly varying shades of gray. Furthermore, the details of these speckles change each time the experiment is repeated. Apparently the exact results of this experiment are sensitive to unintended variations in the initial conditions and gesture parameters. Since the friction forces between bow hair and the string are non-linear, these kinds of chaotic results are to be expected.

If we interpret each pixel of the Guettler diagram as a single measurement of a stochastic process, then we can imagine that the black pixels next to white pixels are not truly black. Demoucron (2015) performed a series of simulations, varying the deceleration before and the acceleration after a bow change. Each run of the simulation started the bow change at a different phase of string oscillation, and the results were averaged over the phases. The result is given in Figure 2.16 in which the color of the pixel indicates the probability of achieving an acceptable attack. This diagram smooths over the speckled nature of the usual Guettler diagram, but it does not change the fact that the outcome of any given bow change could be perfect or terrible depending on initial conditions or uncontrollable tiny differences in the control parameters used to execute the bow change.

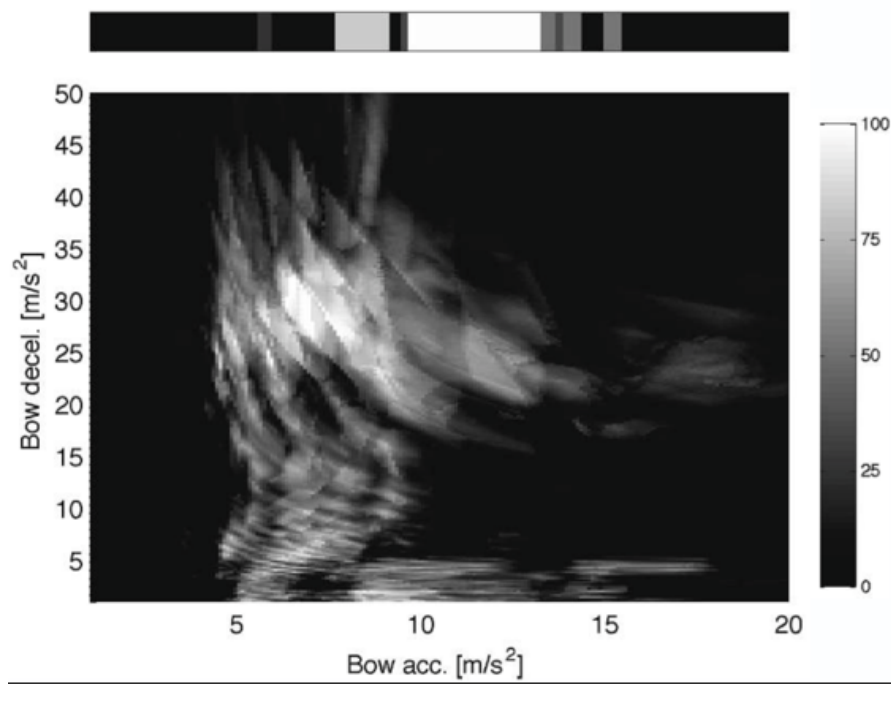


FIGURE 2.16: The probability of achieving Helmholtz motion on a violin within 7 periods or less, from Demoucron, 2015. White pixels have very high probabilities; black pixels, very low. The top panel shows the number (black, 6 or more; white, 0) of periods elapsed before regular triggering for simple attacks from rest.

Problem. This diagram and the way it varies upon repeating the experiment indicate that gestures must be very precisely controlled if you wish to reliably have very short transients. Since these results were produced by a robot with better repeatability than a musician, we must conclude that it is nearly impossible for a musician to reliably produce very short transients. And yet that is not our impression of professional performances.

Hypotheses. We propose two hypotheses for explaining the discrepancy between the implications of the experiment and our impressions of real performances. First, the experiment may be flawed. Musicians probably don't hold the force constant or use constant accelerations. On the other hand, the durations of transients are short, which doesn't give much time for significant departures from these approximations. In any case, the friction interactions between the bow and the string describe a non-linear dynamical system which implies that we shouldn't be surprised to see such chaotic behavior, whatever the true control parameters might be. Second, our impressions may be flawed. When we listen to music, we usually aren't measuring the duration of every attack, though we might notice a particularly long attack duration which doesn't fit the musical context. It may be that the sound of a certain long attack is not disagreeable. Guettler and Askenfelt (1997) found that raucous transients shorter than 50 ms are acceptable, but that multiple slip-type transients as long as 90 ms are acceptable.

Our experiment will not provide the kind of systematic variation of control parameters necessary to produce a Guettler diagram. But we will be able to look at the control parameters that are actually used by the musician. This will allow us to judge whether the control parameters assumed in the previous studies are sufficiently close to reality. It will also help us understand to what extent the musician actively controls the

sound of the cello during an attack. We will also want to look at the distribution of attack transient durations during performances to see whether cellists outperform robots and simulations, and to see how Guettler's results on violin transients translate to cello transients.

2.6 Playability of bowed string instruments

Zhang and Woodhouse (2014a) study the perception of wolf notes and relates the perception to bridge mobility. They placed an adjustable mass on the bridge to make controlled changes to the bridge mobility. Players then stated to what degree the wolf note is worse or better, or gave a rating of the severity of the wolf note. They found a clear relationship between the perceived severity of the wolf-note and the amplitude of the bridge mobility at the frequency of the wolf-note. Among the participants in this experiment were musicians and instrument makers. They found that the experienced musicians were more likely than the makers to be distracted by other perceived properties which were apparently more relevant to them at the time.

2.7 Mental maps between music descriptors and control parameters

Context If we look at the fingerboard of a cello, the most striking feature is the absence of visual cues indicating the precise positions where the cellist must place her fingers to play notes in tune. Furthermore, cellists play while looking at sheet music, the conductor, the audience, or even with their eyes closed. Clearly they do not rely on visual cues to play their instruments. While listening to professional musicians, we don't notice out of tune notes or obvious corrections. It seems like cellists can accurately place their fingers at the precise position required for each note. This is most striking when the cellist moves her entire hand (shifts) to reach the next note. Not only must the musician have an excellent mental model of the positions of notes along the string, but they must have some way of accurately measuring the distances traveled by their fingers while playing. This suggests that they have an ability to play based on proprioceptive or tactile cues.

Pitch accuracy hypothesis Chen et al., 2008 presents a series of experiments to test this hypothesis. They had cellists play alternating notes requiring a shift between them under different conditions. They observed the amount of trial-to-trial and within-trial variation of the fundamental frequency of each note. The first observation was that the difference between the nominal frequency of a note and the mean frequency of repetitions of the note within a trial was often statistically and perceptibly different. This deviation between the preferred frequency and the nominal frequency changed over time from one trial to the other. This indicates that cellists do not have a fixed mental model of pitch. This suggests to me that our impressions of cellists' playing accuracy may be based more on belief than fact.

Role of feedback hypothesis When the musicians did not bow the cello, but plucked it instead, they did not receive continuous aural feedback during the movement. In this case the mean frequency was further displaced from the nominal value and the within-trial variability was greater. The paper (Chen et al., 2008) mentions that for one player the distance along the string between the two notes increased by nearly 6 cm from the beginning of the trial to the end as the low note drifted increasingly flat and the high

note drifted increasingly sharp with each repetition. Proprioceptive and tactile cues are clearly insufficient for measuring distances traveled by the fingers. This suggests to me that proprioceptive, tactile, and visual cues may help the cellist estimate the position of notes, but that each of these models must be continuously updated using aural feedback. While Chen et al., 2008 works with the map between left-hand finger positions and pitch, I suspect that the hypothesis applies equally to the map between right-hand control parameters and timbre and volume.

Other maps Pitch, tempo, and volume stand out among other music descriptors because they are indicated in the music notation, they have widely accepted definitions in terms of physical quantities, and reproducible references can be used to train ourselves to maintain fixed mental models. Tempo and volume are often indicated vaguely: fast, slow, loud, quiet. I know of no attempts to train playing at precise volume levels. Most rhythmic training focuses on rhythms rather than tempo, with certain tempos being trained as a side effect of practicing rhythms at those tempos. Pitch on the other hand is indicated absolutely (within the interpreted intonation scheme) and many exercises aim at developing the ability to name the note associated with a frequency (absolute pitch) and the interval between notes (relative pitch). Yet Chen et al., 2008 indicates that not even in this case do musicians maintain fixed mental models. We should be careful when interpreting comments on even more obscure music descriptors (i.e. timbre) if we suspect that a mental model has had time to change.

2.8 Measuring control parameters

The first calibrated measurements of the control parameters of bowed string instruments were performed by Askenfelt (1983; 1986; 1988). Before that time, studies of the control parameters involved imposing known control parameters to the instrument via various mechanical bowing machines (Raman 1918; 1920). Much of the work in sensing control parameters has been done by the music community in attempts to either use the familiar bowing gestures with new instruments (Trueman and Cook, 2000) or to augment the instrument with electronic or digital effects (Overholt, 2011). Early reviews of the available technologies were given by MIT's Media Lab (Machover, 1992; Paradiso and Gershenfeld, 1997; Paradiso, 1997). The last twenty years have shown improvements in the implementations of those technologies as well as the introduction of two- and three-axis accelerometers, gyroscopes, and inertial measurement units (Young, 2007), 6-DOF electromagnetic pulse sensors (Goudeseune, 2001; Gaus et al., 2007), and infrared video motion capture (Schoonderwaldt and Demoucron, 2009). In addition to sensing technologies, wireless communication technology on small integrated circuits has reduced the need for cables for gathering sensor data (Young, 2002; "The Augmented Violin Project" 2002). While musicians require indicators of control parameters to be playable (i.e. responsive to gesture adaptations), they don't necessarily need them to be calibrated measurements. In this section we review some of the technologies that have been used to indicate control parameters and discuss the possibility of using them for calibrated measurements of control parameters.

2.8.1 Bow kinematics

Wheatstone bridges. The first calibrated measurements of bow position and speed during performance were made by Askenfelt (1983; 1986; 1988). The bow position is measured by laying a thin metal wire among the hairs of the bow forming one leg of

a Wheatstone bridge fed by a DC-supply. This bow hair wire is divided by the metal violin string. At the same time, the metal string forms one leg of a second Wheatstone bridge fed by an AC-supply and is divided by the bow hair wire. The output signal of each Wheatstone bridge indicates the ratio of its divided wire lengths. By multiplying the total length of the wire or string by its division ratio, we recover the frog-to-string distance or bridge-to-hair distance respectively. While Askenfelt's implementation tethered the bow and violin with power supply and data cables, a current implementation could power, sense, and wirelessly transmit the data using batteries and integrated circuits mounted to the bow or wrist strap. Ultimately we did not choose this technique because the build-up of rosin on the strings leads to intermittent electrical contact and noisy signals.

RF field sensing. As part of the Hypercello project, the MIT Media Lab (Machover, 1992; Paradiso and Gershenfeld, 1997; Paradiso, 1997) tracked indicators of the frog-to-string and bridge-to-hair distances by sensing changes in the capacitance between the bow and the bridge (Gershenfeld, 1993). A resistive material served as a receiving antenna embedded in the bow stick which was driven by a radio frequency (RF) transmitting antenna mounted behind the bridge of a cello. The capacitive coupling varied with bridge-to-hair distance while the real impedance varied with frog-to-string distance. Later Young (2002) developed the technology further as the Hyperbow for use with the violin, switching the roles of the two antennas, and replacing the power cable for the driving antenna by a battery mounted to the bow. This allowed the bow to be free of tethers to the computer.

McMillen (2008) incorporated the capacitive sensing technology into the K-Bow which was commercially available for a short time. In this implementation, the bridge antenna was relocated to a circuit board underneath the fingerboard and two loop antennas in the bow stick replaced the resistive strip. As the bow is tilted, the capacitive coupling with one loop antenna increases while the coupling with other decreases. Thus the configuration gives an indication of the tilt angle.

While the implementations discussed only measured one or two dimensions of position, three-dimensional position sensing is possible with more antennas (Paradiso and Gershenfeld, 1997; Smith, 1995; Smith, 1996). The system as implemented by Paradiso and Gershenfeld (1997) is reported to respond linearly to changes in position parallel to the front plate of the instrument and to be insensitive to rotations. The signals from these electric field sensors can be calibrated to measure positions with a reported resolution of 1 mm displacement over the bow length (Paradiso and Gershenfeld, 1997), though care must be taken to avoid electromagnetic interference coming from lighting and other electronics in the environment. However, "The Augmented Violin Project" reports that IRCAM's implementation of the system (the Augmented Violin) yielded inaccurate measurements because the bow presents a reduced surface area to the antenna when played near the tip or frog, because the capacitance is modified by the presence of the performers hand, and because the coupling between the antennas varies with large bow angles. concludes that the distance measurement was only useful for qualitative measurement, but problematic for accurate position measurement.

IR field sensing. McMillen (2008) removed the resistive strip which enabled the frog-to-string distance measurement from the K-Bow in favor of a second loop antenna, which means the RF system could only indicate the bridge-to-hair distance. An infrared light emitting diode located at the end of the fingerboard created a conical field of infrared light which was sensed by a detector in the bow frog. The brightness of the light received by the sensor varied with distance from the emitter so that this signal

indicated the frog-to-string distance. This indicated frog-to-string distance is sensitive to stray reflections and may be affected by other sources of infrared light.

Pérez Carrillo, 2006 uses an infrared range finder to measure the distance from the bridge to the bow. The sensor emits a pulsed infrared beam which reflects off of the target and enters the sensor lens. The location on a CCD array indicates the angle that the light entered the sensor which implies a certain isosceles triangle. The base of the triangle is the distance between the beam emitter and the sensor lens. The height of the triangle is the distance to the target. This system has a few problems: (1) the beam may not hit the bow due to the narrowness of the beam and the narrowness of the bow, (2) the skewed bow may indicate an inaccurate distance because the beam reflects off a portion of the bow which is not directly over the string, and (3) the signal measures the distance to the stick, not the point of contact between the hair and string, so bow tilt leads to inaccurate measurements.

Inertial measurements. Accelerometers, gyroscopes, and magnetometers, are commonplace components of consumer devices used for detecting movement, rotations, and orientation using a variety of microelectromechanical systems (MEMS) techniques. They are often bundled together as Inertial Measurement Units which are smaller and have less alignment error than building the equivalent sensor from separate products.

Accelerometers are generally some variation of a mass connected by a damped spring to a base and enclosing structure. When the system is accelerated, the inertia of the mass will cause the spring to deflect, bringing the mass closer to one of the walls of the enclosure, changing the capacitance between the mass and the wall, or compressing a piezoelectric element between the mass and the wall. Thus an accelerometer can only indicate the acceleration of its enclosure, not its velocity or position. If we know the initial position and velocity, then we can integrate the acceleration from a 3-axis accelerometer to find the current position and velocity of the accelerometer. The gravitational field also acts on the mass causing the spring to deflect in the direction of gravity, so that the accelerometer signal is a sum of the gravitational field and the acceleration of the object. To separate the effect of gravity from the acceleration of the object, it is necessary to measure the orientation of the accelerometer.

Gyroscopes are generally some variation of a pair of masses which oscillate with opposing motion within a plane within a casing. When the system is rotated, the inertia of the masses (i.e. the Coriolis effect) will cause one mass to rise above the plane, changing the capacitance between it and the casing ceiling. The other mass will dip below the plane, changing the capacitance between it and the casing floor. The deflection amount depends on the velocity of the masses, the rate of rotation of the casing, and the angle between the plane of rotation and the plane of oscillation. Accelerations which do not include rotation cause both masses to deflect to the same side of the plane, yielding no net signal. Thus a gyroscope can only indicate the angular velocity (rate and plane of rotation) of its casing. If we know the initial orientation, we can integrate the angular velocity (being careful to take into account that rotations do not commute), to find the final orientation. Depending on the specifications of the gyroscope, large accelerations (such as what may be seen in violin bow changes) might cause one of the masses to reach its maximum allowed displacement from the plane, thus leading to errors which accumulate (Bancroft and Lachapelle, 2012).

Magnetometers are generally some variation of an electric current passing through a wire and a means of measuring its deflection or resonant frequency. When the electric current is placed in a magnetic field, the electrons are deflected to one side or the other due to the Lorentz force, leading to a deflection of the wire itself and a change in the resonant frequency of its mechanical vibrations. These sensors are used to establish

an absolute orientation with respect to the earth's magnetic field, but may be influenced by the magnetic fields of nearby equipment. These sensors are also sensitive to temperature variations as the Young's modulus of the wire changes with temperature.

In theory the signals from an Inertial Measurement Unit may be integrated to perform dead reckoning of the position and orientation of the unit. The use of a magnetometer and a gyroscope gives two signals for estimating the orientation of the unit. The magnetometer could be used to keep the drift from the gyroscope in check, while the gyroscope could be used to help identify and correct for temperature effects in the magnetometer. With the orientation known, the gravitational field can be subtracted from the acceleration, and the acceleration can be integrated to find velocity and position. However numerical integration leads to drift. The error in the orientation and velocity estimate will increase linearly with time (due to one integration procedure), while the position estimate will increase quadratically (due to a second integration). There will be additional errors in the velocity and position estimates due to propagation of the error from the orientation estimate. Because of these errors, the system must be returned to a known configuration to reset the system, or an independent measurement system is needed to keep drift errors bounded.

Schoonderwaldt, Rasamimanana, and Bevilacqua (2006) combined accelerometer signals with a simple video with a 25 Hz frame rate using a Sony Digital Handycam (DCR-TRV245E). The video is used to identify the moment when the bow speed is zero during bow changes. The accelerometer signal is integrated between bow changes and reset each time the video indicates zero bow speed. The reconstructed motion of the bow is validated against measurements from a camera based motion capture system (Vicon) with a frame rate of 150 Hz. Since orientation data is not available from the Handycam video, the accelerometer signals are not corrected for orientation, leading to errors in addition to the drift from numerical integration. The effects of latency and jitter from the Handycam were simulated, indicating that measurements of short rapid bow changes (*spiccato*) are most affected, particularly by latency. They conclude that the system may be useful in cases in which the expensive Vicon system is not available.

Trueman and Cook (2000) used a dual axis accelerometer mounted at the frog to gather signals related to inclination and tilt and acceleration. In this case, these signals became the *de facto* control parameters because the bow was used as a controller for an electronic instrument. Rasamimanana (2004) used a dual axis and a single axis accelerometer to gather the same signals, but for the purposes of distinguishing and identifying bowing gestures on a violin. Young (2007) used 3-axis accelerometers and 3-axis gyroscopes (ie. 6DOF IMU) on both the bow and the violin. The aim was to estimate the relative position, orientation, and motion of the bow with respect to the violin. Young describes a procedure for calibrating the IMUs through a sequence of static measurements in different orientations. The drift errors are kept in check through the use of a Kalman filter and the independent position data from the capacitive measurement of position, which was calibrated by comparison with a camera based motion capture system. Schoonderwaldt and Demoucron (2009) use a 3-axis accelerometer to complement a camera based motion capture system for gathering acceleration data.

While acceleration data is of some use in describing the bow kinematics of a gesture, it is not actually one of the direct control parameters. Integrating acceleration data to get the bow speed and bridge-to-bow distance control parameters requires an independent means of measuring them in order to minimize the drift errors. Field sensing technologies add weight to the bow and have unreliable performance as calibrated measurements of bow position, though the signals they provide are playable.

A dedicated motion capture system seems to be required to get true measurements (as opposed to indicators) from the inertial measurement sensors.

Motion capture. There are several methods of tracking rigid bodies in addition to the inertial measurements and capacitive sensing already discussed. In this section we will review those techniques which we considered using or had been used to track bow movements. Baillot, Davis, and Rolland (2001) give a survey of variations on these techniques and some others that we did not consider using.

Nichols (2002) uses a system of mechanical linkages and goniometers to measure the inclination angle and 3-D position of a rod relative to the chassis of his vBow virtual instrument controller. This kind of mechanical motion capture can give accurate and precise results. Sources of error include flexible linkage arms and inaccurate measurements of the distance between joint axes of rotation. Fitting the musician or instrument with an exoskeleton will certainly be invasive and it will be difficult to argue that the musician's performance is not affected.

Ultrasound emitters and receivers may be used to triangulate the position of the target based on time of flight. The system may be configured with the emitters located at stationary reference points and receivers attached to the targets, or vice-versa. An IR or RF signal is emitted to establish the initial time and to trigger a sound pulse from each of the emitters. The time of flight between when the pulse is emitted to when it is received, multiplied by the speed of sound, gives the distance between each pair of emitters and receivers. With as few as three references (emitters or receivers), the location of the target is fixed relative to the positions of the references. Machover (1992) considered this approach, but concluded that the system would be bulky and difficult to do without coupling some energy into the audible range. Medina, Segura, and Torre (2013) reports an accuracy barely below 10 mm, which is not sufficient for our purposes.

Maestre et al. (2007) use a system based on measuring the magnetic flux emitted from an antenna through three orthogonal sensing coils. The total flux indicates the distance from the field emitter and the ratios of the flux through each coil indicates the orientation of the sensor. The emitted fields induce eddy currents in nearby metal, which may be found in the walls, floor, or ceiling as well as objects in the room or the tracking target itself. These eddy currents cause distortions in the field which lead to inaccurate position and orientation measurements. The system may be implemented with DC pulses or AC pulses. The DC pulse systems take measurements just before the next pulse is emitted to allow the effects of induced eddy currents in the environment to decay, leading to potentially better accuracy. While the weight and size of the sensors themselves can be insignificant, the data collection wires connected to them are a distracting tether.

Schoonderwaldt and Demoucron (2009) uses a system based on images taken from several reference cameras. The images from these cameras, along with knowledge of the position and orientation of each camera, indicate the position of the target through multiscopy (i.e. stereoscopy or parallax) triangulation. The system works by recognizing and identifying features of the image. These features are usually graphic or physical boundaries, such as spots of paint, object corners, or reflective spheres attached to the object being studied. Image-based motion tracking comes in three variations: active markers, passive markers, and marker-less. Active markers broadcast their identities to the cameras, for example by flashing light with specific timings, which makes them easy to recognize and identify. Passive markers reflect light to the cameras, making them easy to recognize. The image processing software then uses rigid body models of the positions of these passive markers to identify each marker. Marker-less systems try

to find recognizable features of an image, such as lines, circles, and points of intersection. Then it tries to identify the correspondences between the features recognized in successive images. Active marker systems generally have larger and heavier markers than passive systems. Passive systems may have trouble when the studied object is not rigid. Marker-less systems are still under development. Currently marker-less systems are useful for animations, gaming, and gross locomotion studies, but they do not seem to have the accuracy required for our study.³ We give more details about the use of passive systems in Section 4.3.

2.8.2 Bow force

Strain gauges at ends of hair. In (Askenfelt 1983; 1986; 1988) the bow force is estimated by measuring the deflection of the bow hair at the frog and tip of the bow using strain gauges. The bow hair is attached to thin metal strips fixed at the frog and tip of the bow. A pair of strain gauges are glued to each strip and all are connected in a Wheatstone bridge. The deflection of the bow hair bends the metal strips and the output of the Wheatstone bridge gives an indication of the bow force. This signal is calibrated by pressing the bow hair against a calibrated scale. In the end, the signal had a poor signal-to-noise ratio and deviations from a desired linear relationship with the force.

Demoucron, Askenfelt, and Causse (2009) made improvements to Askenfelt's system by attaching the strain gauges to removable mounts, treating the strain gauges at the tip separately from those at the frog, and making a detailed analysis of how the position of contact of the string on the hair and the bow force affect the deflection of the hair at the strain gauges.

Guaus et al. (2007) made a variation in which thin plastic strips each with a single strain gauge were used instead of the metal strips with paired strain gauges. This results in some loss of sensitivity as well as the inability to cancel thermal effects in the leadwires. To approximately compensate for thermal effects, the system must be frequently calibrated. Guaus et al. (2009) describes the calibration method. In lieu of a force estimation model based on physical parameters, a Support Vector Regression model interpolates the calibration data.

Capacitor under index finger. The MIT Media Lab's HyperCello project (Machover, 1992) placed copper tape on the stick near the frog and covered it with a urethane foam. Changes in capacitance are measured as the index finger compresses the urethane, giving an indication of the force. This force may be manipulated independently of the force exerted on the string by simply squeezing the stick without applying additional net torque. While suitable as a controllable parameter in an interface with computers, it is not suitable for our project.

FSR under index finger. IRCAM's Augmented Violin project (Rasamimanana, 2004) used a force sensitive resistor on the stick near the frog to sense the force applied by the index finger. Machover had previously considered their use but concluded that the relation between conductivity and pressure is both noisy and hysteretic. Since the force of the finger on the stick can be manipulated independently of the force on the string, we reject this option as well.

Strain gauge on stick. Young (2001; 2002; 2003; 2007) permanently fixed strain gauges on the bow stick and connected them in a Wheatstone bridge configuration. Wires connect the terminals of the Wheatstone bridge to the power supply located at

³Reports of accuracy commonly quote 1° of uncertainty in the joint angles of human limbs. This corresponds to about 8 mm of uncertainty in the position of the far end of a 50 cm limb.

the frog. The relationship between the measured vertical and lateral strains of the stick and the force of the string on the hair depends on the frog-to-string distance in a way that is determined empirically by applying known forces at known locations along the hair. Placing the strain gauges accurately is difficult since the stick is round while the strain gauges are designed to be fixed to flat surfaces. Slight errors in the alignment of the strain gauges are evident and must be accounted for in the empirical model. The strain gauges are temperature sensitive due to the thermal expansion of the alloy within them, requiring occasional recalibration, though incorporating them in a full Wheatstone bridge configuration minimizes the problem.

FSR between stick and hair. Trueman and Cook (2000) placed force sensitive resistors with light, soft sponges between the stick and the hair. The FSRs are most sensitive at low forces, which is appropriate for this application as they are measuring the force required to compress the sponges, not the force applied to the string by the hair. The compression of the sponges is effectively a measurement of the displacement of the bow hair, and thus an indication of bow force. Trueman does not report any calibration procedures or measures of accuracy, but does report that the signal is responsive and playable.

Geometric method. Maestre et al. (2007) noticed that when the hair presses on the string, the line connecting the endpoints of the hair lies at some depth beneath the line connecting the endpoints of the string. The minimum distance between the two lines increases as the force applied increases. The relationship between this minimum distance and the bow force is not linear and depends on the position and orientation of the bow relative to the string. Marchini et al. (2011) uses geometric arguments to model the effects of bow tilt and stick deformation, including taking into account certain systematic calibration errors. Marchini concludes that remaining errors come from inadequate modeling of the stick deformation, neglecting string deformation, and possibly measurement errors from the electromagnetic field-based motion capture system (Polhemus). In an attempt to overcome these errors, Baez (2013) replaced the geometry-based model with a Support Vector Regression model and began using an infrared multiscopy system (Qualisys). Llimona (2014) continued this work, being more careful about identifying appropriate datasets for training, validation, and testing of the Support Vector Regression model to avoid over-fitting, and attempting to take into account the deformation of the string as a constant systematic error.

The studies discussed in the previous paragraph introduced a number of features that may be extracted from motion capture data to estimate the bow force. They include the frog-to-string distance, the minimum distance between the string and the central hair (Maestre et al., 2007), the minimum distances between the string and the left and right edges of the hair ribbon (Marchini et al., 2011), the rotation of the tip relative to the frog Baez (2013), and the tilt angle. The displacement of the central hair is not independent from those of the left and right edge hairs. The relative displacements of the left and right edge hairs are not independent of the tilt angle. The rotation of the tip relative to the frog is not independent of any of the displacements as they are all functions of the force. Information-based models (such as Support Vector Regression) will arbitrarily distribute the influence of a physical effect among the coefficients of correlated features. This means that each time the calibration is performed, the relative influence of each feature may change drastically. This makes it difficult to identify which features are the most important and to assign physical meaning to the values of the coefficients.

Optical reflectance. To measure the bow force, Pardue and McPherson (2013; 2015) used near-field optical reflectance sensors consisting of an IR emitting LED and an IR

sensitive phototransistor in close proximity to each other. These sensors were placed at four points between the stick and the hair. The light emitted by the LED reflects off the hair and is sensed by the phototransistor according to the distance and reflection angle of the portion of the hair ribbon illuminated by the LED. These local measurements of stick-to-hair distance are enough to estimate the shape of the triangle formed by the deformed hair ribbon and the line connecting the endpoints of the hair ribbon, and thus indicates the position and magnitude of the force between the hair and the string. The relationship between the sensor signals and the force depends on the hair tension and the deformation properties of the bow stick which should be modeled empirically. The empirical model should be capable of taking into account the non-linear operational characteristics of the sensor. Since the sensor response is not monotonic with distance, there is a concern that large deformations may be aliased as small deformations. To reduce the risk of this happening, care must be taken when choosing the positions of the sensors; they should be placed neither too close to the middle of the bow where there is little clearance, nor too close to the ends of the hair where there is little change in stick-to-hair distance. As the sensors function by measuring the amount of infrared light received, the ambient lighting conditions may need to be controlled.

Optical fiber. In (Sarlo, Ehrlich, and Tarazaga, 2016), an optical fiber is bonded to the stick or strung among the bow hairs between supports at the frog and tip. The optical fiber is attached to an ODiSI measurement system (*ODiSI*) which interprets the Rayleigh backscattering of light resulting from strains distributed along the optical fiber. While the system provides strain information along the entire length of the bow, the useful information can be obtained from the strain measurement of just one point. The response is roughly linear in the magnitude and in the distance from the frog of the applied force. A separate means of measuring the frog-to-string distance is necessary for interpreting the force from the strain measurements. The system is sensitive enough to be detect the deformation of the bow under its own weight as the inclination angle changes.

2.8.3 String length

The string length is the control parameter used to control the fundamental frequency of the string vibrations. It is also useful for estimating the compliance of the string, determining the displacement of the string under the applied force of the bow. The string length can be determined from the fundamental frequency of the string vibrations, or it can be determined directly by detecting where the string is stopped against the fingerboard.

There are many algorithms for estimating the fundamental frequency of the string vibrations. These include spectral methods, temporal methods, and combinations. A review of methods is given by (Cheveigné and Kawahara, 2001). Two notable pitch tracking algorithms are given in (De Cheveigné and Kawahara, 2002) and (Monti and Sandler, 2002). Pitch tracking algorithms generally divide the signal into analysis windows, with longer windows being required to detect longer frequencies. Longer windows also give more precision in the estimated pitch at the expense of temporal resolution. Algorithms which only try to detect the fundamental pitch occasionally run into octave errors when the octave harmonic has a significant amount of energy compared to the fundamental. Algorithms which assume a harmonic spectrum can sometimes identify a missing fundamental based on the energy distribution in its harmonics. Pitch tracking algorithms generally have problems with polyphonic signals, which happens when two strings are played at the same time.

To detect the position where the string is stopped against the fingerboard in a rough sense, one could place frets (like on a guitar) on the fingerboard as in (Paradiso and Gershenfeld, 1997) or (Kapur et al., 2004). The frets are a resistive material connected in series. When the string touches a fret, making electrical contact, the resistance is divided and the note is identified. Freed (2009) reviews the use of force sensitive resistors to identify the position, including an example of a stringless cello. Grosshauser, Feese, and Tröster (2013) presents a capacitive sensor placed between the strings for detecting the position of the finger.

Pardue, Harte, and McPherson (2015) applies a resistive strip (a single thin layer of velostat; carbon-infused polymer) to the fingerboard. When the metallic cello string contacts the strip, it forms a voltage divider. Comparing the voltage with the string stopped to the voltage with the string open gives an estimate of the stopped length which gives an estimate of the pitch. The position accuracy of this system is reported to be around 6 mm, partially due to noise introduced by the hand. The estimated pitch is then refined using a pitch tracking algorithm on an audio signal. This strategy reduces the latency in real-time systems because (1) shorter analysis windows for finding the frequency of a harmonic may be used rather than the longer analysis window necessary for finding the fundamental frequency, and (2) the range of frequencies that must be checked against is reduced to only those around the expected pitch.

2.8.4 Other measurements

Other measurements are occasionally collected for analyzing the musician's gestures or as control parameters for an instrument connected to a computer. Paradiso and Gershenfeld (1997) measure the wrist flexion/extension angle of the cellist as a controller using a special wrist brace equipped with magnets and Hall-effects. Donnarumma, Caramiaux, Tanaka, et al. (2013) measure muscular activity via electromyogram (EMG) and mechanomyogram (MMG) signals for use as controllers in a musical context. Hsu et al. (2014) placed EMG sensors on eight muscles of the chest, shoulder, and arm to investigate how a violinist uses the muscles to execute bowing motions. Großhauser, Großekathöfer, and Hermann (2010) measures the clamping force of the left and right hands by placing force sensitive resistors under the chin rest and on the neck of the violin, and on the bow under the thumb, forefinger, two middle fingers, and small finger.

Chapter 3

Musician's control parameters

The control parameters describe those parts of the musician's gestures which vary dynamically while playing and are relevant to the friction interactions between the bow hair and the string. These include the effective length of the vibrating string (Section 3.1), the orientation, position, and speed of the bow relative to the cello (Section 3.2), and the normal force of the bow hair against the string (Section 3.3). Other factors which affect the hair-string interactions, such as the choice of rosin, hair tension, string properties such as material, construction, and diameter, and open string tension adjusted for tuning are made before the performance and are not part of the musician's gesture.

3.1 Effective string length

This section describes the string and how the fingers are used to pin it against the fingerboard to define the vibrating length and frequency. Section 3.1.1 describes a setup for measuring string properties and reports a table of measured cello string properties. Section 3.1.2 describes the geometry of the stopped string. Section 3.1.3 describes how the vibrating frequency measured during the musician's performance may be used to estimate the location where the string is stopped against the fingerboard and to estimate the accompanying small increase in string tension.

3.1.1 String model

Our cellos are equipped with medium tension strings. The two highest strings are Larsen Soloist, which have a solid steel core wound with rolled stainless steel flat wire. The two lowest strings are Thomastik Spirocore, which have a steel rope wound with tungsten. We assume the strings have the same behavior as solid strings as modeled by the constitutive equations for longitudinal and bending deformations:

$$T = K_L \epsilon \quad (3.1)$$

$$M = K_B \kappa \quad (3.2)$$

where T and M are the tension and bending torque applied to the string, ϵ is the dimensionless longitudinal strain, κ is the bending curvature with dimensions length^{-1} , and K_L and K_B are longitudinal and bending stiffness coefficients respectively. In the case of solid strings, we can relate the stiffness coefficients to the Young's modulus E and to the the cross-section's area A and second moment of area I assuming a uniform

circular cross section of diameter d .

$$K_{L,solid} = EA, \quad A_{disk} = \frac{1}{4}\pi d^2 \quad (3.3)$$

$$K_{B,solid} = EI, \quad I_{disk} = \frac{1}{64}\pi d^4 \quad (3.4)$$

Rather than trying to calculate these coefficients from material and geometric properties of the string, we use measured values for the coefficients since our strings are not solid.

To measure string properties, we used the device shown in Figure 3.1. The position of the bolts representing the nut and bridge were adjusted to match the distance between the nut and bridge of our cellos. The string was attached to the tuning mechanism and the load cell. The string passed over the nut and bridge with very little tension and nearly zero break angles. We marked the position of the nut and bridge on the string with a black pen to define the length of a segment without tension. Large increases in tension were applied to the string by moving the mass further from the pivot. The tuning mechanism was then used to approximately maintain the longitudinal position of the string and to make fine adjustments of the tension. After the string was initially brought to approximate playing tension, the string was left to set for about ten minutes. This should have given the strings enough time to fully stretch under the load provided the strings are sufficiently similar to the metallic core (Supersensitive and Jargar) violin strings reported in (Pickering, 1986). No time was given for the strings to stretch after the small incremental changes in tension as the effect of creep in this case should be well below our measurement precision (a few tenths of a millimeter). Using our thumbs to stop the string at the edges of the nut and bridge, we then pluck the string and use an electronic tuner to measure the frequency of vibration. The stretched distance between the marks on the string were recorded along with the frequency of vibration and tension of the string.

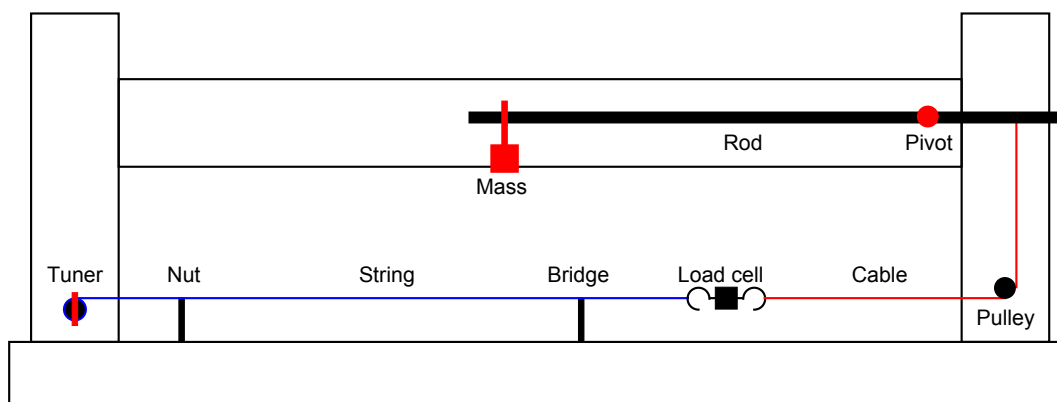


FIGURE 3.1: Aluminum extrusions were used to construct a frame. Two bolts serve as the nut and bridge. The cello string is attached to a tuning mechanism and a load cell. The load cell attaches to a steelyard and allows us to measure the tension in the string. By moving the relatively small mass further from the pivot point, the tension in the string can be increased. The tuning mechanism allows us to maintain the string in approximately the same longitudinal position and to make fine adjustments to the tension.

The longitudinal stiffness (Equation 3.1) was estimated from the data. Using the diameter of the string, an effective Young's modulus was calculated using Equation 3.3 and an upper limit for the bending stiffness was calculated assuming a solid string model (Equation 3.4). Since this upper limit was negligible in our application (see Section 3.1.3), we did not bother to measure the true bending stiffness. If we had found the contrary, we would have used an electromagnetic pickup or optical forks to record the free vibrations of the plucked string and analyzed the inharmonicity of its spectrum to estimate the effective bending stiffness.

Table 3.1 shows the results of our measurements. The tension measurements are within about 1% (5% for String II) of those collected from manufacturers at (Aitchison, 2016) after compensating for the difference in string length and converting from pounds-force to newtons. The stiffness coefficients may be comparable to the elasticity coefficients of violin strings reported by Pickering (1986). No references were found for comparing the string densities.

	L_{ref} [mm]	f_{ref} [Hz]	T_{ref} [N]	K_L [N]	μ_0 [10^{-6} kg/mm]
I (A_3)	690	220	174	23500	1.90
II (D_3)	690	147	135	17300	3.31
III (G_2)	690	98.0	133	7960	7.42
IV (C_2)	690	65.4	130	9550	16.1

TABLE 3.1: String properties measured using the device in Figure 3.1 as described in the text. The vibrating length of string was set to L_{ref} by adjusting the distance between the nut and bridge bolts. The vibration frequency of each string was set to its nominal frequency f_{ref} by adjusting the tension T_{ref} . The longitudinal stiffness K_L was estimated by fitting the data to Equation 3.6. The linear mass density was estimated by fitting the data to Equation 3.5 using Equation 3.7.

3.1.2 Finger model

Since we are only concerned with capturing control parameters, we reduce the finger to a constraint force at a point. The force is orthogonal to the open string, and follows the material point until it is pinned against the fingerboard at the stopping point (see Figure 3.2).

3.1.3 Stopped string length estimation

The deformation implies a slight stretching of the string accompanied by a corresponding decrease in the linear mass density according to the conservation of mass

$$\mu = \frac{\mu_0 L_0}{L} \quad (3.5)$$

where μ_0 and L_0 are the mass density and length of the string at zero tension.

The slight stretching of the string implies a slight increase in the tension T of the string according to the linear constitutive relation Equation 3.1, repeated here for convenience.

$$T = K_L \epsilon = K_L \frac{L - L_0}{L_0} \quad (3.6)$$

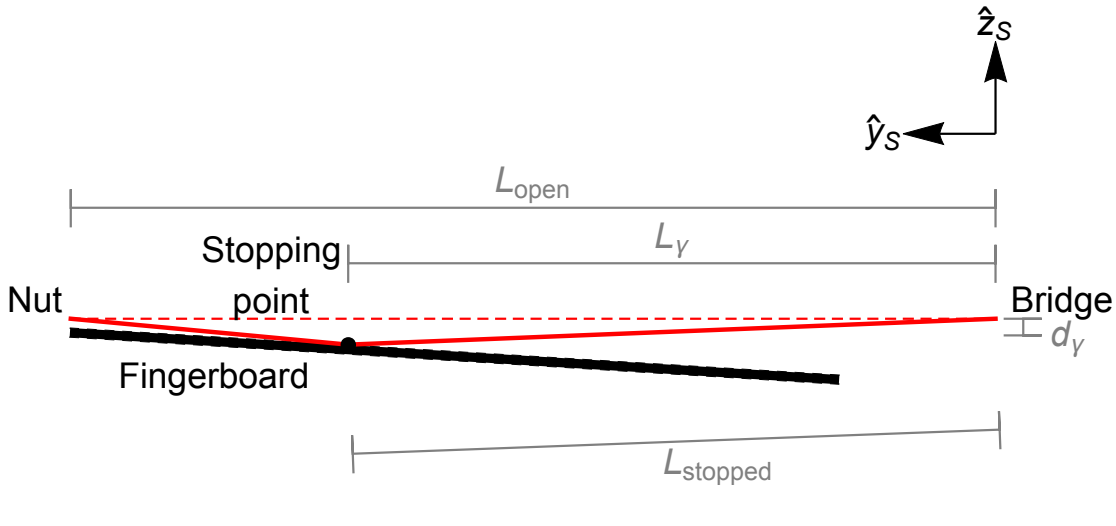


FIGURE 3.2: The string is called "open" when no fingers touch it. The length of the open string is the distance from the bridge to the nut. The string is called "stopped" when a finger has pinned the string against the fingerboard. The point of contact between the string and the fingerboard is called the "stopping point." The effective length of the stopped string is the distance from the bridge to the stopping point.

Using the length, tension, and linear mass density of the string, we can determine the fundamental frequency of its vibrations according to a stiff-string model. In practice, the term including the bending stiffness is on the order of 10^{-4} and can be ignored.

$$f = \frac{1}{2L} \sqrt{\frac{T}{\mu}} \left(1 - \frac{\pi^2 K_B}{L^2 T} \right)^{1/2} \approx \frac{1}{2L} \sqrt{\frac{T}{\mu}} \quad (3.7)$$

The major effect of stopping the string is to limit vibrations to a shorter portion of the string giving a higher fundamental frequency.

To calculate the effective string length, tension, and linear mass density of the stopped string, we compare four states of the string. We consider a segment of string with an unstretched length of L_0 and mass density μ_0 . That segment is stretched until it spans the distance between the bridge and nut, representing the open string. The segment is stretched even further until it reaches the tension of the stopped string. Finally, we isolate a portion of the segment representing the effective string length of the stopped string. The four states, their lengths, tensions, mass densities, and vibrating frequencies are summarized in Table 3.2.

state	length	tension	density	frequency
unstretched	L_0	0	μ_0	n/a
open	L_{open}	T_{open}	μ_{open}	f_{open}
tensioned	$L_{tensioned}$	$T_{stopped}$	$\mu_{stopped}$	$f_{tensioned}$
stopped	$L_{stopped}$	$T_{stopped}$	$\mu_{stopped}$	$f_{stopped}$

TABLE 3.2: Hypothetical string states are used to relate measurements and string properties for estimating the length of the stopped string.

Before mounting the string on the cello, we can measure its mass density μ_0 , and its longitudinal stiffness coefficient K_L (see Section 3.1.1). Once mounted, we can measure

the length L_{open} and frequency f_{open} of the open string. After stopping the string, we can measure its frequency $f_{stopped}$. All other variables in the table above may be calculated through appropriate applications of the conservation of mass (Equation 3.5), constitutive relation (Equation 3.6), and string frequency (Equation 3.7) equations.

Having calculated the effective length of the stopped string $L_{stopped}$, we can use the measured geometry of the fingerboard to estimate the stopping point. This is the point on the fingerboard which is located at a radial distance $L_{stopped}$ from the bridge. For now, we express this point as a pair of coordinates: the distance L_γ from the bridge along the axis of the undisplaced string \hat{y}_S and the transverse displacement d_γ toward the fingerboard along the vertical axis \hat{z}_S (see Figure 3.2). Once the position and orientation of the cello are known, the position of the string's bridge endpoint \vec{r}_{bridge} is known and the position of the stopping point \vec{r}_{stop} can be calculated by

$$\vec{r}_{stop} = \vec{r}_{bridge} + L_\gamma \hat{y}_S - d_\gamma \hat{z}_S. \quad (3.8)$$

3.1.4 Discussion of string modeling

While this section is supposed to be about calculating the effective length control parameter from the measured vibrating frequency of the string, it is actually more about making corrections to the position and orientation of the line segment which represents the bowed string (Equation 3.8), estimating the tension of the string, and collecting string properties needed for the bow force model described in 3.3.

The calculation took into account the change in mass density of the string and the longitudinal stiffness of the string without consideration of whether these complications were necessary. The difference in mass density between the reference measurements and the experimental condition are negligible since the string tension has not changed much. We can then estimate the tension of the open string during the experiment using the following simplified relationship which yields an error of less than 0.01%.

$$T_{exp} = \left(\frac{f_{exp}}{f_{ref}} \right)^2 T_{ref} \quad (3.9)$$

In fact if you simply assumed the open string tension was equal to the reference tension, ignoring differences due to a slightly different tuning, then you would only incur up to 0.6% error.

Stopping the string has three effects on the bow force model: it shortens the string, it rotates the bowed string line segment toward the fingerboard, and it increases the tension of the string. Ignoring the change in mass density for a string stopped at the octave harmonic results in 0.6% error in the estimated tension. This is significant to the musician. If the musician plays the harmonic, and then stops the string at that point, she will find the stopped string is slightly sharp compared to the harmonic. The musician must use a slightly longer effective string length for the note to remain in tune. On the other hand, the slight increase in tension and the slight difference in stopping point it implies are almost certainly negligible effects when estimating the bow force due to the motion capture measurement error.¹

¹So why did we go through all this effort? I developed these calculations early on during the thesis when I had no equipment, no measurements, and no idea about the size of the effects. Having already programmed the calculations into the pipeline I simply couldn't be bothered to change it.

3.2 Bow kinematics

This section defines the scalar bowing parameters (bow angles, bridge-to-hair distance, frog-to-string distance, and speed) in terms of the positions and orientations of rigid body frames which may be measured using a motion capture system. The definitions provided here are similar to those of Schoonderwaldt and Demoucron, 2009 and Maestre et al., 2007 adapted for the cello, but here we use a string-centric basis rather than an instrument-centric basis for defining the bowing angles. The definitions of the frog-to-string distance, bridge-to-hair distance, and total depth come from Maestre et al., 2007. Maestre describes the calculation through a minimization process and calculating Euclidean distances, though he doesn't offer an explicit implementation of the algorithm. In Section 3.2.2 I present explicit solutions for each of these distances based on skew projection which avoids using any minimization algorithms or Euclidean distance calculations.

3.2.1 Orientation of the bow

The orientation of the bow is described by three rotations which are meaningful to musicians (see Figure 3.3). We begin with the longitudinal axis of the bow hair running parallel to the top plate of the cello and orthogonal to the string with the hair lying flat against the string. First, we rotate the bow through the *inclination angle* about the longitudinal axis of the string so the bow is no longer parallel to the top plate of the cello. Second, we rotate the bow through the *skew angle* about the vertical axis of the bow, so the bow is no longer orthogonal to the string. Finally, we rotate the bow through the *tilt angle* about the longitudinal axis of the bow, so the hair no longer lies flat against the string.

From these reference frames, we can immediately identify the first rotation axis as \hat{y}_S and the last rotation axis as $-\hat{x}_H$. The second rotation axis is orthogonal to the other two, which we calculate as $\hat{z}_{HS} = \frac{\hat{x}_H \times \hat{y}_S}{\|\hat{x}_H \times \hat{y}_S\|}$. The rotation angles themselves are then calculated as follows, taking into account our sign conventions described in Figure 3.3.

$$\begin{aligned} \text{inclination} & \quad \theta_I = \frac{\pi}{2} - \arccos(\hat{x}_S \cdot \hat{z}_{HS}) \\ \text{skew} & \quad \theta_S = \frac{\pi}{2} - \arccos(\hat{x}_H \cdot \hat{y}_S) \\ \text{tilt} & \quad \theta_T = -\frac{\pi}{2} + \arccos(\hat{y}_H \cdot \hat{z}_{HS}) \end{aligned} \quad (3.10)$$

The expressions for the skew angle and tilt angle can be used for the cello, bass, viola, and violin. The inclination angle changes sign for the violin and viola because the bow frog is held on the treble side of the violin and viola, but the bass side of the cello and bass. Schoonderwaldt uses slightly different definitions, choosing to reference the violin body rather than the string. Simply replacing the violin reference frame with the string reference frame in his expressions gives my skew and tilt angle. His inclination angle remains slightly different from mine as he uses \hat{z}_S rather than \hat{z}_{HS} .

3.2.2 Position and speed of the bow

We define the hair line as the line which connects the endpoints of the middle of the hair ribbon at the frog and tip. Likewise, the string line connects the endpoints of the string at the nut and bridge. These two lines usually do not intersect, but we can always find the point on each line which is closest to the other line. Having identified the positions of these two points of closest approach as well as the position of the endpoints of the string and hair, we can now describe the position of the bow relative to the cello using three distances which are meaningful to musicians.

The first distance (fig. 3.4, a) describes the location of the string between the hair endpoints. It is calculated as the distance along the hair line from the frog to the point of closest approach on the hair line. The second distance (fig. 3.4, b) describes the position of the bow between the string endpoints. It is calculated as the distance along the string line from the bridge to the point of closest approach on the string. The final distance (fig. 3.4, c) is the height of the bow hair above the string, or equivalently the total depth of the hair line below the string line. It is calculated as the distance between the points of closest approach on the hair and string. While the total depth is not meaningful to musicians, it will be useful to us as an indicator of the bow force.

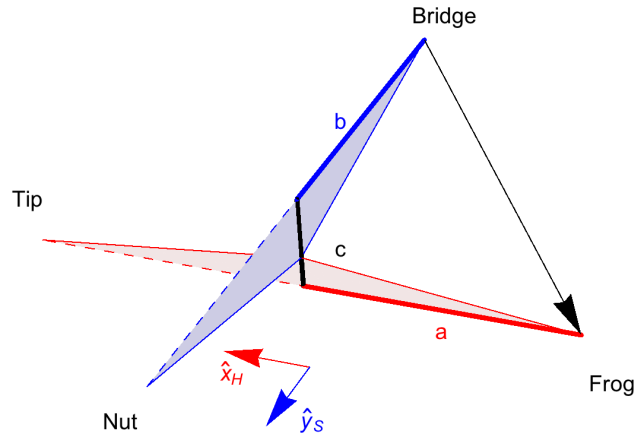


FIGURE 3.4: The position of the bow relative to the cello is described by the string-frog distance (a), the hair-bridge distance (b), and the total depth (c).

The calculations described in the paragraph above are easily realized by noting that the axis along the hair line \hat{x}_H , the axis along the string line \hat{y}_S , and their cross product form a skewed basis upon which we can project the displacement vector from the position of the string's bridge endpoint \vec{r}_{S_b} to the hair's frog endpoint \vec{r}_{H_f} .

$$\begin{aligned}
 \text{frog-to-string distance} \quad a &= -(\vec{r}_{H_f} - \vec{r}_{S_b}) \cdot \frac{\hat{x}_H - (\hat{x}_H \cdot \hat{y}_S)\hat{y}_S}{1 - (\hat{x}_H \cdot \hat{y}_S)^2} \\
 \text{bridge-to-hair distance} \quad b &= +(\vec{r}_{H_f} - \vec{r}_{S_b}) \cdot \frac{\hat{y}_S - (\hat{x}_H \cdot \hat{y}_S)\hat{x}_H}{1 - (\hat{x}_H \cdot \hat{y}_S)^2} \\
 \text{total depth} \quad c &= -(\vec{r}_{H_f} - \vec{r}_{S_b}) \cdot \frac{\hat{x}_H \times \hat{y}_S}{\|\hat{x}_H \times \hat{y}_S\|} \\
 \text{bow height} \quad h &= -c
 \end{aligned} \tag{3.11}$$

The bow speed is an indicator of the length of hair which passes over the string per unit time, which we calculate as the rate of change of the string-frog distance. We are particularly interested in the part of the bow movement which causes transverse displacement of the string. For this reason, we take only the bow speed component which is orthogonal to the string by multiplying by the cosine of the skew angle.

$$\text{bow speed} \quad v_{bow} = \frac{da}{dt} \cos \theta_S \tag{3.12}$$

3.3 Bow force

The bow applies a reaction force normal to the contact surface and a friction force tangent to the contact surface. The friction force varies over each stick-slip cycle of the string vibration. Coupling between polarizations of the string vibrations imply that the normal force will also vary over each stick-slip cycle. Vibrations in the bow stick and hair ribbon further modulate the normal force. The player does not have control

over these variations in the normal bow force. The normal force that the player does have control over is an average over the duration of a stick-slip cycle. It is this average normal force that we are identifying as the bow force control parameter.

The most significant changes in bow force occur during bow changes and string crossings. Changes in bowing direction do not often occur at frequencies above 12 Hz (semiquavers/16th notes at 180 bpm) due to physical limitations. This allows us to estimate the minimum duration of a bow change at about 0.1 seconds. The motion capture data is sampled at 120 Hz which should give us enough data points during the bow change to allow us to follow the variation in bow force.

In the sections that follow, we will develop a model for estimating the bow force from motion capture data. The model is based on an analysis of the string in static equilibrium, and slowly changing deformations of the bow. Applying these models to our experimental measurements depends on the validity of the inherent quasi-static approximation. The quasi-static approximation is valid when we can ignore inertial effects. We suspect that such an approximation is valid most of the time, as we have observed the bounce frequency of the bow around 15 Hz which is typical (Askenfelt and Guettler, 1998). The only concern is at moments when the bow undergoes sudden rotations or high accelerations in the normal direction, such as when bouncing the bow on the string during spiccato.

The method of estimating the bow force presented here was originally suggested by Maestre et al. (2007). My original contribution to this method is to take into account the compliance of the string and the observation that the bow force is approximately quadratic in the hair depth.

3.3.1 String compliance

The string compliance relates the transverse displacement of the string to the applied static bow force which causes it. It depends on the tension of the string, its resistance to stretching, the length of the string, and the position of the applied force. The goal of this section is to find the relationship between the transverse force F applied at a given point and the resulting displacement c_s (which we call the string depth) of that point.

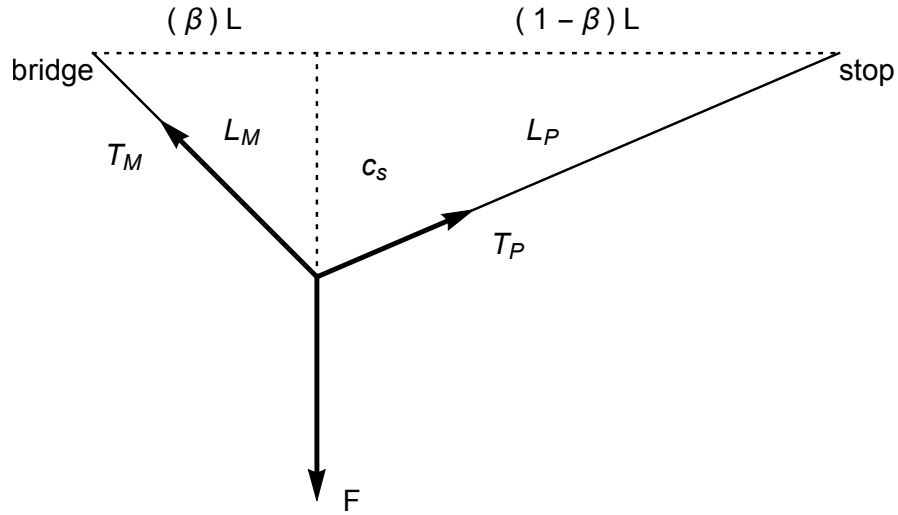


FIGURE 3.5: The string compliance model assumes a static force is applied in a transverse direction, the string forms two straight line segments, and that we can measure the final position of the corner where the force is applied. The string is stretched to a length L and tension T before applying the force. After deformation, the string is divided into two segments, having tensions T_M and T_P and lengths L_M and L_P .

When the force is applied, the string is displaced forming two sides of a triangle. In fact, the bending stiffness of the string rounds over the sharp corner, reducing d by less than 2% for typical forces and string properties, which we ignore. From Figure 3.5 we can apply the Pythagorean theorem to find the lengths L_P and L_M of the two string segments.

$$\begin{aligned} L_P &= (c_s^2 + ((1-\beta)L)^2)^{1/2} \\ L_M &= (c_s^2 + ((\beta)L)^2)^{1/2} \end{aligned} \quad (3.13)$$

where c_s is the string depth and $0 \leq \beta < 1$ is the final horizontal position of the applied force, measured along the line from the bridge to the stopping point and expressed as a fraction of the distance L from the bridge to the stopping point. $\beta = 0$ corresponds to the bridge and $\beta = 0.5$ corresponds to the midpoint of the string.

We assume that there is no longitudinal component to the applied force. This assumption is satisfied when either the agent applying the force follows the material point of the string (as is the case for stopping with a finger), or if the string slips underneath the agent (as is the case during the slip phase of stick-slip interactions). Balancing the horizontal and vertical forces relates the force F and string depth c_s to the tensions T_P and T_M in each of the segments.

$$\begin{aligned} \text{Horizontal equilibrium:} & \quad T_P \frac{(1-\beta)L}{L_P} - T_M \frac{(\beta)L}{L_M} = 0 \\ \text{Vertical equilibrium:} & \quad T_P \frac{c_s}{L_P} + T_M \frac{c_s}{L_M} - F = 0 \end{aligned} \quad (3.14)$$

Before the force is applied, the portion of the string between the bridge and the stopping point has tension T and length L . If the tension were removed, this segment would contract to its original length L_0 according to its longitudinal stiffness K_L (see Equation 3.1). We can write similar constitutive relations for the two segments of length

L_P and L_M in terms of an unknown fraction α analogous to β . The fraction α varies according to the angle and magnitude of the applied force.

$$\begin{aligned} T &= K_L \frac{(L-L_0)}{L_0} \\ T_P &= K_L \frac{(L_P-(1-\alpha)L_0)}{(1-\alpha)L_0} \\ T_M &= K_L \frac{(L_M-\alpha)L_0}{\alpha L_0} \end{aligned} \quad (3.15)$$

Assuming known values for T , L , K_L , β , and c_s , we are left with seven equations and seven unknowns (L_P , L_M , L_0 , T_P , T_M , α , and F). The geometry equations (3.13) give L_P and L_M directly. The first constitutive equation (3.15) can be rearranged to solve for L_0 . The other two constitutive relations can be used to eliminate T_P and T_M from the horizontal equilibrium equation (3.14) and solve for α . With α known, the constitutive equations then give us T_P and T_M directly. Finally, the vertical equilibrium equation can be used to find the force as a function of the string depth c_s and the bridge-to-bow distance $b = (\beta)L$.

$$F = F(b, c_s) \quad (3.16)$$

Solving these equations analytically may not be possible without making further simplifying assumptions and approximations. Numerical solutions, however, are found easily enough so we did not bother to investigate any errors that would have been introduced if we had used a simpler model.

3.3.2 Hair compliance

The hair compliance describes the transverse displacement of the hair caused by an applied force. It depends on the tension of the hair, its resistance to stretching, the length of the hair, the distribution of force across the width of the hair ribbon, the stiffness of the bow stick, and the position of the applied force. The goal of this section is to find the relationship between the transverse force F applied at a given point and the resulting displacement c_h which we call the hair depth.

It is tempting to look for an analytic model as we did for the string, but the bending of the stick depends on its material properties, cross-sectional area, and curvature, all of which vary along the length of the stick. While we could measure the taper and camber of the stick, the material properties cannot be measured directly. In any case, the equations involved are not likely to have solutions in terms of known analytic functions.

Ablitzer, 2011 created a numerical finite element model of a bow subjected to static forces and moments and taking into account the large deformations of the stick. The model includes the measured geometry, assumed elastic constitutive relations, and force and moment balances. By applying external forces and moments and measuring the resulting deformations of the stick, it is possible to estimate effective material properties which lead to the observed behavior. The estimated material properties and measured deformations can then be used with the finite element model to estimate the necessary forces and torques. The advantages of the finite element model are (1) that its parameters are the material properties (which may be interesting in their own right), and (2) that it can be used to both interpolate between and extrapolate beyond the data used to calibrate the model. The disadvantages of the finite element model are that (1) it requires a specific set of calibration data which may take longer to collect and (2) it will be inaccurate if the underlying assumptions of the model are violated.

Another approach is to develop an empirical model with arbitrary parameters which doesn't require any prior knowledge about how available measurements are related to the bow force. As in the case of the finite element model, the parameters of the empirical model are estimated through a process of applying external forces and observing the resulting deformations. The empirical model with its estimated parameters can then be applied to measured deformations to estimate the necessary forces and torques. Advantages of the empirical model are that (1) almost any quickly collected data is suitable for calibration, and (2) the model can be improved by adding knowledge about the physics of the bow. The trade-off is that the empirical model does not tell us about the material properties and may or may not be able to extrapolate beyond the calibration data.

Since we are not interested in the material properties of the bow, and we need a fast calibration procedure during the experimental context, we decided to use an empirical model approach.

After the musician brings the bow hair to playing tension, data for building a hair compliance model is collected by pressing the bow hair against a force transducer (Figure 3.6) at various fixed positions along the bow hair. The force transducer is mounted with an aluminum blade which acts as a perfectly rigid string with its string axis \hat{y}_S pointing along the edge. One endpoint of the edge may be taken as the location of the bridge

The force transducer and bow each have a set of markers which allow us to measure their positions and orientations using a motion capture system as described in Section 4.3. Taking one endpoint of the edge to represent the location of the bridge, we can use the motion capture data to calculate the frog-to-"string" distance and the hair depth as in Section 3.2.2. The total depth when applied to the rigid force transducer gives just the hair depth since the string depth is zero.



FIGURE 3.6: An HBM U1A force transducer with an aluminum blade measures bow forces up to 10 N for calibrating the hair compliance model.

Figure 3.7 shows typical data from a calibration procedure. The force is increased for about two seconds (red highlight) until either the capacity of the force transducer

is reached or the bow stick almost touches the force transducer. The force is decreased for about two seconds (blue highlight) until the bow hair is lifted off the force transducer. The bow is moved about 1 cm (green highlight) to repeat the press and release procedure at a new position along the bow hair.

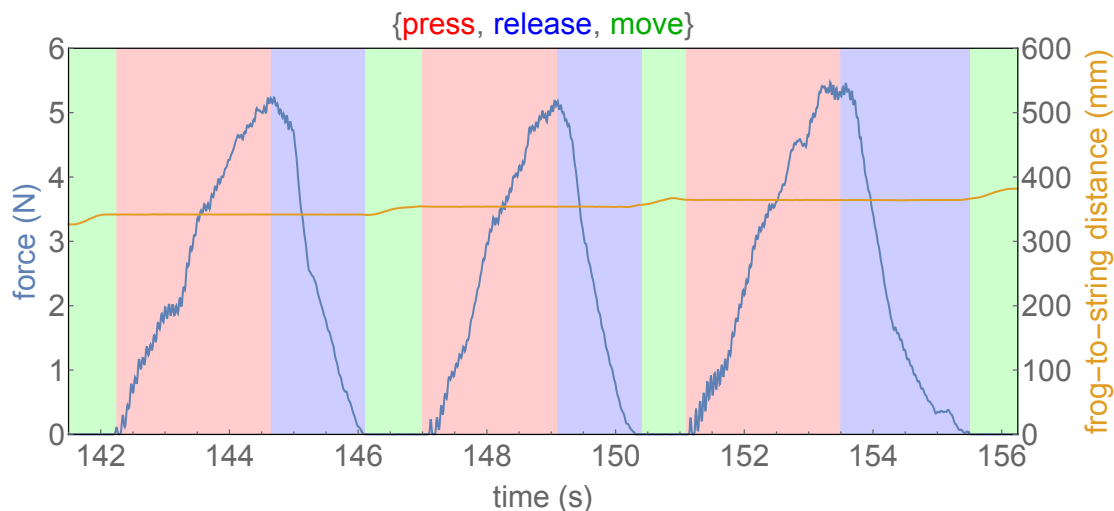


FIGURE 3.7: Force and frog-to-string distance as functions of time while collecting data for the hair compliance model.

The tip rotation is a noisy indicator of bow force which may be useful in the upper half of the bow where an applied bow force is accompanied by significant stick deformation. The sensitivity of the tip rotation to the force increases as the force is applied closer to the tip, suggesting that the precision increases. Unfortunately, the sensitivity near the tip is so great that the accuracy of the model is sensitive to errors in calibration data. The errors in the calibration data for tip rotation come mostly from the small size of the rigid bodies associated with the tip and frog. For this reason, we do not use the tip rotation in our bow force estimation model.

Our main predictor of bow force is the deformation of the bow as measured by the hair depth (Equation 3.11). If the bow stick were perfectly rigid, then we could apply the compliance model developed for the string. However, the stick bends quite easily, so we look for an empirical relationship. Figure 3.8 shows that a simple quadratic relationship gives a reasonable model. The coefficients of the fit shown in Figure 3.8 reflect the compliance of the hair at a single position on the bow. At other positions along the bow hair, we find that a quadratic model still fits the data well, but that different coefficients are needed.

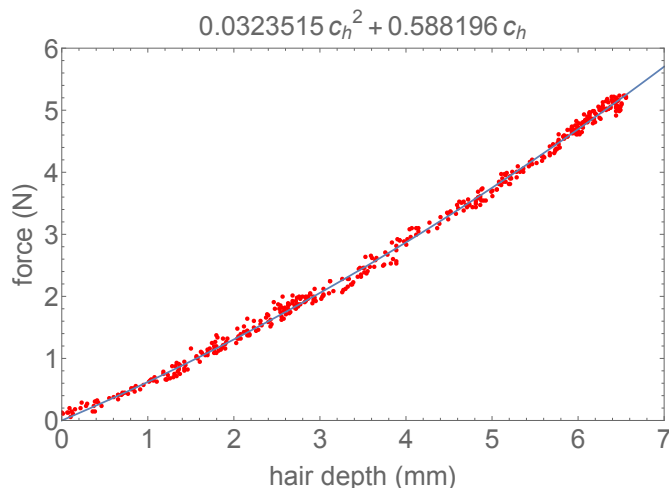


FIGURE 3.8: Data taken while pressing and releasing the bow at a single frog-to-string distance. A quadratic model constrained to pass through the origin fits the force versus hair depth data well.

Modelling the quadratic coefficients as a function of the frog-to-string distance completes the bow force model as a function of frog-to-string distance a and hair depth c_h .

$$F = F(a, c_h) \quad (3.17)$$

We originally attempted to model the force as a function of the hair depth using Support Vector Regression and various sets of features. We initially tried naively "playing" the force transducer as if it were a string in an attempt to capture the dynamics of the bow in real playing situations as suggested in (Baez, 2013). We did some feature engineering (for example, using the cosine of the tilt angle instead of the raw tilt angle) and used various Elastic Nets (combinations of ridge regularization and lasso feature selection) to create information-based models. We quickly realized that Support Vector Regression is just an interpolation scheme, and is incapable of predicting values more extreme than those observed in the training data. We eventually realized the problems associated with using correlated features, and began to reduce the feature set.

We identified the inclination angle as a source of noise. The hair is deformed by the total force applied, but the force transducer only measures the force along its axis. We correct for this difference by dividing the measured force by the cosine of the inclination angle (Equation 3.18). In practice this is a small correction because we attempt to maintain the force parallel to the transducer axis during the calibration procedure. Having included the expected effect of the inclination angle, we can now eliminate it from the list of features used for predicting the bow force.²

$$F = \frac{F_{measured}}{\cos \theta_I} \quad (3.18)$$

We identified the "bridge-to-bow" distance as noise. The force transducer is rigid, so there shouldn't be any effect. Any effect the model attributes to this distance is merely

²One might question whether the bow's weight significantly deforms the stick and whether such a deformation significantly affects the predicted forces. This would require incorporating measurements of the bow orientation relative to the gravitational field, and cannot be simply estimated from the inclination angle alone.

coincidental. This had little effect on our models as the lasso feature selection had already identified it as a feature to be effectively ignored. The lasso feature selection also identified the skew angle as having little influence within the model. Thus the set of features used to estimate the bow force were the frog-to-string distance, the cosine of the tilt angle, and either the hair depth or the rotation of the tip relative to the frog in the $\hat{x}_H\hat{z}_H$ -plane.

During this time we were still hunting down the sources of errors. We came to realize that the bow was bouncing on the load cell as we tried to bow in a way that gave a similar sensation as the stick-slip interactions with a real string. We suspect that this bouncing and/or the torque applied by the bow lead to additional noise in the force ground truth measurements. We then started using the press-and-release procedure indicated in Figure 3.7 which greatly reduced the noise. At this time, the effect of tilt was still noisy, and we still didn't understand where the noise was coming from. We decided to reduce the number of features to just the hair depth and frog-to-string distance and to use a simple polynomial model, rather than a Support Vector Regression model. Having done that, we were able to identify systematic errors coming from the estimation of the positions of landmarks (see Section 4.3.4). Unfortunately, the time for developing the bow model had been exhausted and we were not able to develop the model further. We would have liked to develop a more sophisticated model which includes a physically motivated dependence on frog-to-string distance, incorporating the tilt angle, and possibly switching between using the total depth and using the rotation of the tip relative to the frog as its primary indicator of force.

The model for the bow force in terms of the frog-to-string distance and the hair depth is

$$F = k_1(a)(c_h - c_0) + k_2(a)\frac{1}{2}(c_h - c_0)^2 \quad (3.19)$$

where c_0 allows us to estimate any remaining systematic error in the estimation of the ends of the hair ribbon. The hair stiffness functions are arbitrarily modeled as fourth order polynomials.

$$k_1(a) = k_{1,0} + k_{1,1}a + k_{1,2}a^2 + k_{1,3}a^3 + k_{1,4}a^4$$

$$k_2(a) = k_{2,0} + k_{2,1}a + k_{2,2}a^2 + k_{2,3}a^3 + k_{2,4}a^4$$

We use a least total squared residuals algorithm to estimate the coefficients $k_{i,j}$. Figure 3.9 shows the best fit model based on calibration data taken during the experiment.

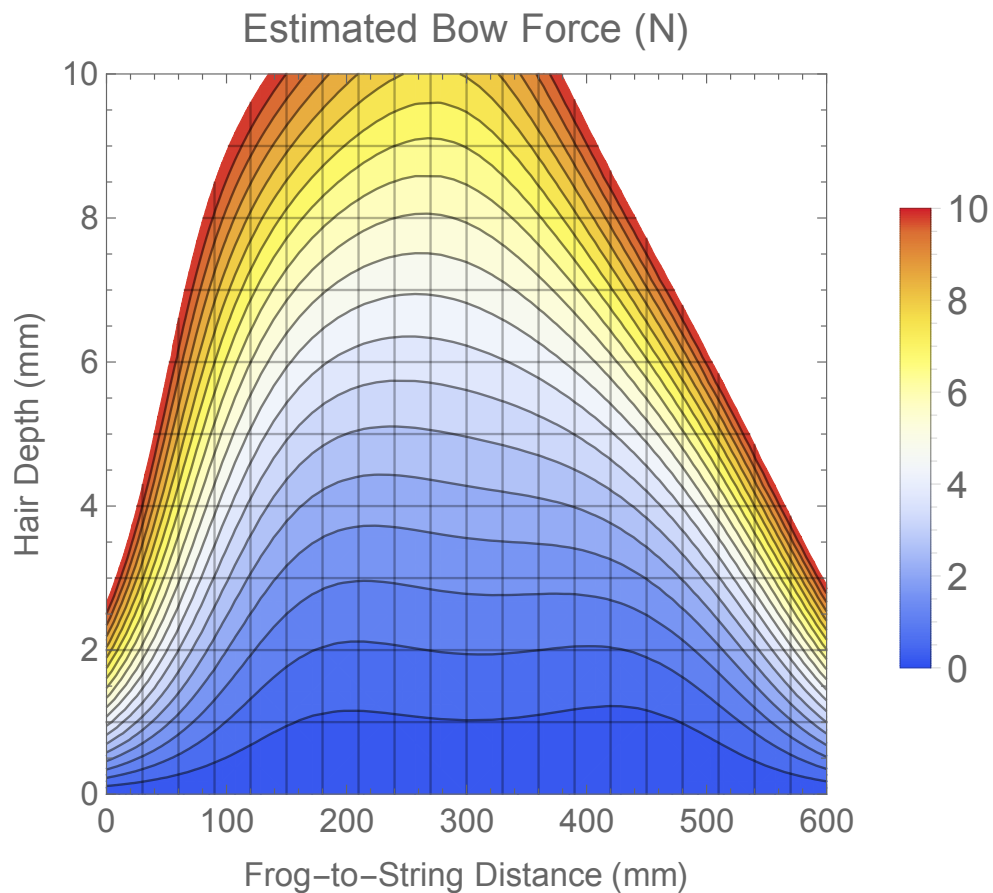


FIGURE 3.9: The best-fit model of Equation 3.19 after compensating for systematic error (c_0). Contours are plotted every 0.5 N up to 10 N. Note that not all regions of this diagram are accessible as the hair will touch the stick before reaching 10 N in the middle of the stick and mechanical disadvantage makes it impractical to apply more than a few Newtons of force near the tip.

To estimate the accuracy of the model, we divide the bow into twenty sections and calculate the expected absolute residual error and standard deviation in each section. Figure 3.10 shows that the errors near the frog and tip are quite large (large mean value) and that the calibration is not very stable (large standard deviations). From about 180 mm from the frog to about 540 mm from the frog, the errors are small and we feel comfortable quoting a thumb rule of about 0.3 N as the error.

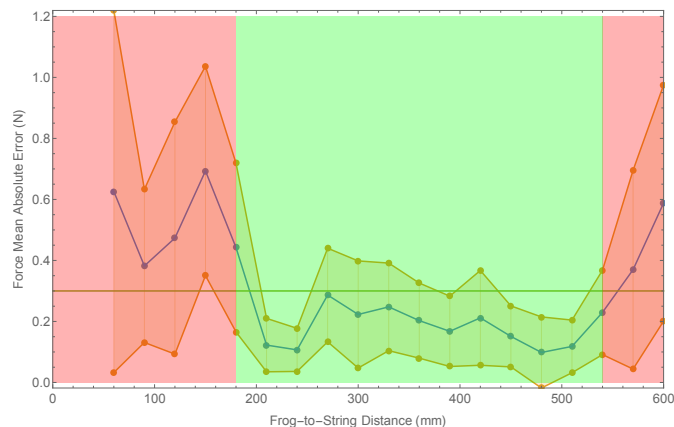


FIGURE 3.10: An estimate of the accuracy of the hair model.

3.3.3 Bow force model

We now have two models to estimate the force; one depends on the deformation of the string as measured by the string depth c_s , the other depends on the deformation of the hair as measured by the hair depth c_h . Unfortunately, neither of these measurements are available individually; it is only possible to measure their sum (see Figure 3.11).

The total depth c is the sum of the string depth c_s and the hair depth c_h . Its division into string depth and hair depth depends on the relative compliance of the string and hair. The compliance of the string depends on the bridge-to-hair distance (Section 3.3.1). The compliance of the hair depends on the frog-to-string distance (Section 3.3.2). The total depth c , frog-to-string distance a , and bridge-to-hair distance b can be calculated from the positions of the bridge \vec{r}_{S_b} , stop (or nut) \vec{r}_{S_n} , frog \vec{r}_{H_f} , and tip \vec{r}_{H_t} (Equation 3.11).

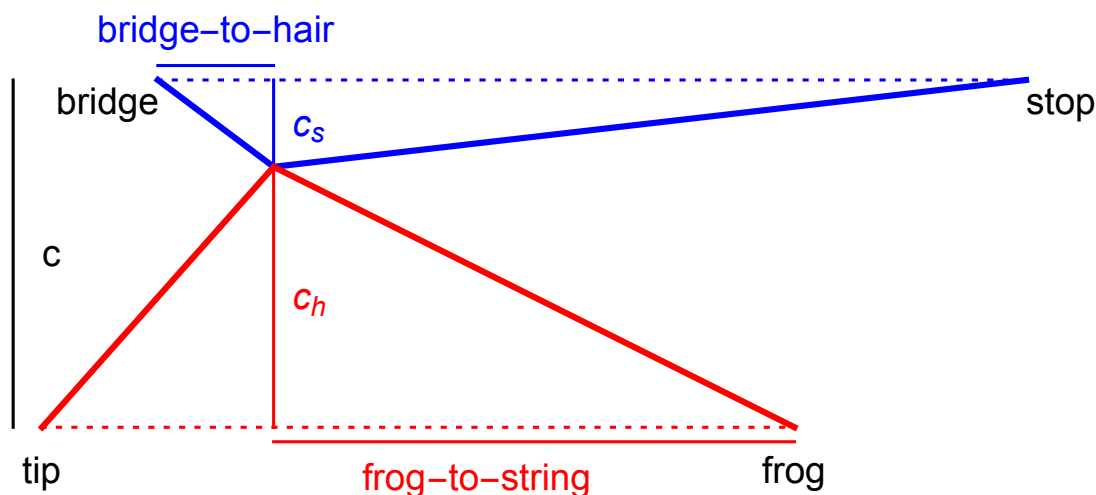


FIGURE 3.11: The total depth c is the sum of the string depth c_s and the hair depth c_h .

The problem is to find a model of the force which depends on the measurable total depth. Such a model is trivially found by realizing that the definition of string, hair, and total depth along with the two previous force models make a system of three equations with three unknowns (c_s, c_h, F).

$$\begin{array}{ll}
 \text{force from string deformation} & F = F(b, c_s) \\
 \text{force from hair deformation} & F = F(a, c_h) \\
 \text{total depth relation} & c = c_h + c_s
 \end{array} \tag{3.20}$$

Finding the solution numerically is easy if we constrain the search to the domain $c_s > 0, c_h > 0, F > 0$. The result is a complete model giving us the bow force in terms of the observable frog-to-string distance a , bridge-to-hair distance b , and total depth c .

$$F = F(a, b, c) \tag{3.21}$$

It can take a few hours for my computer to calculate the bow force for all the data from the experiment, taking into account the deformation of the string, and one might ask whether it is necessary. The string depth accounts for about 10-20% of the total depth, which leads to a systematic overestimation of 10-40% in the bow force if the total depth is used instead of the hair depth in the model of the previous section (Equation 3.19).

Chapter 4

Experimental equipment

We want to relate the musician's perception of the cello to the response of the cello and the control parameters which generated the response. The cello responses which are most likely to influence the musician's perception of playability are the radiated sound (which the musician hears) and the string vibrations (which affects the bow-string interactions). Section 4.1 briefly describes the microphone and its placement, while Section 4.2 describes a modified bridge with embedded piezoelectric sensors allowing us to measure the string vibrations.

We previously reviewed technologies for measuring control parameters in Section 2.8, and in Chapter 3 we defined the control parameters in terms of position and orientation data. Section 4.3 of this chapter describes the motion capture system used to measure the position and orientation data.

4.1 Microphone

In order to record the audio from the cello, we use a free-field 1/2" microphone (Brüel & Kjaer 4391) placed directly in front the cello about 1.6 meters away and 1 meter off the ground. The microphone can be seen in Figure 4.9 directly above the video camera which is behind the music stand.

4.2 Bridge sensor

The sounds recorded by the microphone include information not only about the vibration of the cello, but also about the acoustics of the room in which the cello was played.

Since we are interested in the physical behavior of the cello itself, we want a signal that does not include the effects of the room. A few options for such a signal are using accelerometers or contact microphones attached to the front plate of the cello, placed underneath the feet of the bridge, or clipped onto the bridge. All of these options tell us about the motion where the sensor is attached, thus mixing the signals from each string and capturing only a portion of all the vibrations of the cello body. This is problematic because it is possible that the results of our study could be sensitive to the placement of the sensor.

In any case, we are interested in the interactions between the string and bow which we think are related to playability. Since contact microphones give only limited information about these interactions, we looked for more direct means of measuring the string vibrations. After considering magnetic pickups and optical forks, we decided to use piezoelectric sensors embedded in the bridge underneath each string following

the design by Jim Woodhouse as seen in (Zhang, 2015) which is reportedly based on a design by Reinicke (1973).

In Section 4.2.1 we describe our implementation of the bridge sensor including dimensions, cautionary notes, and some improvements that we made to make the sensor less fragile. Section 4.2.2 describes the measurement procedure and calculations for calibrating the sensor, and a new analysis for interpreting the calibration coefficients.

4.2.1 Design

The sensor design is shown in Figure 4.1. The dimensions are based on the thickness of the thickest string, the distance between strings, and the area needed on the upper support to make the electrical connections. Other designs were considered to reduce the size and mass of the sensor, but this sensor is easier to build and robust against clumsy handling. Our luthier chose and carved the bridges keeping in mind the effects of replacing parts of the wood under each string with sensors. He also cut the right-angled notches underneath each string at the proper angle and depth, and provided an initial fitting of the sensors.

The sensor design begins with a lower and an upper plastic support. The lower support forms a right angle and includes some material in the corner. The upper support forms a right triangle with the right angle being shaved off. The long surfaces of each support are lined with copper tape. Piezoelectric elements are placed between the pieces of copper tape, making electrical contact. The long surfaces of the lower support hold the piezoelectric elements at right angles to one another, while the material in the corner of the lower support prevents them from touching each other. The upper support transfers the force from the vibrating string to the piezoelectric elements. Shaving off the right angled corner of the upper support prevents the two supports from touching each other and ensures that the string is completely supported by the piezoelectric elements. The copper tape wraps onto the front surface of the sensor for attaching wires.

Following the suggestion by Jim Woodhouse, thin plastic plates are glued to the front and back of the bridge, preventing the sensor from tearing itself apart by sliding forward (while bringing the string up to tension) or backward (while sitting under string tension). Take care that the plates do not pinch the upper support or become glued to it. While the angled profile of the bridge causes the plates to trap the upper support in the sensor, the upper support should be more or less free to move up and down a few tenths of a millimeter before applying string tension. If your signal is weak or has an unexpected form, this is likely the source of the problem.

Woodhouse reported problems with failed electrical connections at the solder points. To address this problem we drilled holes through the sensor, passed the wires from the back of the sensor, and soldered the wires to the copper tape on the front of the sensor. Passing the wires through the sensor gives them some structural support. When the wires move, stress is applied where the wire enters the back of the sensor rather than at the solder points. This reduces the amount of movement near the solder points, helping to maintain good electrical connections.

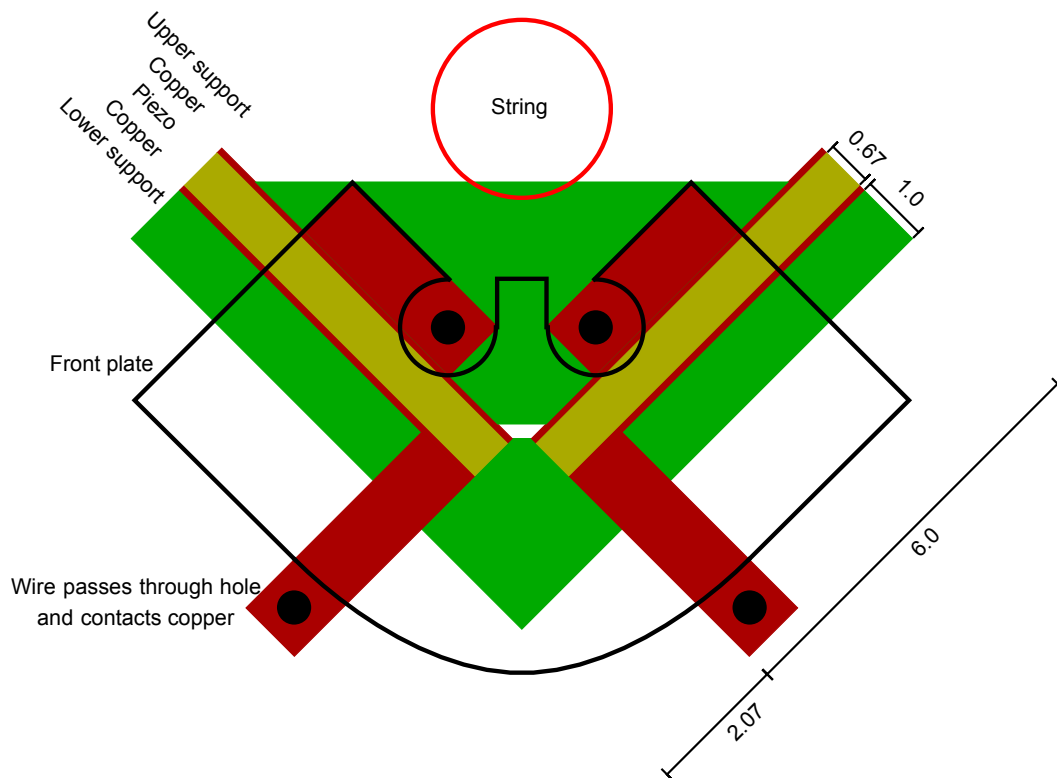


FIGURE 4.1: The bridge sensor design including explicit dimensions, based on the sensor shown in Zhang, 2015.

The piezoelectric elements are made of a transversely isotropic ceramic, with the axis of symmetry (the piezoelectric axis) spanning the thickness of the element. The element produces an electric potential difference across its thickness in response to strains along the piezoelectric axis. These strains are produced by forces applied orthogonally to the surface (ie. along the piezoelectric axis). The potential difference is proportional to the normal force supported by the element.

When connecting the wires to the sensor, one side of the piezo is assigned the signal; the other side, the reference (ground, zero potential). The choice is established through an arbitrary convention; we choose to have a positive signal when the piezo is compressed. This is easily checked by bowing across the string and comparing the shapes of the periodic waveforms (see figure 4.2). When bowing down-bow, the string is pulled toward the bass piezo and away from the treble piezo before slipping. During down-bows, the bass piezo waveform is a sawtooth which climbs up gradually and then jumps down suddenly when the Helmholtz corner arrives at the bridge. Meanwhile, the treble piezo waveform slides down gradually and then jumps up suddenly at the arrival of the Helmholtz corner at the bridge.

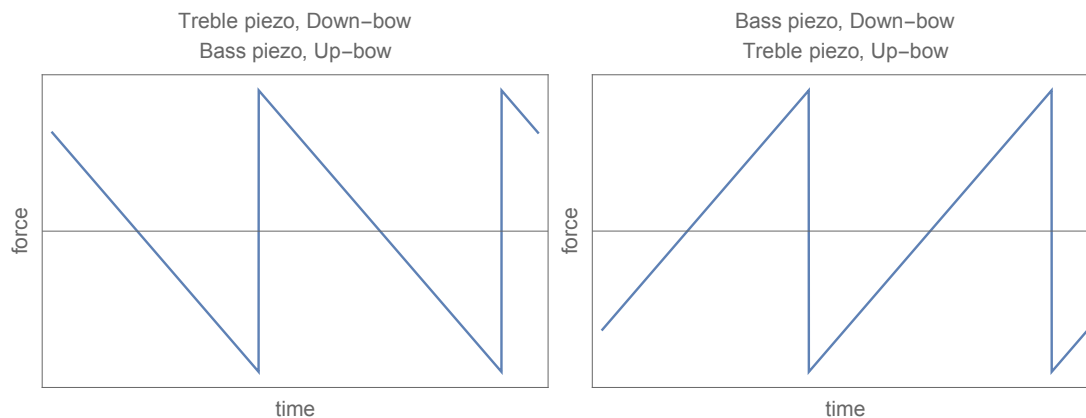


FIGURE 4.2: These are the expected waveforms for the treble and bass piezos during up-bows and down-bows according to the sign convention of positive signals under compression.

The sixteen wires from the bridge (four strings, two piezos per string, two wires per piezo) are collected into a 16-pin connector¹ (Figure 4.3). This allows us to quickly disconnect one cello from the computer and connect the other without fear of mixing up signals. A common 16-pin cable is used to connect the cello to a circuit containing a charge amplifier for each of the eight piezos. We made a cable which connects the 16-pin output of the charge amplifier circuit to the eight BNC interfaces at the data acquisition board². The circuit design is given in Appendix A.



FIGURE 4.3: The piezo signals run through a charge amplifier before being recorded by the computer.

¹Actually, only nine pins are used: eight signals and one common ground.

²These homemade BNC cables were often the source of bad signals. It is recommended to spend some time making the connector mechanically robust to avoid electrical shorts after repeated connections and disconnections

4.2.2 Calibration

With the raw signals (potential differences) from the bridge piezos we can compare the relative amplitudes of a single piezo at different times and we can analyze the temporal and harmonic content. Calibrating the signals to give us forces will allow us to study the polarization of the transverse vibrations by comparing the two piezos underneath a string. It also allows us to compare results between strings, cellos, or other experiments. A calibrated force signal also allows us to estimate the amplitude of the string vibrations. It may be interesting to compare the amplitude of string vibrations with the amplitude of the radiated sound on different cellos. The calibrated force signal may even be used with the bridge mobility to study the motion of the bridge. It might be used along with radiation transfer functions to synthesize sounds of model instruments.

Measurement procedure

To calibrate the bridge sensors, we use the wire-break method described in (Zhang, 2015). The cello is held vertically between two heavy supports (see figure 4.4). A small table with a guide post is placed in front of the cello. A thin copper wire is looped around the string, passes tangent to the guide post, and is attached to a force transducer resting on the table. A protractor (figure 4.5) is placed against the bridge and the table is positioned so that the copper wire runs along the desired direction. Once the protractor is removed, the guide post serves as a reference to ensure the direction of the wire remains the same. Finally, the force transducer is pulled away from the cello along the table until the copper wire breaks. The signals from the force transducer and the two piezos underneath the string are recorded and the peak (or valley) corresponding to the wire-break in each measurement is kept (figure 4.6).



FIGURE 4.4: A HBM U1A force transducer is used to measure the magnitude force applied to the string when the wire breaks. Sliding the force transducer along the surface of the table ensures the force is applied within the bridge plane. A guide post is used as a reference to set the angle of the applied force.



FIGURE 4.5: A protractor along with a guide post is used to set the angle of the applied force relative to a global reference frame. The protractor registers against the strings and curve of the bridge. The gridded paper indicates the two reference axes in the plane of the bridge. Several positions are marked along the edge of the protractor. Four angles are marked at each position corresponding to the angles of the lines connecting the point to each of the four strings.

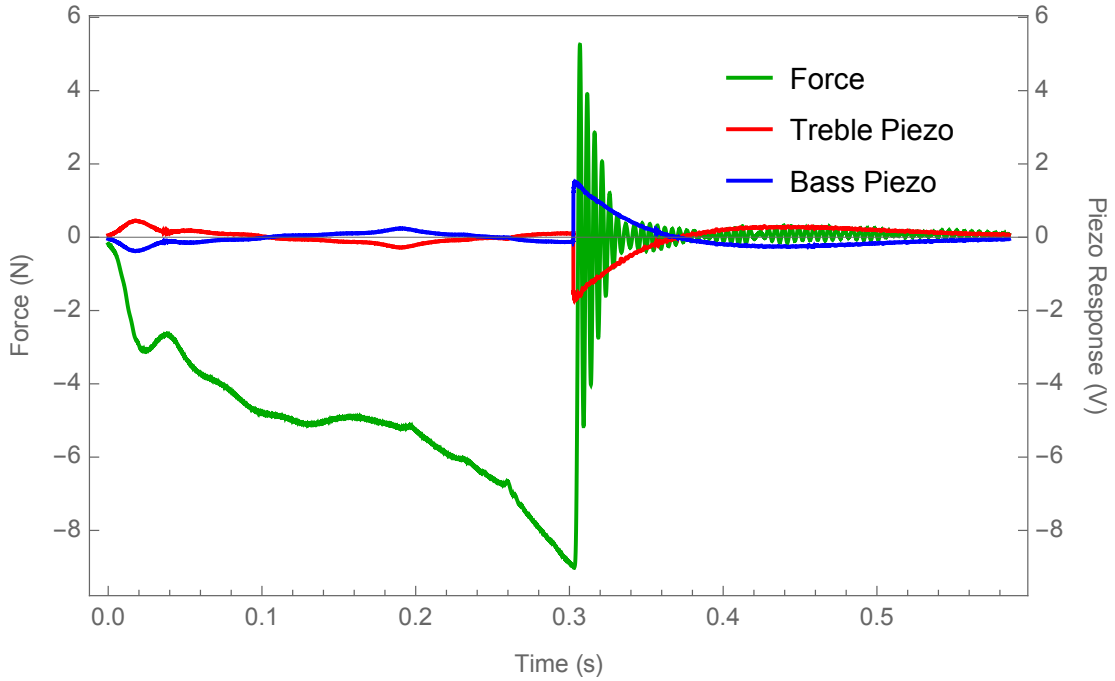


FIGURE 4.6: The signals from the force transducer and bridge piezos during a wire-break measurement. The peak force is taken as the magnitude of the applied force. The height of the first peak (or valley) is taken as the response amplitude of each piezo.

Parameter estimation

The data from the wire-break measurements consists of the magnitude and angle of the applied force (F_i, θ_i) and the potential differences across the treble and bass piezos (V_i^T, V_i^B) for each measurement $i = 1 \dots n$. After measuring a few wire-breaks at each measurement angle, we collect the data from the n measurements into an overdetermined set of linear equations.

$$\mathbf{F} = \mathbf{V}\mathbf{C} \quad (4.1)$$

where \mathbf{F} is the set of force measurements projected along the horizontal x and vertical z axes

$$\mathbf{F} = \begin{pmatrix} F_1^x \\ F_1^z \\ \vdots \\ F_n^x \\ F_n^z \end{pmatrix} = \begin{pmatrix} F_1 \cos(\theta_1) \\ F_1 \sin(\theta_1) \\ \vdots \\ F_n \cos(\theta_n) \\ F_n \sin(\theta_n) \end{pmatrix}, \quad (4.2)$$

\mathbf{V} is the set of potential differences measured across the treble T and bass B piezos

$$\mathbf{V} = \begin{pmatrix} V_1^T & V_1^B & 0 & 0 \\ 0 & 0 & V_1^T & V_1^B \\ & & \vdots & \\ V_n^T & V_n^B & 0 & 0 \\ 0 & 0 & V_n^T & V_n^B \end{pmatrix}, \quad (4.3)$$

and \mathbf{C} is the set of unknown calibration coefficients we are trying to estimate

$$\mathbf{C} = \begin{pmatrix} C_T^x \\ C_B^x \\ C_T^z \\ C_B^z \end{pmatrix}. \quad (4.4)$$

We then find the values of the calibration coefficients which minimize the total squared differences

$$J = (\mathbf{F} - \mathbf{V}\mathbf{C})^\top(\mathbf{F} - \mathbf{V}\mathbf{C})$$

Finding the ordinary least squares estimators of linear parameters in an overdetermined system of equations is a common problem with a well-known solution (see for example, Draper and Smith, 2014). Formally, the solution is given by

$$\mathbf{C} = (\mathbf{V}^\top\mathbf{V})^{-1}\mathbf{V}^\top\mathbf{F}.$$

Calculating the pseudo-inverse $\mathbf{A} = (\mathbf{V}^\top\mathbf{V})^{-1}\mathbf{V}^\top$ by composing matrix transposes, multiplications, and inverses can be susceptible to numerical problems when the $\mathbf{V}^\top\mathbf{V}$ matrix is ill-conditioned. In that case, it is preferable to calculate the pseudo-inverse directly using other algorithms such as those implemented as built-in functions in modern scientific computing languages:

Wolfram Mathematica: `C = LeastSquares[V, F];`

MathWorks MATLAB: `C = V\F;`

Python: `C = numpy.linalg.lstsq(V, F)[0];`

Interpretation of calibration coefficients

To establish the relationship between the calibration coefficients and the gains and orientations of the piezos, we present the following analysis, which differs from the one shown in (Zhang, 2015), arriving at a different result.

I believe there are two mistakes in Zhang's presentation. The first is a sign error and angle swap when she converts from one set of basis vectors to the other near the end of the presentation. The second mistake is the assumption that the potential difference across a piezo is proportional to the *orthogonal projection of the force* onto the piezo surface normal. This is fine when there is only one piezo or when the two piezos are orthogonal. However, the piezos are not assumed to be orthogonal, so skew projection should have been used consistently to avoid the double counting that happens when orthogonal projection is used inappropriately.

The force of the string can be decomposed into a component which is orthogonal to the treble piezo and a component which is parallel to the treble piezo (see red arrows in Figure 4.7). The treble piezo can clearly support the component which is orthogonal to it (the labeled red arrow), but the parallel component must be supported by the bass piezo. If the two piezos are orthogonal to each other, then the force component which is parallel to the treble piezo will be orthogonal to the bass piezo and will be completely supported by the bass piezo. In that case, we can stop the analysis here. But if the two piezos are not orthogonal, then the force component which is parallel to the treble piezo (the unlabeled red arrow) can be decomposed into a component which is orthogonal to the bass piezo and a component which is parallel to the bass piezo (the blue arrows). The bass piezo supports the orthogonal part (the labeled blue arrow) and

leaves the parallel part for the treble piezo. The analysis continues *ad infinitum* until the entire force of the string is supported by the two piezos.

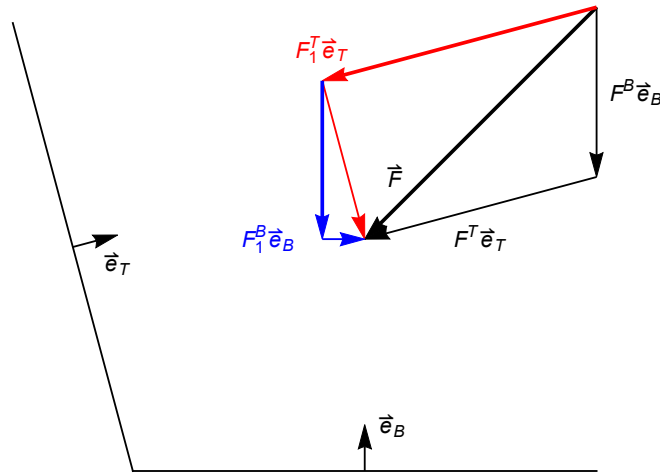


FIGURE 4.7: The normal force supported by each piezo can be visualized as an infinite sum through orthogonal decomposition of successive remainders (red and blue arrows). Skew projection provides the result directly (thin black arrows).

Equation 4.5 gives the magnitude of the net normal forces F^T and F^B applied to the treble and bass piezos in terms of the total force \vec{F} and the unit normal vectors \vec{e}_T and \vec{e}_B . Appendix B derives the equation as an application of skew projection.

$$\begin{aligned} F^T &= \left((\vec{F} \cdot \vec{e}_T) - (\vec{F} \cdot \vec{e}_B)(\vec{e}_T \cdot \vec{e}_B) \right) / (1 - (\vec{e}_T \cdot \vec{e}_B)^2) \\ F^B &= \left((\vec{F} \cdot \vec{e}_B) - (\vec{F} \cdot \vec{e}_T)(\vec{e}_T \cdot \vec{e}_B) \right) / (1 - (\vec{e}_T \cdot \vec{e}_B)^2) \end{aligned} \quad (4.5)$$

The electric potential V^T measured by the treble piezo is proportional to the normal force F^T that it supports. The proportionality constant is its gain g_T . Likewise for the bass piezo.

$$\begin{aligned} V^T &= g_T F^T \\ V^B &= g_B F^B \end{aligned} \quad (4.6)$$

The force supported by each piezo points along the normal to its surface, i.e. parallel to the unit vectors \vec{e}_T and \vec{e}_B (see figure 4.8). Their vector sum is equal to the total applied force.

$$\vec{F} = F^T \vec{e}_T + F^B \vec{e}_B \quad (4.7)$$

To find the horizontal and vertical components of the total force, we project it onto the orthonormal basis \vec{e}_x and \vec{e}_z .

$$\begin{aligned} F^x &= \vec{F} \cdot \vec{e}_x = F^T \vec{e}_T \cdot \vec{e}_x + F^B \vec{e}_B \cdot \vec{e}_x \\ F^z &= \vec{F} \cdot \vec{e}_z = F^T \vec{e}_T \cdot \vec{e}_z + F^B \vec{e}_B \cdot \vec{e}_z \end{aligned} \quad (4.8)$$

Representing the forces in terms of potentials with equation 4.6 and reading the dot products from figure 4.8, the expression for the force components (equation 4.8)

becomes

$$\begin{aligned} F^x &= \frac{\cos \theta_T}{g_T} V^T + \frac{\cos \theta_B}{g_B} V^B \\ F^z &= \frac{\sin \theta_T}{g_T} V^T + \frac{\sin \theta_B}{g_B} V^B \end{aligned} \quad (4.9)$$

from which we can read the calibration coefficients in terms of the piezo gains and angles.

$$\begin{aligned} C_T^x &= \frac{\cos \theta_T}{g_T} & C_B^x &= \frac{\cos \theta_B}{g_B} \\ C_T^z &= \frac{\sin \theta_T}{g_T} & C_B^z &= \frac{\sin \theta_B}{g_B} \end{aligned} \quad (4.10)$$

Inverting these relations, we can estimate gains and angles from the estimated calibration coefficients.

$$\begin{aligned} \theta_T &= \arctan \frac{C_T^z}{C_T^x} & g_T &= \frac{C_T^x}{\cos \theta_T} = \frac{C_T^z}{\sin \theta_T} \\ \theta_B &= \arctan \frac{C_B^z}{C_B^x} & g_B &= \frac{C_B^x}{\cos \theta_B} = \frac{C_B^z}{\sin \theta_B} \end{aligned} \quad (4.11)$$

Values of calibration coefficients for our two cellos are found in Appendix C.

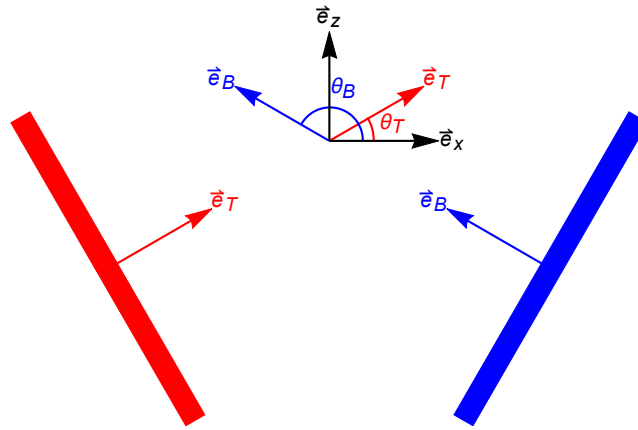


FIGURE 4.8: This diagram shows the orientation of the piezo surface normals relative to the global horizontal and vertical axes. Note the normals are not assumed to be orthogonal to each other. With the orientation of the normals chosen in this figure, the piezo gains are negative so that the piezos have positive potentials under compression. This can be achieved by exchanging the signal and reference leads attached to the piezo, or by turning over the piezo.

4.3 Motion capture

Chapter 3 defined the bow force model and kinematic control parameters in terms of the positions and orientations of the bow and cello within a three-dimensional space. In this section, we describe cameras and markers used to measure the musician's control parameters. We give the algorithm for pre-processing marker position data to estimate the positions of landmarks from previously constructed rigid body models (reference frames and estimated landmark positions). We then describe how each of the rigid body models are constructed, including methods for defining the positions of landmarks and discussing systematic errors. In particular, we describe the placement of markers and how the markers are used to estimate the positions of points of interest

on the force transducer (used to calibrate the bow force model, see Section 3.3.2), cello, and bow.

We use a commercial motion capture system (OptiTrack) based on tracking several passive markers using ten infrared cameras (1280×1024 resolution, 56° field of view, 120 fps frame rate). The cameras are placed about 2m from the cello and are oriented so that most of the markers on the cello as well as both ends of the bow are always within the frame (Figure 4.9). One camera was mounted near the ceiling, slightly behind and to the left of the cellist giving a good view of the scroll. A second camera was placed on a convenient support near the ceiling in front and to the right of the cello. Two cameras were placed near the floor on either side and slightly in front of the cello. The other six cameras were distributed at various heights between one and two meters along an arc in front of the cello. After calibration, the system reports a spatial precision of about 0.3 mm, which is consistent with the variations seen during measurements of the stationary cello, and is limited by the camera resolution.



FIGURE 4.9: Here we can see the positions of eight of the ten motion capture cameras. The two cameras mounted near the ceiling are out of frame.

The motion capture software (Motive:Tracker) collects images from each of the cameras in which markers and stray reflections form white blobs against a black background (see Figure 4.10). Circles are fit to the blobs with the center of each circle corresponding to a ray extending from the camera. If rays from multiple cameras nearly intersect at a point, then the reconstructed position is recorded as an observed marker. Previously defined rigid body models are then compared with the observed markers. If a set of observed markers corresponds well with a rigid body, then they are labeled. The positions of the labeled markers are then broadcast to the synchronization software (The MotionMonitor). The synchronization software records the data streams from the motion capture system, the microphone, and the bridge sensors. After the experiment is over, we export the data from the synchronization software for pre-treatment and analysis in Mathematica, Matlab, or Python.

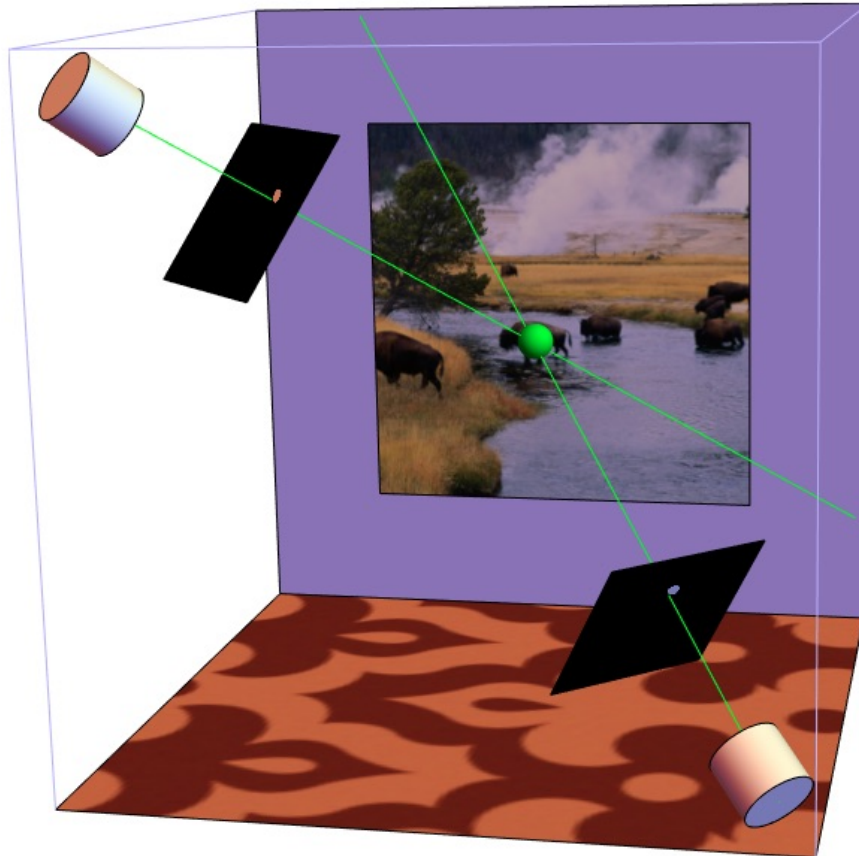


FIGURE 4.10: A conceptual schematic of the motion capture system. The two cylinders represent cameras. The data collected by the camera is projected onto the imaging planes. Rays extending from the cameras through the blobs in the images nearly intersect. The position of the object is reconstructed by finding the point which best describes the approximate intersection of all involved rays.

The MotionMonitor software collects the broadcast motion capture signals from Motive:Tracker and samples the data acquisition card for the signals from the bridge sensor or force transducer. Nothing else is running on the computer, so presumably the operating system is not inserting interrupts in queue which would affect synchronization. Beyond that we are only looking for synchronization accuracy at 120 Hz (the rate of motion capture). The shape of the load cell signal follows the shape of the hair depth measurement (Figure 4.11), and the piezos and motion capture signals agree on the moment when the bow changes direction (Figure 4.12).

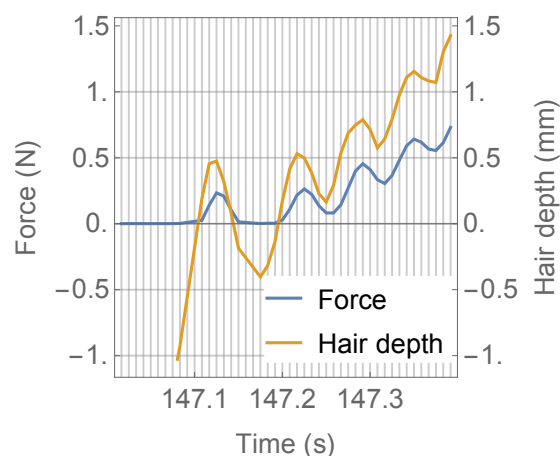


FIGURE 4.11: The force signal measured by the force transducer follows the hair depth signal from motion capture measurements. The vertical grid lines indicate when motion capture measurements were taken. The 15 Hz variation in the force is due to the bow bouncing when placed on the load cell.

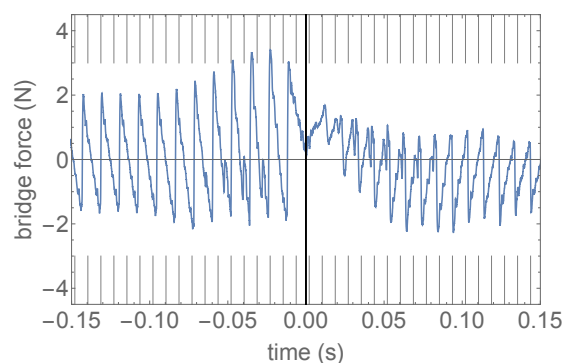


FIGURE 4.12: The force signal measured by the piezos during a bow change. The vertical grid lines indicate when motion capture measurements were taken. The origin of time is defined as the moment when a linear interpolation of the bow speed crosses zero. The piezo signal shows the final slip before the bow change, a period of constant sticking as the bow pulls the string first in one direction and then in another, followed by the first slip after the bow change. That the piezo signal goes through its minimum at $t = 0$ is an indication of good synchronization between the signals.

4.3.1 Using rigid body models to find landmarks

When we described the extraction of bowing parameters from motion capture data in Section 3.2, we assumed that we knew the positions of certain landmarks; namely, the endpoints of the hair ribbon and the endpoints of the string. Unfortunately, we

cannot place markers directly at these landmarks because they might bother the musician. In this section, we discuss how we create rigid bodies before the experiment and how we use them to estimate the positions of landmarks during pre-processing after the experiment.

Before the experiment, markers are placed in convenient locations on the force transducer, cello, and bow as described in the sections that follow. The markers are labeled in the motion capture software, and a recording of their static positions is made. We then use various strategies (described in the sections that follow) to define the positions of interesting landmarks with respect to the positions of the markers. The set of marker and landmark positions constitutes a rigid body model.

During the experiment, the marker positions are tracked. The motion tracking data has three problems: (1) positions of landmarks are unknown, (2) sometimes a marker is occluded giving no position information, and (3) often the rigid body constraints are not respected exactly. All three of these problems are solved by finding an optimum translation and rotation which maps the rigid body model as closely as possible to the observed markers (Figure 4.13). The optimization minimizes the total squared distances between the rigid body markers and the corresponding observed markers.

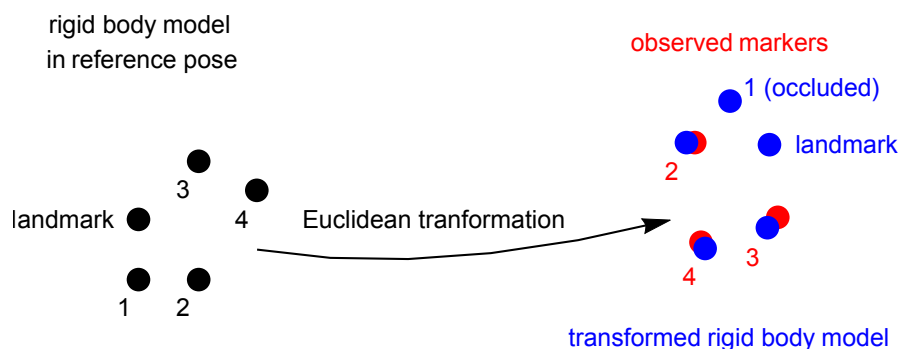


FIGURE 4.13: A rigid body model includes the relative positions of its markers and landmarks. The set of observed markers (red) are missing landmarks and occluded markers. An optimal Euclidean transformation maps the rigid body model from its reference position (black) to a position and orientation (blue) close to the corresponding set of observed markers, reducing measurement error by enforcing rigid body constraints. The positions of landmarks and occluded markers are reconstructed from the transformed rigid body model.

Finding the least squares rigid body transformation between two corresponding sets of points is a well-known problem. It is usually described as finding an ideal rotation and translation. Finding the best translation is trivial: just map the centroid of one set of points onto the centroid of the other set. Finding an arbitrary matrix which minimizes the total squared distances is also relatively easy when posed as an ordinary least squares linear parameter estimation problem (section 4.2.2). The problem lies in restricting ourselves to orthogonal matrices (i.e. rotations) while performing the minimization. This problem is known as the Orthogonal Procrustes Problem and was solved in (Schönemann, 1966) based on the singular value decomposition of the covariance matrix between the reference and rotated data sets. Explicitly applying Schönemann's solution to the rigid body transformation problem was shown in (Arun, Huang, and Blostein, 1987). Arun's algorithm is presented below for convenience.

Begin with the two ordered sets of points {model: $\vec{x}_i = x_i^1 \vec{e}_1 + x_i^2 \vec{e}_2 + x_i^3 \vec{e}_3$ } and {measurements: $\vec{y}_i = y_i^1 \vec{e}_1 + y_i^2 \vec{e}_2 + y_i^3 \vec{e}_3$ } for $i = 1, \dots, n$ in which points with the same indices correspond to each other.

1. Calculate the centroids of each set of points.

$$\vec{x}_0 = \frac{1}{n} \sum_{i=1}^n \vec{x}_i = x_0^1 \vec{e}_1 + x_0^2 \vec{e}_2 + x_0^3 \vec{e}_3 \quad \vec{y}_0 = \frac{1}{n} \sum_{i=1}^n \vec{y}_i = y_0^1 \vec{e}_1 + y_0^2 \vec{e}_2 + y_0^3 \vec{e}_3$$

2. Calculate the deviations of each point from its centroid.

$$\vec{X}_i = \vec{x}_i - \vec{x}_0 = X_i^1 \vec{e}_1 + X_i^2 \vec{e}_2 + X_i^3 \vec{e}_3 \quad \vec{Y}_i = \vec{y}_i - \vec{y}_0 = Y_i^1 \vec{e}_1 + Y_i^2 \vec{e}_2 + Y_i^3 \vec{e}_3$$

3. Calculate the 3×3 cross-correlation matrix of the deviations.

$$\mathbf{C} = \left(\sum_{i=1}^n X_i^r Y_i^c \right)_{[r \in \{1,2,3\}, c \in \{1,2,3\}]}$$

4. Calculate the singular value decomposition (SVD) of the cross-correlation matrix.

$$\mathbf{U} \mathbf{\Lambda} \mathbf{V}^T = \mathbf{C}$$

5. Calculate the rotation matrix

$$\mathbf{R} = \mathbf{V} \begin{pmatrix} 1 & 0 & 0 \\ 0 & 1 & 0 \\ 0 & 0 & \det(\mathbf{V} \mathbf{U}^T) \end{pmatrix} \mathbf{U}^T$$

where the determinant $\det(\mathbf{V} \mathbf{U}^T) = \pm 1$ ensures that \mathbf{R} is a rotation matrix rather than a reflection matrix.

6. Calculate the translation vector

$$\vec{t} = \vec{y}_0 - \mathbf{R}(\vec{x}_0)$$

7. Calculate the corrected positions

$$\vec{y}_i' = \vec{t} + \mathbf{R}(\vec{x}_i)$$

4.3.2 Force transducer markers and reference frame

The force transducer is used for building a model of the effective hair compliance (see section 3.3.2). The force transducer consists of an aluminum wedge mounted on a sensor which is held in position by a wooden support (see figure 3.6). Markers placed on the force transducer allow us to track its pose with the motion capture system while the sensor itself measures the force applied by the bow on the wedge. From the markers we need to establish the position of at least one of the corners of the aluminum wedge's upper edge, the orientation of that edge, and the orientation of the sensor's measurement axis.

Six markers are attached to the force transducer: one on each corner of the upper edge defining the edge line, two on the base forming a line which is approximately orthogonal to the edge line, and two more on the wedge for redundancy (see figure 3.6). We decided to identify landmarks directly by placing markers exactly at the positions of the landmarks. This was possible because the markers will not interfere with the bow during the hair compliance measurements.

Placing a marker at a landmark is the easiest method of defining a landmark position. However, systematic errors may occur due to human error when placing the marker. There is always a slight offset between the geometric center of a marker and the surface it is mounted on. This presents a problem because a landmark is represented by the geometric center of the marker, but we usually want the landmarks to lie on the surface. We minimize this kind of error by using small markers (3 mm hemispheres) whenever necessary. In the case of the load cell, we need two markers to define the edge line representing a perfectly rigid string. Rather than mounting these markers on top of the edge surface (see the red marker in Figure 4.14), we place them on the ends of the edge line so that the centers of the markers are aligned with the upper edge (see the blue marker in Figure 4.14). This should eliminate the systematic error coming from marker geometry, leaving only human placement error.

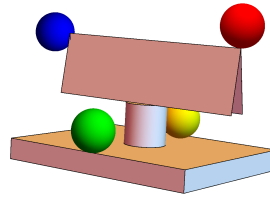


FIGURE 4.14: Schematic of the force transducer. The red and blue markers in this figure are intended to define the edge line which is orthogonal to the vertical axis of the force sensor. The centroid of the red marker is well above the edge line, giving a systematic error. The blue marker is placed well. The green and yellow markers define a second direction orthogonal to the load cell axis.

While the markers on the ends of the edge line must be placed accurately, the markers on the base can be placed somewhat arbitrarily. This is because the edge line and the support base are both orthogonal to the axis of the force sensor. As long as the markers on the base do not form a line parallel with the edge line, then we will be able to construct an orthonormal set of basis vectors indicating the direction of the edge line \hat{y} , the direction along the force sensor axis \hat{z} , and the approximate direction of bow movement from frog to tip \hat{x} . The calculations are as follows:

The markers lying on the edge line represent the position of the string endpoint at the bridge (\vec{r}_B) and nut (\vec{r}_N). These markers define the direction of the edge line unit vector \hat{y} . We just need to find their difference vector and normalize it to get the unit vector pointing from bridge to nut.

$$\hat{y} = \frac{\vec{r}_N - \vec{r}_B}{|\vec{r}_N - \vec{r}_B|} \quad (4.12)$$

The markers lying on the support base represent the positions of the treble (\vec{r}_L) and bass (\vec{r}_R) corners of the cello's front plate. They define a direction which is orthogonal to the force sensor axis, and they approximate the expected direction of bow movement from frog to tip. To define \hat{x} , we use the standard Gram-Schmidt orthonormalization procedure. We find the orthogonal projection of the difference vector onto \hat{y} (the part parallel to \hat{y}) and subtract it from the complete difference vector. This leaves us with a vector which is orthogonal to \hat{y} . The final step is to normalize this orthogonal vector.

$$\hat{x} = \frac{(\vec{r}_L - \vec{r}_R) - ((\vec{r}_L - \vec{r}_R) \cdot \hat{y})\hat{y}}{|(\vec{r}_L - \vec{r}_R) - ((\vec{r}_L - \vec{r}_R) \cdot \hat{y})\hat{y}|} \quad (4.13)$$

The axis of the force sensor is assumed to be orthogonal to both \hat{y} and \hat{x} due to the construction of the wedge and support base. The three-dimensional vector cross-product of \hat{y} and \hat{x} gives a vector which is orthogonal to both of them, proportional to both of their lengths and the sine of the angle between them, and is oriented according to the "right hand rule." Since \hat{y} and \hat{x} are orthonormal, their cross-product will already be normalized.

$$\hat{z} = \hat{x} \times \hat{y} \quad (4.14)$$

4.3.3 Cello markers and reference frames

The cello is used as a reference for describing the relative motion of the bow (see sections 3.2.1 and 3.2.2). From the cello markers, we need to identify the positions where each string meets the bridge and nut, and the orientation of each string (figure 4.15).

We cannot place markers directly at the points of interest on the cello as we did with the force transducer. We can only place the marker on top of the string, rather than in line with its axis as we did on the force transducer. Additionally, the cellist may touch the marker at the nut with their finger or the marker at the bridge with the bow, thus disturbing the experiment when the marker moves or falls off completely. We could just ask the musician to be careful with the markers, but that raises their awareness of the experimental condition, possibly leading to unnatural behaviors. Fortunately, there are a few methods for tracking landmarks without needing markers at those locations during the experiment.

We first tried a method using a stylus to indicate the landmark positions relative to more conveniently placed markers. The stylus was a piece of plastic having three markers arranged in a triangle and a corner designated as the tip. The stylus was calibrated by measuring the positions of the stylus markers as it is pivoted on its tip about a fixed point. Sphere-fitting algorithms are then used to define the position of the stylus tip with respect to its own markers. We then temporarily place the tip of the stylus at the desired landmark and measure the position of the tip (as calculated from the stylus markers) with respect to the positions of the cello markers. This sounds great in theory, but in practice, the stylus should be quite large with many markers forming a 3-dimensional branching tree. At the time, we only had a few markers to use as a stylus and the stylus suggested to us was rather small. Beyond issues of stylus design, there is the fundamental problem of estimating the position of its tip via sphere-fitting. Sphere-fitting algorithms tend to predict smaller radii and require data points over

large angles. It turns out that "large angles" seems to mean about 270° around a great circle.

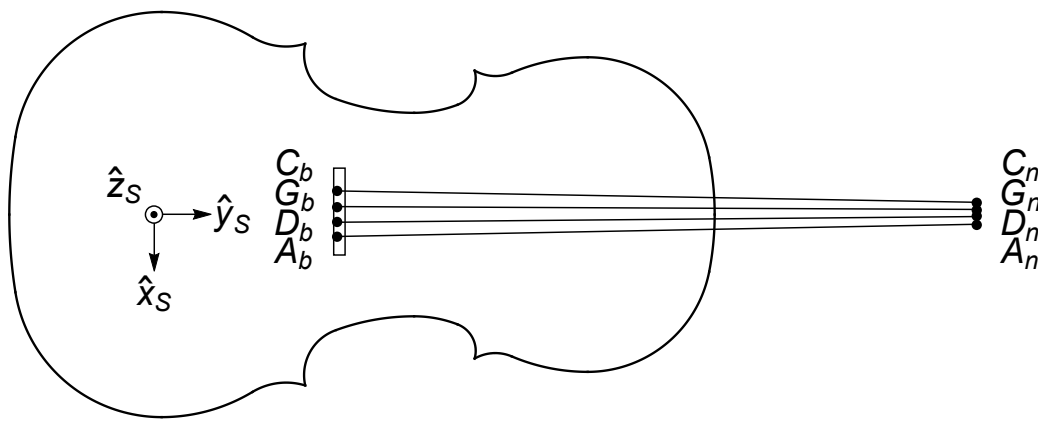


FIGURE 4.15: Landmarks are placed at the intersections of each string with the bridge and nut.

Better methods for defining landmark positions include using two sets of markers: one temporary and one permanent. The temporary markers are used to define landmarks at the nut and bridge with respect to the positions of the permanent markers. The permanent markers are placed at convenient locations which will not disturb the player and the temporary markers will be removed during the experiment; thus the markers will not present any problems to the musician.

We tried to place temporary markers as close to the desired landmarks as possible. In our case, this meant finding the smallest markers that can be tracked by our system (3 mm diameter hemispheres) and placing them directly on top of the strings. This gives some systematic error as discussed in section 4.3.2, but it is much less than the errors we got using a stylus.

The best method we came up with was to place several temporary markers along the length of the string. The markers were not all placed on top of the string, but also on the sides of the string, so that a projection of the markers along the string axis would form a circular arc. We aimed to occupy about 270° of arc with markers. It is important to make sure that the centers of the markers are well aligned with the radii of the string and that you use an adhesive with a very thin, uniform thickness, such as double-sided tape. We then calculated the First Principal Component of the temporary marker positions to find the orientation of the string axis. The temporary marker positions are then projected onto a plane orthogonal to the string axis. Next, we use a circle-fitting algorithm (hyperSVD) having no intrinsic bias from (Al-Sharadqah, Chernov, et al., 2009) to locate the position of the string axis.

Having found an infinitely long line which represents the string, we need to identify the endpoints which represent the nut and bridge. To define the nut endpoint, we placed a temporary marker on the nut between strings I and II and another between strings III and IV. These two markers define the "nut line" which passes close to the desired endpoint. We then found the point on the string axis which is closest to the nut line. To define the bridge endpoint, we placed three markers on the top edge of the bridge (one between each pair of strings). These temporary markers define the "bridge plane" which is approximately orthogonal to the string axis. The intersection of the string axis with the bridge plane defines the bridge endpoint of the string.



FIGURE 4.16: Here we see four markers on the front, three markers on the side, three markers on the scroll, two temporary markers on the nut, and three temporary markers on the bridge.

Now we need to decide where to place permanent markers on the cello (Figure 4.16). The markers have to be visible to the cameras, but cannot disturb the musician. These markers will define the orientation of the cello axes, so we might as well choose the marker positions so that defining these axes is easy. For this reason, we place one marker in each of the lower bout corners. These markers define a direction \hat{x} which is parallel to the bridge plane.

We need at least three markers in the form of an asymmetric triangle to define a rigid body. To have better estimates of the landmarks, they should lie within the region bounded by the permanent markers if possible (i.e we want to interpolate, rather than extrapolate positions). For these reasons, the next marker we place is on the scroll. This allows us to interpolate the positions of the landmarks in the plane of the top plate. We will still have to extrapolate the height of the landmarks, but there is no getting around that since the landmarks are elevated above the front plate.

The more spread out the markers are, the better we can estimate the orientation of the cello. The problem is that having markers spread out makes it difficult to make sure that they are all within the camera frame at the same time, particularly with one marker next the cellist's head. So we add some redundant markers and create separate

rigid body models which can be combined in pre-processing. That way if the scroll is completely hidden from view, we can still use the visible markers on the front plate to estimate the position and orientation of the cello. Since the markers on the scroll are far from the markers on the front plate, we placed a few redundant markers on the scroll to reduce the influence of errors in any one of them. This may also reduce the chances of having all of them occluded by the cellists head.

Finally, the position and orientation of the cameras tends to favor certain measurement planes over others. In particular, if our cameras were placed in a plane, then we would have good measurements parallel to that plane, but we would not have good depth measurements orthogonal to that plane. We have already taken steps to reduce this problem by arranging the cameras on a spherical shell, creating several preferred planes. We can further reduce the problem if the rigid body has multiple planes to present to the cameras. For this reason we added another three markers on the ribs of the treble side. One was placed on the upper bout near the front plate corner, the other two were placed near the front and back plates of the lower bout where it is widest.

With these markers placed and the landmarks defined, we can then define the reference frames attached to each string. Each string has an origin where it meets the bridge which is one of our landmarks. Each string has an axis \hat{y}_S from the bridge (\vec{r}_B) to the nut (\vec{r}_N).

$$\hat{y}_S = \frac{\vec{r}_N - \vec{r}_B}{|\vec{r}_N - \vec{r}_B|} \quad (4.15)$$

The markers located at the bass (\vec{r}_R) and treble (\vec{r}_L) corners of the front plate define a line that is parallel to the bridge plane. This line defines horizontal in the global reference frame of the bridge, which we can take advantage of for easily applying string vibration polarizations to the bridge mobility measurements to get an idea of how the bridge moves while playing. Instead of taking the direction of this line as it is, we will use only the part which is orthogonal to the string axis because we want to build an orthonormal reference frame for the string.

$$\hat{x}_S = \frac{(\vec{r}_L - \vec{r}_R) - ((\vec{r}_L - \vec{r}_R) \cdot \hat{y}_S)\hat{y}_S}{|(\vec{r}_L - \vec{r}_R) - ((\vec{r}_L - \vec{r}_R) \cdot \hat{y}_S)\hat{y}_S|} \quad (4.16)$$

The third direction \hat{z}_S of the string's reference frame is orthogonal to the other two and is oriented from the plate to the strings. We take advantage of the vector cross-product to create an orthogonal vector with the correct orientation. Since \hat{x}_S and \hat{y}_S are orthonormal, their cross-product is already normalized.

$$\hat{z}_S = \hat{x}_S \times \hat{y}_S \quad (4.17)$$

4.3.4 Bow markers and reference frames

The bow has been modeled by other groups as a single rigid body for the purposes of motion tracking (Marchini et al., 2011). A 6-degree-of-freedom sensor was placed at the frog and a bow force model based on the frog-to-string distance and hair depth were created using methods similar to what we described in Section 3.3.2. Marchini et al. report problems with the performance of their bow force model near the tip, and suggests the problem lies in the model failing to completely account for the deformation of the bow. However, a more important problem, as I see it, is that the bow is

quite long, and small errors in the measured orientation of the rigid body at the frog cause large errors in estimating the bow depth of a rigid bow near the tip. A typical orientation error of 0.5° gives 1 mm errors in bow depth at distances from the frog of just $1/5$ of the 600 mm hair length. Whenever possible we should interpolate positions between markers, rather than extrapolating positions beyond a set of markers. By placing a second rigid body at the tip, we can minimize the orientation error of the hair and achieve better estimates of the bow depth.

While the presence of a second rigid body allows us to measure the rotation of the tip with respect to the frog (another measure of bow deformation), this extra measurement is a monotonic function of the previously known bow depth, and thus its inclusion does not necessarily introduce extra information or produce a better model. Including the tip rotation might improve the model in cases where the tip rotation is more accurately measured than the hair depth, i.e. near the tip. Unfortunately, such a model becomes very sensitive to errors in the calibration measurements near the tip. Using the tip rotation instead of the bow depth only presents a possible improvement in the region between $4/6$ and $5/6$ of the bow length from the frog. I believe the improved performance of the model presented in (Llimona, 2014) over that presented in (Marchini et al., 2011) may be attributed to the increased accuracy of measuring bow depth.

For the purposes of motion tracking (i.e. improved estimates of bow depth), we model the bow as two rigid bodies: one at the tip and one at the frog (Figure 4.17). Each of these rigid bodies has its own reference frame and its own origin. The origin of the frog rigid body is located in the middle of the hair where it meets the ferrule H_F . The origin of the tip rigid body is located in the middle of the hair where it meets the tip plate H_T . The frog and tip reference frames are initially aligned with the hair reference frame (see section 3.2.1), but rotate when the stick bends.

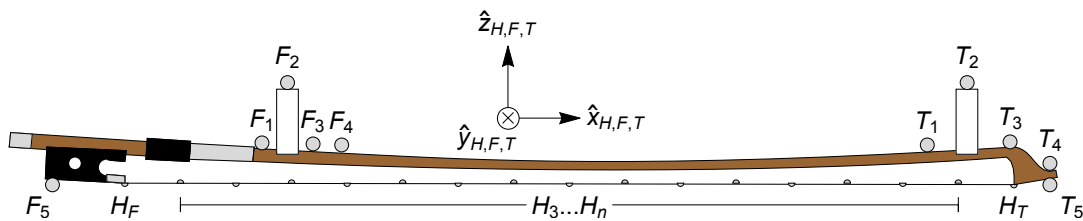


FIGURE 4.17: The bow is modeled as two rigid bodies. Styrofoam antennas are placed near the frog and tip. Spherical passive reflective markers with 6.4 mm diameters are used to track the position of the two rigid bodies. Hemispherical markers with 3 mm diameters are temporarily placed on the hair ribbon to define the positions of the endpoints relative to the larger markers. The smaller markers are removed before the experiment. We are interested in the positions of the points H_F and H_T and the orientations of the three reference frames (Hair, Frog, and Tip).

Markers are shown three times larger for clarity.

The position and orientation of a rigid body can be determined by as few as three markers arranged in an asymmetric triangle. To have reliable orientations, the base and height should be as large as possible. While the bow stick offers plenty of length for a large base, it does not have much vertical height. An obvious solution is to place markers underneath the tip T_5 and the frog F_5 . We do this, but it is not ideal because those markers are often occluded by the player's hand or by the bow itself. To make

sure that a planar set of markers is always visible, we attach small styrofoam antennas to the bow using an easily removable sticky putty (Pat-a-Fix). Special care should be taken in orienting the antennas to avoid the base of the frog antenna from touching strings and to avoid the top of the tip antenna from touching the upper corner of the cello's c-bout when the musician tilts the bow toward the thumb.

Markers are attached to the bow using sticky putty at the locations shown in figure 4.17 for the duration of the experiment. The markers $F_1 \dots F_5$ are used to estimate the position of the end of the hair ribbon at H_F . The markers $T_1 \dots T_5$ are used to estimate the position of the end of the hair ribbon at H_T . Note, although markers F_5 and T_5 protrude only slightly below the hair ribbon, they cannot be brought closer to H_F and H_T because they may get caught on the adjacent strings while playing, and thus disturb the player.

Most of the bending occurs in the middle of the stick. The tip rigid body markers do maintain their rigid body relations. But the markers $F_1 \dots F_4$ are a bit further from the frog than the ideal. The bending of the stick causes these markers to move closer to the line defined by F_5 and H_F . This means that the rigid body relation used to estimate the position of H_F relative to $F_1 \dots F_5$ introduces some systematic error depending on the amount of stick bending. This shouldn't be a problem though because the empirical model for the hair compliance (section 3.3.2) should automatically take this error into account.

We originally tried to estimate the positions of H_F and H_T using a stylus as described in Section 4.3.3, but had large systematic errors as explained in that section. We then tried using markers placed with putty, but found unacceptable errors due to the marker centroids not lying on the surface of the hair. Additionally, the inconsistent thickness of the putty lead to a systematic error which varied linearly from frog to tip. We finally used a procedure using many markers temporarily placed on the bow hair, similar to the procedure used for estimating the endpoints of the string in Section 4.3.3. It is quite easy to miss the centerline when placing a marker on the hair ribbon. Fitting a line to these misplaced markers would give errors in the plane of the hair ribbon as well as the unavoidable errors in the direction orthogonal to the ribbon. For this reason we decided to fit the markers to a plane and then identify a line within the plane. This should concentrate all the within-plane errors into the placement of the H_F and H_T markers, which is minimized by placing them with care.

To define the position of the hair ribbon endpoints relative to the rigid body markers, we use double sided tape³ to temporarily add small markers at H_F , H_T and at several staggered positions spanning the width and length of the hair ribbon on both its top and bottom surfaces. We find the plane which best fits these markers by minimizing the total squared distances between the markers and the plane. Then we find the points in this hair ribbon plane which are closest to the markers that we placed at H_T and H_F .⁴ Finally, we calculate the position of H_F relative to the frog rigid body markers, and the position of H_T relative to the tip rigid body markers.

The axes of the hair are based on the position of the tip H_T and frog H_F and the orientation of the stick as indicated by one of the frog markers F_1 . The axes are constructed using the previously described Gram-Schmidt orthonormalization procedure.

³It was not fun removing the tape from the bow hair. The temporary markers were attached using double sided tape because it is thin and has a constant thickness.

⁴We tried to identify these endpoints using a stylus and we also tried using a marker attached with putty, but the method described in the text gives the smallest systematic error. The error is reduced because measurement errors are averaged out over the many markers attached to the hair ribbon.

The \vec{x}_H axis points from frog to tip.

$$\vec{x}_H = \frac{\vec{r}_{HT} - \vec{r}_{HF}}{\|\vec{r}_{HT} - \vec{r}_{HF}\|}$$

The \vec{z}_H axis points from hair to stick.

$$\vec{z}_H = \frac{\vec{r}_{F1} - \vec{r}_{HF} - ((\vec{r}_{F1} - \vec{r}_{HF}) \cdot \vec{x}_H)\vec{x}_H}{\|\vec{r}_{F1} - \vec{r}_{HF} - ((\vec{r}_{F1} - \vec{r}_{HF}) \cdot \vec{x}_H)\vec{x}_H\|}$$

The \vec{y}_H axis points from fingers to thumb.

$$\vec{y}_H = \vec{z}_H \times \vec{x}_H$$

4.4 Discussion of errors

In the previous three sections, we presented a number of techniques for estimating the positions of landmarks from the measured positions of markers. The two methods which seemed to minimize systematic errors were placing small markers directly on the landmark (at least temporarily), or using temporary markers to define a plane (in the case of the hair ribbon) or a cylinder (in the case of the string). After the experiment was completed, we tried to estimate the endpoints of a cello string using both of these methods. Temporary markers were placed along the string, including one at the nut and one at the bridge. Then ten seconds of data were recorded while the cello sat motionless. The temporary markers were removed. We attempted to replace the markers at the nut and bridge at their original positions. The other markers along the string were placed without reference to their previous positions, and another recording was taken. The process was repeated for a total of five recordings.

Calculating the variability in the position of the fixed markers between recordings gives a measurement precision between 0.2 mm and 0.3 mm. The same analysis on the temporary markers at the nut and bridge gives a standard deviation of 0.9 mm, an indication of human error in placing markers. We then apply the cylinder-fitting algorithm to the temporary markers on the string to estimate the landmarks at the nut and bridge. The variability of those estimates was 2.0 mm. One of the estimates failed to fit a cylinder with a reasonable radius. After discarding that measurement, the variability was reduced to 1.3 mm. I could not believe such a terrible result, after all, the method seemed to give good results before. So I made a simulation of the procedure (placing markers, cylinder-fitting, repeat for 1000 measurements) and found that the errors followed a Maxwell-like distribution with a heavier tail. The most-probable error was around 0.6 mm, only slightly better than our observed human error, but errors around 1.3 mm were still quite probable. The error seems to come from slight errors in the estimated orientation of the axis and over-estimation of the circle radius, leading to significant errors in the estimated positions of the endpoints.

Given that the cylinder- and plane-fitting algorithms involve so much extra effort and time while not even guaranteeing more than a slight improvement, I suggest that we simply place temporary markers on top of the landmarks and develop a robust procedure for correcting the placement error. I think the first step toward reducing the placement error is to make an object which registers against the nut/bridge and the

strings which acts as a physical stop. When placing the markers on the landmarks, you will know they are in the correct place because they are touching the physical stop.

Chapter 5

Experiment

Before a musician will buy an instrument, they will borrow it for an extended period of time (several days to several weeks) and play it in various venues with other musicians. They will compare it with other instruments and ask the opinions of other musicians. It may take more than a year to become fully aware of what can be done with the instrument. But before they borrow the instrument, they first perform a short evaluation of the instrument at the seller's studio to determine whether the instrument has any potential. It is this initial encounter with the instrument that we wish to study. What do musicians do during the initial evaluation? What qualities must the instrument have to pass to the next phase of the purchasing decision? How do the actions of the musician affect her perception of the qualities of the instrument? This thesis is an exploratory observation of initial evaluations. As such, we don't expect to answer these questions, but to generate a few hypotheses for further research. In any case, this context defines some parameters of our experiment: we will need at least one professional musician with experience evaluating instruments, at least two cellos, and plausible contexts for performing on, evaluating, and comparing these instruments.

Suppose the musician were to describe a difference between the sounds of two instruments. We could examine the recordings of these sounds and study the differences of sound attributes, but we would not be able to say whether the difference is because the instruments are different or because the musician played the instruments differently. For this reason, not only do we need a microphone to record the sounds produced by the instrument, but also a system for measuring the control parameters used to generate those sounds. Our system includes an optical motion capture system and a bow force model based on the motion capture data.

We are particularly interested in the perception of playability because the literature has proposed a hypothesis about it. Namely the mobility of the bridge affects the motion of the string, and the player perceives this effect as she tries to control the string's vibrations. If the player is more able to reliably and quickly initiate and sustain a desired string motion (usually Helmholtz motion), then the instrument is more playable. This hypothesis guides our interpretations of the results of simulations and the design of future experiments. But the hypothesis itself has not yet been tested, and questions remain about how to interpret the existing results outside of the experimental context which produced them. For example, the Schelleng diagram is defined in terms of steady-state gestures, but we would like to use it to frame our discussions of non-steady gestures. Also, the Guettler diagram—based on a small set of possible control parameter gestures—leads to predictions which contradict our impressions of real playing. So in addition to recording the radiated sound and the applied control parameters, we will also need to measure the bridge mobility and record the string motions to test the playability hypothesis. We use a common procedure for measuring the bridge mobility using an accelerometer and an impact hammer. We use piezoelectric sensors

embedded in the bridge underneath each string to measure the string motions (see Section 4.2).

5.1 Prior observations

We developed our protocol based on our observations of how cellos are evaluated and compared. Violoncelle En Seine was a competition in Paris, 2014 for cello makers where we observed four professional cellists evaluating forty cellos. They were asked to identify the four best cellos and rank them, ultimately choosing a favorite. Although a questionnaire was provided to give structure to their evaluations, none of the cellists respected it, finding it confusing, tedious, or unnecessary. They made only brief comments in certain fields of the questionnaire or assigned only an overall pass/fail judgement.

After evaluating about six cellos, all cellists began using initial evaluations of 1-2 minutes to reject cellos which were worse than at least four of the previously evaluated cellos. Further rounds of rejections were performed until about eight cellos remained. Then the musicians compared cellos, usually in pairs but sometimes taking up to four at a time. During this phase, the cellos were played about 30 seconds to 2 minutes each before switching to another cello, with the number of swaps depending on the decisiveness of the cellist. Once the top four cellos were identified, rankings four and three were quickly assigned, with ranking two and the favorite taking longer.¹ One cellist evaluated all the cellos in a hallway, another performed the first round of eliminations in practice rooms and finished the evaluations in a large classroom, the other two cellists evaluated the cellos in a large classroom. Each cellist used his own bow.

We noticed that only one cellist used scales and sounds outside of a concrete musical context, and that all cellists primarily used a few excerpts from their solo repertoire to form their opinions. Each excerpt was used to evaluate multiple aspects of the cello, such as its response in quick passages, its expressiveness in slower passages, its power in the lower register, its projection in the upper register, or its homogeneity across registers. Among the commonly used excerpts were various movements from the Bach suites, the introduction to the Brahms' Sonata No. 1, and the beginnings of several concertos (Saint-Saëns, Elgar, Dvořák, . . .).

5.2 The musicians

We report on the observations of a single cellist playing two of our cellos using our bow. She has fifteen years of professional experience participating in soloist competitions, chamber music groups, and orchestras. She regularly uses two cellos, corresponding to the two cities in which she divides her time. She often tries other cellos out of curiosity and is constantly keeping an eye out for another instrument for personal use. Two other professional cellists, two amateur cellists and myself were observed playing these two cellos during the development of the equipment and experimental protocol. While quantitative measurements are not available for these players, I will refer to their comments as appropriate.

¹It is interesting to note that there was considerable overlap in the top four instruments of each cellist. However, these shared instruments were ranked differently by each cellist.

5.3 The two cellos

In the beginning, we thought it would be useful to cello makers if we could connect any perceived differences directly to known changes in setup. For this reason, we commissioned two identical cellos and a bow of corresponding quality. The construction of the instruments was completed about a year and half before the experiment at a european workshop and were setup and adjusted by our luthier. Initially, the cellos were perceived as being effectively identical; bridge mobility measurements were very similar and amateur and professional players could not reliably distinguish between them while playing. We then modified the bridges by embedding sensors under each string as described in section 4.2. After several evaluations of the cellos by amateur cellists, the luthier determined that one cello (Cello A) could be made more "souple" [flexible] and the other (Cello B) more "rigide" [rigid] by replacing the sound-posts. A small mass was also added to the underside of the "rigide" cello's tailpiece near the fine tuner of string IV. The cellos are consistently rated as good quality student cellos.

The goal of the sound-post adjustments was to make the instruments distinguishable. We wanted each cello to correspond to the playability preferences of different hypothetical musicians. We didn't want to introduce obvious playability *problems* though. The musicians would be asked to evaluate each instrument for half an hour to an hour, which is something they would not normally do for instruments that have problems. The amateur and professional cellists were capable of distinguishing the two after their evaluations.

5.4 The bow

The cellists at Violoncelle En Seine each used their own bow. They admitted that they could assess cellos using another bow, just as they can perform on cellos which are not their own when necessary. However, they did insist that they would prefer to use their own bow and doubted whether their assessments of the cellos would be as accurate using another. This motivated us to find ways of tracking the bowing parameters using only temporary modifications to bows, which could possibly be applied to the musician's bow if permitted. The modifications should not noticeably change the playing characteristics of the bow or disturb the player's use of the bow. We decided to use optical motion tracking using markers placed on the bow (Section 4.3.4) to track the bowing parameters (Section 3.2 and to estimate the bow force (Section 3.3).

Our luthier provided us with a bow of a quality commensurate with the quality of the cellos. We attached markers to the bow using a sticky putty which does not damage the bow. During early evaluations, a professional cellist and three amateurs accepted the bow as the tool for doing the assessment and made no complaints about not using their own bow. Moreover, even though the musicians were assured that their bows would be safe, they were still reluctant to allow mounting the markers to their own bows. For this reason we decided that we would impose our bow on the musician during the experiment. We gave the bow to the musician the day before the experiment with the agreement that she would practice at least an hour with the bow to become familiar with it.

5.5 Repertoire selection

The repertoire was chosen based on our observations at Violoncelle En Seine and comments made by cellists who evaluated our cellos while we were developing the hardware and experimental protocol. We restricted ourselves to music that is likely to be familiar to the musician, would be easy enough to adequately prepare before the experiment with little notice, and which would be useful for evaluating instrument. We deemed a set of excerpts to be potentially useful if it represented notes on all four strings, played at different dynamic levels, with different articulations, and different tempos.

Gabriel Fauré - Élégie

The figure shows two excerpts from Gabriel Fauré's Opus 24, Élégie. The first excerpt is marked *f* and the second is marked *pp*. Each excerpt consists of a melodic line with fingerings and bowing directions, and a corresponding string location line with fret numbers.

Excerpt 1 (f):

- Melodic line: $\overset{2}{\downarrow}$ $\overset{1}{\downarrow}$ $\overset{1}{\downarrow}$ $\overset{3}{\downarrow}$ $\overset{1}{\downarrow}$ $\overset{3}{\downarrow}$ $\overset{4}{\downarrow}$ $\overset{2}{\downarrow}$ $\overset{1}{\downarrow}$ $\overset{2}{\downarrow}$ $\overset{1}{\downarrow}$ $\overset{4}{\downarrow}$ $\overset{3}{\downarrow}$ $\overset{2}{\downarrow}$ $\overset{2}{\downarrow}$ $\overset{4}{\downarrow}$ $\overset{2}{\downarrow}$ $\overset{1}{\downarrow}$ $\overset{4}{\downarrow}$ $\overset{3}{\downarrow}$ $\overset{1}{\downarrow}$
- String location line: 6-5-3-5-3-5 | 8-6-5-6-5-8 | 12-10-8-10-8-5 | 8-7-5

Excerpt 2 (pp):

- Melodic line: $\overset{3}{\downarrow}$ $\overset{2}{\downarrow}$ $\overset{2}{\downarrow}$ $\overset{3}{\downarrow}$ $\overset{2}{\downarrow}$ $\overset{1}{\downarrow}$ $\overset{4}{\downarrow}$ $\overset{2}{\downarrow}$ $\overset{1}{\downarrow}$ $\overset{2}{\downarrow}$ $\overset{1}{\downarrow}$ $\overset{4}{\downarrow}$ $\overset{3}{\downarrow}$ $\overset{2}{\downarrow}$ $\overset{2}{\downarrow}$ $\overset{4}{\downarrow}$ $\overset{2}{\downarrow}$ $\overset{1}{\downarrow}$ $\overset{4}{\downarrow}$ $\overset{3}{\downarrow}$ $\overset{1}{\downarrow}$
- String location line: 13-12-10-12-10-5 | 8-6-5-6-5-8 | 12-10-8-10-8-5 | 8-7-5

FIGURE 5.1: Excerpt from Gabriel Fauré's Opus 24, Élégie. The upper lines indicate the fingers and bowing directions used by the musician during the experiment. The lower lines indicate the string played and the location of the note on the string.

Earlier studies on the playability of cellos focused on the perception of the wolf note. So we decided to use an excerpt which includes notes in the region where wolf notes are usually found on cellos (around F_3 played on string III). This consideration lead us to the beginning of Fauré's Élégie (Figure 5.1) which includes notes in this region. This is a slow piece which is suitable for evaluating the expressiveness of the cello. It begins with a phrase played loudly with marked bow changes to evoke feelings of anger and sadness at the loss of a loved one. The phrase is then repeated but this time it is played quietly with less marked bow changes, demonstrating the repetition of thoughts and the changing emotions associated with grieving. The cellist further differentiates the repetitions by changing the string on which she plays the first few notes of the phrase. This repeated phrase contains three notes in the region associated with wolf notes: $E\flat_3$, F_3 , and G_3 played on string III. If the cello has a playability problem due to the presence of a wolf note, this excerpt is likely to demonstrate it when the cellist attempts to play softly during the second repetition. Unfortunately, our cellos do not have a prominent wolf note, so we were not able to observe its effect on the evaluations. Nevertheless, this excerpt is still useful for evaluating expressive passages on the upper two strings.

Johannes Brahms - Sonate

FIGURE 5.2: Excerpt from Johannes Brahms' Opus 38, Sonata No. 1 in E minor. The upper line indicates the fingers and bowing directions used by the musician during the experiment. The lower line indicates the string played and the location of the note on the string.

After modifying the cellos, one of the amateur cellists commented that the "souple" cello was slightly more powerful in the lower register but had a different tone as predicted by our luthier. Having identified this difference, we decided to include an excerpt which highlights it. We chose the opening phrase of Brahms' Sonata No.1 in E minor (Figure 5.2) because it was used by nearly every cellist we observed evaluating cellos. Played on the two lowest strings, it is especially useful for evaluating the power and tone of the lower register. The beginning of the phrase is played strongly while the end of the phrase ends in a decrescendo which allows the cellist to explore the range of timbres available in the lower register.

While Fauré covers the mid-high register and Brahms covers the low register, we still needed a piece which allows us to compare the two registers. The musicians at Violoncelle En Seine favored the Bach suites for this purpose which narrows our search. Since both Fauré and Brahms are both slower and more expressive pieces, we felt that we should balance the evaluation by including a faster movement which includes many bow changes and string crossings to test the response of the instrument. While many movements from the Bach suites feel fast and have many string crossings, most of them tend to connect notes without changing the bow direction. The Prelude to the Fourth Suite (Figure 5.3) however is exactly what we need. Additionally it features jumps from string IV to string I which juxtaposes the two registers that had the most differences between cellos according to the amateur musicians. We hoped that this juxtaposition might augment the perceived differences between the two cellos, leading to more easily understood comments during the experiment.

Bach - Suite IV, Prelude

The figure displays four systems of musical notation for an excerpt from Johann Sebastian Bach's Prelude to Cello Suite No. 4. Each system includes a bass clef staff with a treble clef staff below it. The upper staff shows the melody with bowing directions (V for up-bow, v for down-bow) indicated above notes. The lower staff shows the string positions and fingerings (numbers 1-5) for each note. The key signature is E-flat major (two flats) and the time signature is common time (C).

FIGURE 5.3: Excerpt from Johann Sebastian Bach's the Prelude to Cello Suite No. 4 in E \flat major, BWV 1010. The upper line indicates the bowing directions used by the musician during the experiment. The lower line indicates the string played and the location of the note on the string.

The Fauré and Brahms excerpts are familiar and easy enough to prepare in a short time. The Bach excerpt is well known, but it is more difficult than the other excerpts. The amateur cellists struggled with this excerpt, though the professional cellists did not. We wanted the musician to feel at ease during the experiment. We also wanted any noticed difficulties to be due to the limitations of the cello and not due to a lack of preparation of the cellist. For these reasons, we decided to provide the excerpts to the musicians before the experiment. The selected excerpts by Fauré, Brahms, and Bach as provided to the musician are in Appendix E. The excerpts were given to the musician the day before the experiment with the agreement that she would prepare them on her own instrument (and with our bow). While the excerpts have some suggested fingerings and bowings, the musician was given the freedom to choose her own fingerings and bowings.

5.6 Framing the experiment

We did not want the musician thinking that she was the object of our study because we did not want her to adopt unnatural behaviors. For example, (1) she could try to describe what she thinks most other cellists would have perceived, (2) she might play scales or other exercises that she believes should be done during a proper evaluation, but which she normally wouldn't do, or (3) she might act as if she were being judged personally. To elicit a natural performance from the musician in our laboratory setting, we needed to define an authentic task with a plausible context, explain the presence of our equipment, and reassure the musician that she was not the object of study.

We framed the experiment as an authentic evaluation task which explains the presence of the bridge sensors. The text given to the musician can be found in Appendix E. The musician was told that a composer at a music school had asked us to equip a pair of cellos with sensors that allow his students to interact with a computer during their final year exam. Before we can deliver the cellos, we need a few professional players to evaluate the cellos and record a few excerpts so that we can decide whether any adjustments are needed. The musician is asked to evaluate the two cellos, discussing any merits or faults that they may have, and to record a few excerpts.

The scenario doesn't explain the presence of the motion capture setup or why the evaluation had to be done in our studio. To explain this, we simply acknowledged that we *are* researchers, and that we are taking advantage of the opportunity to study how the instrument behaves in real playing situations. The motion capture system allows us to record real bow movements that could potentially be used as inputs in simulations of different cellos. We further explain that analyzing the data is difficult and that we rely on her expert comments to help us interpret the data. The effect is to present ourselves as incapable of judging the musician, thus assuring her that we are using her to study data; not using data to judge her.

5.7 Eliciting comments

From our observations at Violoncelle En Seine, we identified three distinct tasks that musicians do during their first encounter with cellos: perform on each cello, evaluate each cello, and compare pairs of cellos. We designed our experiment to include these three tasks.

The musician begins with at least ten minutes of free evaluation. She is free to tell us what she perceives during the free evaluation, but we pose no questions and we make it clear that we do not expect her to tell us anything. We do this because we don't want to influence how she evaluates the cellos with our comments/questions. We also don't want to distract her from the task by asking her to stop and find a way to express her perceptions using words. By being a non-participant observer, we hope to allow the musician to evaluate the cello as she would do naturally.

After ten minutes of free evaluation, if the musician is not ready to perform for the recordings, we encourage her to prepare the excerpts. Once the musician is ready to record her performance, we remind her of the goal of the task: to produce a recording which she is comfortable sharing with others and which gives an example of what is possible to do with the instrument. We permit as many recordings as she wishes and will only send the recording that she is comfortable sending. Specifically we are not asking her to perform her best (because we are not judging her), to make a recording she is happy with (because it may not be possible), or indicating any expectation of how

the music should be interpreted (because musicians are not told how to play the music used to evaluate an instrument). Thus, she is free to interpret the music according to her tastes and to the particularities of the cello without worrying that she will be judged by her performance.

After each recording of each excerpt we ask the musician two questions (Table 5.1). We ask whether the musician is satisfied, meaning that she is comfortable sending the recording to the school. If the musician is not satisfied, then we ask what she would like to change. The indicated changes help us to identify meaningful differences in the control parameters and instrument response between recordings. These differences tell us that properties should be less like what is shown in the first recording and more like what is shown in the final recording. If the musician is satisfied with the recording, then we ask what properties of the instrument are highlighted by the excerpt. This question gives the musician an opportunity to discuss observations (like positive impressions) which were not elicited by the previous question.

- Are you satisfied with this recording?
- If not, what would you like to change?
- If so, what properties (merits or faults) of the instrument are demonstrated by this extract?

TABLE 5.1: Questions asked after each recording of each excerpt.

Once the musician has finished recording all the excerpts, we then ask the musician to tell us about the evaluation. We did not want to ask these questions before the recordings because the musician may not have finished forming her impressions. As the musician performs the excerpts and works out the changes in control parameters necessary to get a recording she is satisfied with, her impressions of the instrument may change. If we had asked her to give us her impression before the recordings and she had declared that the instrument has some particular property, she may be resistant to allowing herself to change her impression and she may change the way she plays to reinforce her statements.

While we are interested in the concept of playability, musicians do not usually use that term specifically. Furthermore, playability may not be the most relevant feature for the musician. We use open-ended questions which encourage different kinds of statements, but we do not try to direct the musician into talking about any particular aspect of the cello or suggest any vocabulary that she hasn't already used. While specifically asking about certain properties heightens the musician's awareness of those properties and may enable her to distinguish small differences, it may also lead to imagining non-existent differences or overemphasizing the unimportant properties. We use the first two questions in Table 5.2 to get descriptions of the instrument's properties and the musician's value judgements applied to those properties. The third question encourages positive statements and comparisons with other cellos. The final question allows the musician to talk about the negative aspects of the cello in a constructive way. This question was particularly delicate: we didn't want the musician to feel she had just played an instrument with problems, leaving her with a negative impression of her experience. We don't ask what is wrong with the instrument. Instead, we ask in what ways she would like the instrument to be changed. Since the musician believes that we

will try to make these changes, hopefully she will leave the experience feeling helpful, which we reinforce by telling her so and thanking her.

- Please describe this cello. (descriptions)
- What do you think about this cello? (value judgements)
- What did you appreciate particularly? (Encourage positive statements)
- If the luthier could change the instrument, what outcome would you ask him to achieve? (Talk about negative features in a constructive way.)

TABLE 5.2: Questions asked after finishing evaluating and performing on each instrument.

Once the musician has finished evaluating both cellos, we then ask her to compare the two cellos. Formally speaking, the comparison is outside of the frame of the experiment (evaluating the instruments individually), but it falls naturally in our request for comments which helps us interpret data as explained earlier. Additionally, musicians usually compare cellos during their evaluations and the musician is likely to have already made comparative comments when describing the second cello during this experiment, so asking for a comparison just formalizes what the musician would have done naturally. The questions posed in Table 5.3 are designed to identify perceptual differences, suggest moments in our recordings to look at more closely, suggest particular features in our control parameter to pay attention to at those moments, and get feedback which we can use to modify the experiment.

- What differences did you notice?
- Which of these differences were demonstrated in the extracts?
- How did these differences affect your way of playing the extracts?
- Could you propose another excerpt which would demonstrate the differences between these instruments?

TABLE 5.3: Questions asked after comparing the two cellos.

5.8 Discussion

The approximate duration of the experiment was three hours, slightly longer than expected due to some technical difficulties. The musician seemed to be content with her participation in the experiment, and did not express feeling tired, though I would not ask for a longer duration. The musician understood that we were recording and would later analyze her gestures, using her comments to help interpret the data. She understood that we were trying to understand the relationships between the control parameters applied to the instrument and the behavior of the instrument. The musician was not aware that our study focused on issues of playability during the experiment (by design), and I did not tell her afterwards, though I do not object to doing so.

There is an ethical concern associated with framing the experiment as we did. The frame is fabricated, there is no third party composer. Framing the experiment in this way was necessary to ensure a natural performance. The musician's contentment with the experiment seemed to be based on knowing that her comments would be helpful, not only to us as we tried to understand the data we collected, but also to the imagined composer in the context of the frame. I was concerned that the musician's primary motivation was tied to the frame of the experiment, so I did not inform her that the composer didn't exist. In future experiments we should reconsider how we we can make our research the primary motivation of the musician without compromising the naturalness of the performance.

Chapter 6

Data processing and exploration

In Section 6.1, we describe the raw dataset and review the processing necessary to extract the playing parameters. In Section 6.2 we discuss how the data was segmented by string, bowing direction, and pitch using the available score. Section 6.3 demonstrate typical values of the bowing parameters in a real playing situation and looks at the distribution of single-note averages across cellos and strings.

6.1 Data pre-processing

Here we review the data processing pipeline to give us, in one place, a list of all the measurements, explaining how each contributes to the complete set of data, and thus justifying why each measurement was necessary.

The recorded data includes an audio recording from the microphone, 8 audio-like recordings from the bridge sensors, and position data for several labeled markers. The motion capture data was recorded at a frame rate of 120 frames per second and the microphones and piezos were sampled at a sampling rate of 30720 samples per second¹. The data is synchronized and partitioned into frames of data. Each frame contains one measurement of motion capture data and 256 audio samples from each piezo and the microphone. To interpret this data, we also have measurements for defining rigid bodies, calibrating the bridge sensors, and calibrating the bow force model, as well as measurements of the bridge admittance and string properties.

6.1.1 Fundamental frequencies.

The first step in the pre-processing pipeline is to estimate the fundamental frequency of the note played in each frame of data using an algorithm (Monti and Sandler, 2002). In particular we estimate the fundamental frequency of the plucked open strings after tuning the instrument and of the bowed strings during the performance. We use a window size of 256 samples so the algorithm returns one pitch per frame of data. At this stage of processing, we have not yet identified which string is played, so we run the fundamental frequency estimation algorithm on all piezo signals and the microphone signal. We then convert the fundamental frequencies to pitches (i.e. $440Hz \rightarrow A_4$) which will be useful for segmenting and labeling the data later.

¹For reasons unknown, The MotionMonitor sampled at 30729 samples per second, so we had to slightly down-sample to 30720 samples per second to get the desired 2^8 samples per frame for passing to the pitch-estimation algorithm.

6.1.2 Open string tension

Using the string properties (K_L and μ_0) measured in Section 3.1.1, the distance between the nut and bridge on our cello L_{open} (686 mm), and the estimated frequencies f_{open} of the plucked open strings, we use Equations 3.5, 3.6, and 3.7 to solve for the unstretched length L_0 , the open string mass density μ_{open} and most importantly, the tension T_{open} which is necessary for incorporating the string compliance into the bow force model.

6.1.3 Stopped string length, stopping point, and stopped string tension.

Using the open string properties (length, tension, frequency) and the geometry of the fingerboard (i.e. the height of the open string at various positions along the fingerboard), we can use the frequency of the stopped string to estimate the length $L_{stopped}$ and tension $T_{stopped}$ of the stopped string (again, using Equations 3.5, 3.6, and 3.7) as well as the stopping point coordinates (L_γ, d_γ) of Figure 3.2. The stopped string length is necessary for calculating the bridge-to-bow distance as a fraction of the effective string length (i.e. the horizontal axis of the Schelleng diagram). The stopped string length and tension are both necessary for incorporating the string compliance into the bow force model. The stopping point coordinates give us corrections to our estimated string axis using Equation 3.8 to prevent a systematic over-estimation of the bow force.

6.1.4 Rigid body models.

The next step in the data pipeline is to define the rigid body models for the force transducer, bow, and each cello. These models are defined from static measurements of the temporary and permanent markers on each object, made before the experiment. Defining the landmarks on the force transducer and bow are described in Sections 4.3.2 and 4.3.4 respectively. To define the rigid body model of the cello we made four measurements: one for each string as we moved a set of temporary markers from one string to another. We then combined the four measurements by finding optimal transformations as described in Section 4.3.1 to carry three of the datasets onto the fourth. We then estimated the endpoints of each string as described in Section 4.3.3.

6.1.5 Landmark estimation.

For each frame of motion capture data, we find optimal transformations to carry the rigid body models onto the measured positions of markers within the recording studio. In particular, the transformation maps the positions of the landmarks within the rigid body onto their estimated positions within the recording studio. We thus have the positions within the recording studio of the endpoints of the bow hair and the endpoints of the string (during performance) or force transducer (during bow force calibrations) as well as all markers.

6.1.6 Orientation of reference frames.

Using the positions of the markers and landmarks, we can now calculate the orientation of the reference frames for the force transducer, open strings, and hair ribbon as described in Sections 4.3.2, 4.3.3, and 4.3.4 respectively. After calculating the open

string reference frame, we can apply the stopping point correction to estimate the stopping point (see Equation 3.8 and Figure 3.2). The stopped string reference frame is then calculated as we did for the open string but using the stopping point instead of the nut.

6.1.7 Kinematic control parameters.

Once we have the positions and reference frames of the hair ribbon and force transducer during bow calibration, we can calculate the inclination angle, frog-to-string distance, and hair depth (Equations 3.10 and 3.11). The equation for total depth when applied to the rigid force transducer gives the hair depth since the string depth is zero.

Using the positions and reference frames of the hair ribbon and the stopped strings during performance, we can calculate the bowing angles (inclination, skew, and tilt), the frog-to-string distance, the bridge-to-hair distance, and the total depth (see Equations 3.10 and 3.11 again). Once the frog-to-string distance and skew angle are calculated for each frame, we can calculate the bow speed (Equation 3.12), which we implement using a three-point Lagrange interpolation of the previous, current, and next frame of data. We revert to forward difference, central difference, or backward difference estimations whenever the previous, current, or next data point is missing data respectively.

6.1.8 Bow force model.

We now turn our attention to estimating the bow force which is done in three steps.

First, we build the hair compliance based force model (Section 3.3.2) by processing the calibration data. The calibration data consists of the force measurements and motion capture data taken during the calibration procedure. We have already processed the motion capture data to get the kinematic control parameters (frog-to-string distance a , hair depth c_h , inclination angle θ_I) of the bow. The force transducer measures the force along the sensor axis, but the deformation of the bow is due to the entire force. We correct for this difference by dividing the measured force by the cosine of the inclination angle (Equation 3.18). With the pre-processing done, we then fit the hair compliance based force model (Equation 3.19) using a least total squared residuals algorithm.

Second, using the string properties (K_L from Table 3.1, tension $T_{stopped}$, length $L_{stopped}$), and bridge-to-bow distance b (Equation 3.11), we create the bow force model based on string compliance (Equation 3.16).

Finally, the system of equations relating the bow force, hair depth, string depth, and total depth (Equation 3.20) is solved for each frame of performance data to give us the estimated bow force.

6.1.9 Piezo calibration.

Before we look at the control parameters in the next chapter, there are still two more pre-processing calculations we can do to help us interpret the results. The first is to calibrate the piezo signals by calculating the calibration coefficients for the piezos (Section 4.2.2.2) using the data from wire-break measurements (Section 4.2.2.1), and then applying the calibration coefficients to the piezo signals to transform the signals from uncalibrated treble/bass pairs to calibrated horizontal/vertical pairs. We calibrate the piezos for three reasons:

- to compare signals between strings on the same cello or different cellos

- to compare the amplitude of the string vibrations to the amplitude of the radiated sound
- to observe whether the polarization of the vibrations shows anything interesting

6.1.10 Schelleng's Limits.

Finally, we calculate Schelleng's predicted maximum and minimum bow force limits for each frame of performance data using Equations 2.1 and 2.2. In addition to the string properties, bow speed, and bow position, these calculations require an estimate of the coefficients of friction and measurements of the bridge mobility.

We use the values $\mu_s = 0.643$ and $\mu_d = 0.346$ from (Mores, 2016). We do not assume that these numbers are correct for our combination of bow hair, cello strings, rosin, and temperature, but we do assume that their difference $\mu_s - \mu_d = 0.297$ is within a factor of about 3 of the value which best represents our setup. We note that Demoucron (2015) uses $\mu_s - \mu_d = 0.5$ in his simulations, similar to the value we have selected.

We use an impact hammer and an accelerometer as in (Zhang, 2015) to measure the four bridge mobility transfer functions (horizontal / vertical force with horizontal / vertical velocity) as functions of frequency f . We then calculate the mobility Y of the bridge as a function of frequency f for forces and velocities tangent to the bowing direction given by the bow inclination angle θ_I , corresponding to the transverse polarization considered by Schelleng.

$$\begin{aligned}
 Y(\theta_I, f) = & \cos(\theta_I) \cos(\theta_I) Y_{HH}(f) \\
 & + \cos(\theta_I) \sin(\theta_I) (Y_{HV}(f) + Y_{VH}(f)) \\
 & + \sin(\theta_I) \sin(\theta_I) Y_{VV}(f)
 \end{aligned} \tag{6.1}$$

6.2 Data segmentation

During the pre-processing phase, before we have identified the string being played, we blindly process the data on each string as if it were played. This costs some extra processing time and computer storage, but it greatly simplifies the calculations since no logic for recognizing segmentation boundaries needs to be programmed. Once these preliminary calculations are done, we can use them to find informed criteria for defining segmentation boundaries.

We would like to have a semi-automated way of segmenting the data by note, string, and bow-direction using the available data. The dataset for a performance includes time, pitch, bow force, bow speed, frog-to-string distance, bridge-to-hair distance, inclination angle, skew angle, and tilt angle. We can also revisit the raw data, such as the microphone and calibrated piezo signals, as well as intermediate calculations such as stopped string length, string depth, hair depth, and total depth. In this section we will explore various strategies for using some of this data to segment a performance.

6.2.1 Segmentation based on the inclination angle

To identify the string being played, Schoonderwaldt and Demoucron (2009) and Maestre et al. (2007) used their versions of the inclination angle, so we will begin with

that strategy. The largest difference between the values of the inclination angle calculated using each string is less than 0.7° , so for the purposes of string classification, it doesn't matter which string is used to calculate the inclination angle.

Each string can only be played within a certain range of inclination angles. The ranges for adjacent strings overlap slightly since they may be played at the same time. The exact placement of the boundaries depends on the geometry of the deformed strings and bow. To calculate the boundaries, we have to take into account the stopping point, the bridge-to-bow distance, the skew angle, and the bow force.

Figure 6.1 shows the inclination angle as a function of time for a recording of the Bach excerpt. We can see that the player quickly passes from one string to the other and settles at inclination angles far from the boundaries. If the music does not include playing two strings simultaneously, then nominal inclination angles used for playing each string may be determined from an excerpt, and an arbitrary boundary may be drawn to separate them.

If a previous recording is not available, or if you want to have an idea of when an adjacent string might be accidentally touched, then the segmentation boundaries may be estimated based on geometry. In Figure 6.1, the segmentation boundaries are calculated using open strings, a range of typical bridge-to-bow distances, a large range of skew angles, and zero bow force. This is the best a priori approximation of the classification boundaries that can be made without knowing the playing parameters.²

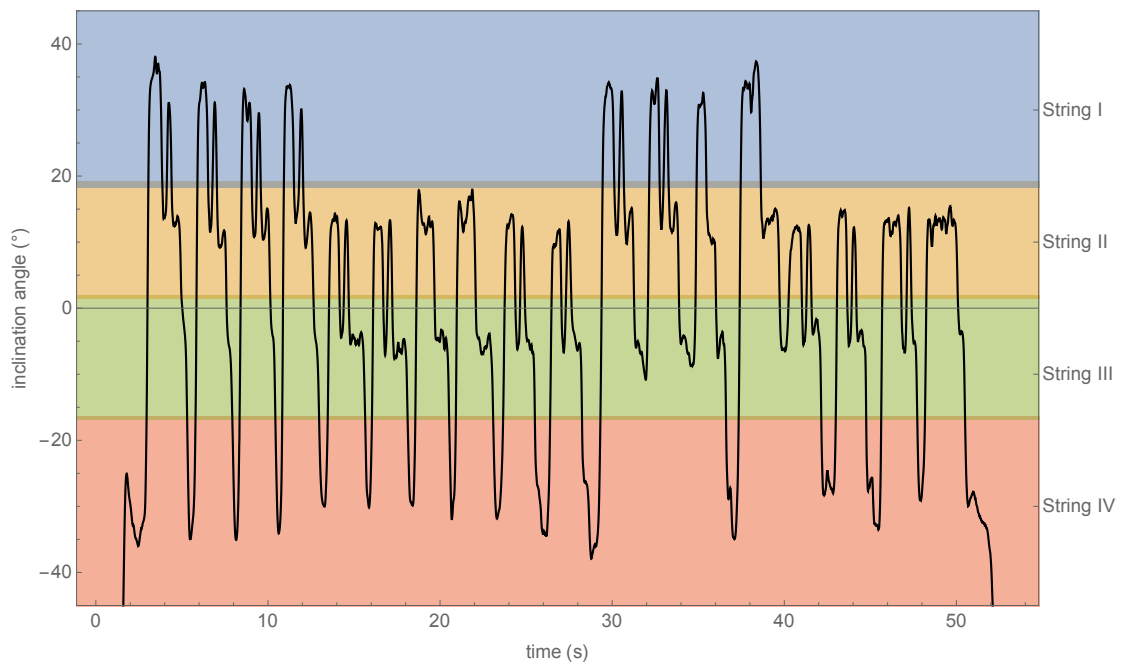


FIGURE 6.1: Inclination angle versus time for a recording of the Bach excerpt. The background colors indicate the string classification boundaries based on zero-force, open-string geometry.

²It is sometimes possible to play three strings at the same time. An example is when playing over the fingerboard with a sufficiently large force. Thus the playing parameters can greatly change the string classification boundaries.

6.2.3 Segmentation based on the bow force or total depth

Next we look at the bow force (or total depth) as a function of time (Figure 6.4). At nearly every instant, the total depths calculated for multiple strings are positive. This is because the deflection of the hair and the string allows the line connecting the endpoints of the bow to pass underneath adjacent strings while the hair itself clears them.

If a string were played, then not only would it have a positive total depth, but it would also vibrate. By looking at the calibrated piezo signals of each string (Figure 6.3), we could try to filter out strings with small vibrations, but how exactly do we define a small vibration? The two light touches on strings II and III are arguably small, yet they are really played. The two sympathetic vibrations³ are the same size as the light touches, but they are not played. And just after a string crossing, the initial string has large vibrations, but the bow is no longer actively playing the string.

While vibration amplitudes might not help, the frequency of the vibrations are of some use. If the frequency is too low to be played on a string, then we can conclude it is the result of the bridge moving underneath it as a lower string is driven by the bow⁴. In this way we can sometimes eliminate higher strings from the list of played strings.

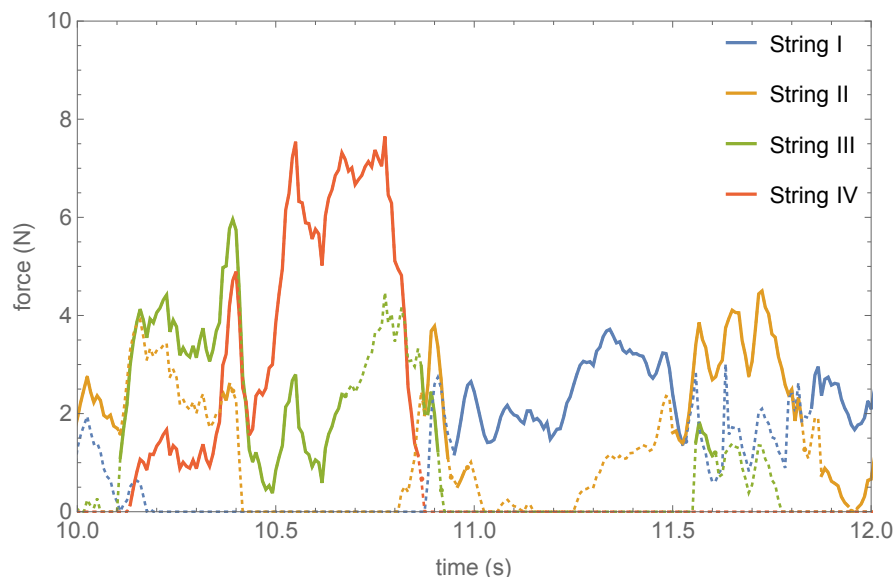


FIGURE 6.4: The bow force versus time for a portion of the Bach excerpt. The dotted lines show when the bow force indicates touching, but the piezo signal does not indicate a pitch that can be played on the string.

³When one string is driven, it causes vibrations in the bridge and top plate which causes the bridge to move underneath the other strings, driving their vibrations. The other strings all start to vibrate at the frequency of the driven string, but the vibration amplitudes will typically remain negligibly small. However, if one of the other strings shares a harmonic frequency with the driven string, then that string will vibrate with a noticeably large amplitude. When this happens, the two strings are said to vibrate sympathetically.

⁴While non-sympathetic vibrations typically have negligible amplitudes, they can usually be detected. Furthermore, if the bridge has large amplitude movements (due to playing loudly or due to the mobility of the bridge) then the measured signal can be quite large.

Note that the pitch tracking algorithm does not require a large amplitude to find the frequency. It is likely that lower strings will have small vibrations with a detectable pitch when playing on higher strings. However, if we are certain that only one string is being played, then we can simply take the string with the greatest force. This allows us to estimate string crossings with nearly the same result as using the inclination angle as shown in Figure 6.5.

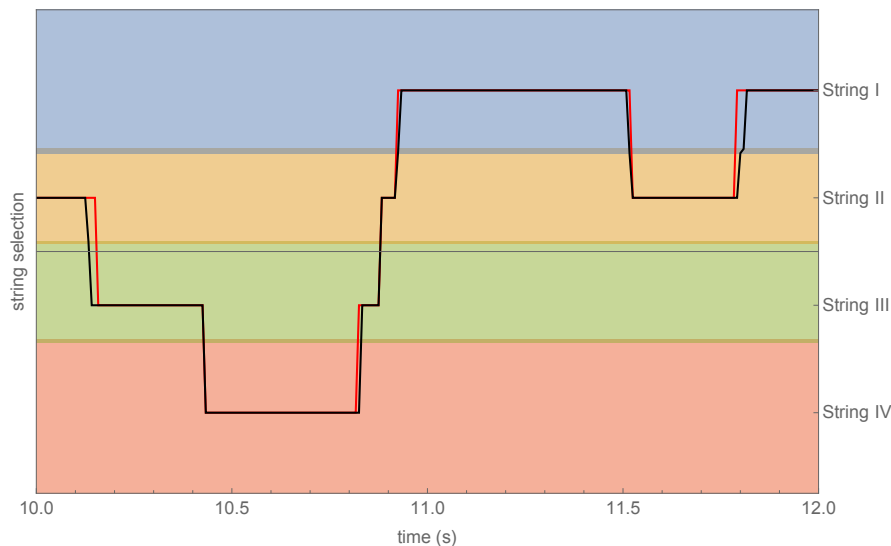


FIGURE 6.5: String selection and estimated string crossings based on the inclination angle (black) and bow force (red).

6.2.4 Segmentation using the score, pitch, and control parameters

If we look at the pitch as a function of time (Figure 6.6), we may see coupling between the strings via the bridge as overlapping curves (G_3 just after 11.5 seconds on strings II, III, and IV), vibrations from left hand finger movements ($E\flat_2$ at 10.1 seconds), and ringing of recently played strings ($B\flat_2$ at 10.4 seconds), though they are difficult to identify without extra information from the control parameters. We saw these features when looking at the piezo signal amplitudes. Additionally, we see confirmation of an accidental touch of String II due to pressing String III too hard at 10.4 seconds and vice versa at 11.6 seconds. These touches are suggested by the estimated bow forces, but are not expected based on the inclination angle, and are not evident from just looking at the piezo signal amplitudes.

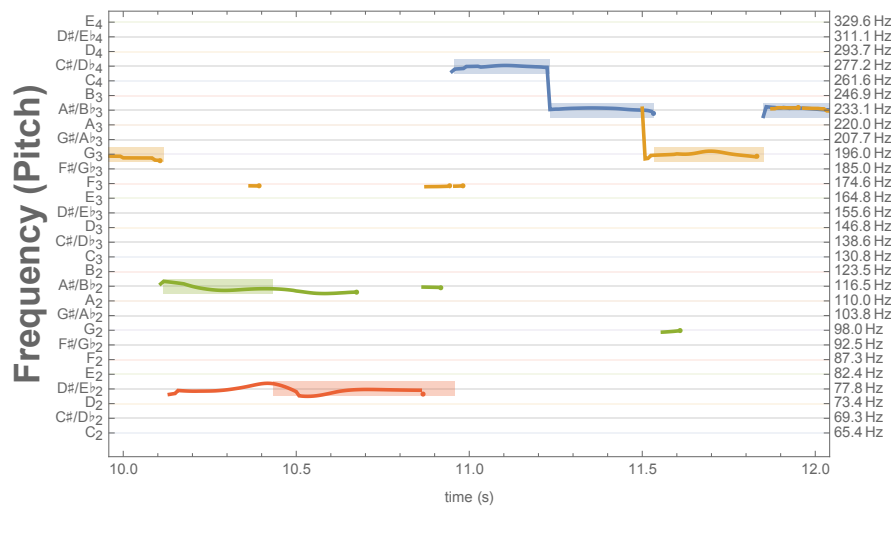


FIGURE 6.6: A segmentation of the bow performance.

Accurately estimating which string is touched by the bow requires knowledge of the control parameters and how they affect the geometry of the deformed string and bow hair. This is important if the dataset has double stops or when we are interested in the occurrences of accidental touches. However, in our dataset there are no intentional double stops, and for the purposes of segmentation, we are not interested in accidental touches. Under these conditions, using either the inclination angle with zero-force, open-string geometry or the string with the greatest force leads to acceptable estimates of string crossings. Since we have the score available, we use the following algorithm for segmenting the dataset.

Whenever multiple strings are vibrating with a defined pitch and have a non-zero reported force, we select only the string with the greatest force. We use the score to identify the expected string and note. Then we look for the first moment when the expected string has the greatest force and is playing the note. This moment marks a segmentation boundary. Once the beginning of one note is found, we start looking for the beginning of the next note until the entire performance is segmented. The result is shown in Figure 6.6.

6.3 Statistics of control parameters

Now that the control parameters are calculated and the dataset is segmented into individual notes, we can begin asking questions about extreme values, typical values, and variability. We will address these questions using the data available from all recordings of Fauré, Brahms, and Bach on both instruments. There are 1297 notes taken from one repetition of Fauré, four repetitions of Brahms, and four repetitions of Bach on Cello A ("souple"), and two repetitions of Fauré, two repetitions of Brahms and three repetitions of Bach on the Cello B ("rigide").

6.3.1 Extreme values

It is important to be aware of extreme values when designing methods of measuring the control parameters. Extreme values occur for only an instant and are typically far in

the tails of the distributions, but they may be meaningful when describing a particular gesture. It is important that the chosen method of measuring the control parameters is capable of measuring these extreme values. The extreme values observed in our dataset are presented in Table 6.1. In the table, the negative bow speed is an up-bow; the positive, down-bow. The extreme values of the frog-to-string distance indicate that the player used neither the 3 cm of the hair at the frog nor at the tip. It is tempting to suggest that measurement devices may be placed in these regions, but even a small marker on the ferrule of the frog disturbs the player as it clips adjacent strings. The sensor we used to calibrate the bow force model has a maximum limit of 10 N. It is possible to apply much more than 10 N of bow force, but this cannot be sustained. We were not certain about our accuracy when extrapolating beyond 10 N, so it is a welcome observation that the maximum bow force was only 9.6 N.

	min	max
force	0 N	9.6 N
speed	-1575 mm/s	1258 mm/s
bridge-to-bow distance	18.8 mm	102 mm
frog-to-string distance	30 mm	574 mm
inclination angle	-40°	40°
skew angle	-12°	15°
tilt angle	-2°	69°

TABLE 6.1: Extreme values of control parameters.

6.3.2 Typical values

Simulation studies usually include gestures which go beyond the range of control parameters that are actually used by musicians. This is computationally expensive and the extra information can be distracting. To help identify the regions of control parameters which are the most relevant, we describe probable typical values which complements the possible extreme values already discussed.

When we are not interested in extreme values of control parameters, we are usually interested in typical values or averages. Sometimes we are interested in other statistics which describe the range of values a control parameter covers during a note, such as the standard deviation or maximum and minimum. By calculating the statistic of a control parameter for each note and then averaging the statistic over all notes, we get a typical value for the statistic. In addition to the typical value of the statistic, we often want to know how much that typical value can change from one note to another. This is calculated as the standard deviation of the statistic over all notes.

Table 6.2 gives the range of typical values for the mean, standard deviation, minimum, and maximum of each control parameter. Since the Bach excerpt is longer, has more notes, and was repeated more times, the values given here are skewed toward the averages of the Bach excerpt. The first line of the table may be read as follows: The mean force during a note is typically around 1.0 to 2.4 N. The force typically varies 0.2 to 0.6 N about the mean during a note. The minimum and maximum forces during a note are typically around 0.4 to 1.4 N and 1.6 to 3.4 N respectively.

	mean	std	min	max
force (N)	1.7 ± 0.7	0.4 ± 0.2	0.9 ± 0.5	2.5 ± 0.9
speed (mm/s)	339 ± 111	141 ± 74	61 ± 62	581 ± 221
bridge-to-bow distance (mm)	70 ± 8.8	2.2 ± 2.3	66 ± 10	74 ± 8.4
frog-to-string distance (mm)	239 ± 65	44 ± 25	173 ± 70	310 ± 83
tilt angle ($^{\circ}$)	34.8 ± 7.2	4.0 ± 1.8	27.8 ± 7.6	41.9 ± 6.0
skew angle ($^{\circ}$)	0.8 ± 2.9	1.6 ± 1.1	-1.8 ± 3.6	3.4 ± 2.7
String I inclination angle ($^{\circ}$)	29.7 ± 3.8	3.6 ± 1.7	20.5 ± 6.2	33.1 ± 3.6
String II inclination angle ($^{\circ}$)	11.6 ± 2.1	2.6 ± 1.7	5.5 ± 6.2	14.8 ± 3.2
String III inclination angle ($^{\circ}$)	-5.7 ± 1.9	2.6 ± 2.1	-10.9 ± 6.6	-1.0 ± 5.0
String IV inclination angle ($^{\circ}$)	-27.1 ± 2.6	3.7 ± 3.3	-30.7 ± 2.9	-15.5 ± 13.2

TABLE 6.2: Typical values of control parameter statistics.

While Table 6.2 is supposed to indicate typical values, it must be pointed out that there are different schools of thought on the role of tilt and how much the bow should be tilted toward the fingerboard. Some of the supposed roles of tilt include: 1) Tilt may be coordinated with bow force, especially when playing with low force. 2) Tilt may be used to decouple the bouncing of the hair from the bouncing of the stick. 3) Tilt may be used to change the color of the sound. 4) Tilt may be used to relieve strain on the wrist. Personally, I have had teachers advocating three tilt strategies: 1) Use a very tilted bow to avoid wrist flexion and to approach an ideal point excitation. 2) Use a flat bow so that the flexed wrist allows supination and pronation to reduce ulnar and radial deviation. 3) Vary the tilt according to the desired color while continuously monitoring and occasionally releasing the tension in the wrist, generally resulting in more tilt on shorter and higher strings; less tilt on longer and lower strings. The tilt angles in Table 6.2 correspond to a player who uses a very tilted bow as part of her playing strategy.

Table 6.2 gives statistics for the inclination angle on each string separately. The mean values indicate the nominal angles for each string on our cellos and describe the perceived geometry of the strings. The average minimum and maximum values are limited by the adjacent strings and the edges of the top plate, but do not necessarily indicate the string-crossing boundaries. The average standard deviations indicate the amount of freedom taken by the player. The inner strings have a smaller standard deviation of the mean (2.1° and 1.9° compared to 3.8° and 2.6°), indicating that the same angle was returned to more consistently and the nominal angle is more precisely defined. The inner strings have a smaller average standard deviation about the mean (2.6° and 2.6° compared to 3.6° and 3.7°), indicating that the player held the bow angle more constant during each note. The player may feel slightly more constrained by the adjacent strings. I suspect that making the bouts wider or the bridge shorter will cause the standard deviations on the outer strings to be smaller while making the bridge more curved will make the standard deviations on the inner strings to be higher. Such changes might lead to a more homogeneous playing experience, though I refrain from any predictions about whether it is preferable.

Chapter 7

General results

In Chapter 6 we presented some initial exploration of the statistics of each control parameter over the entire set of 1297 recorded notes. In this chapter we look closer at the coordination of the control parameters.

7.1 On the perception of Schelleng's bow force limits

In section 2.4, we presented the Schelleng diagram and various features we would like to study: the upper and lower bow force limits, their intersection point, and the range of forces between them (see Figure 7.1). The first set of objectives was to determine whether, how often, and under what circumstances the musician plays in each region of the Schelleng diagram. Our original idea was to plot the trajectory of control parameters on the Schelleng diagram, but we soon realized that there is no single Schelleng diagram; every bow speed and every frequency has its own diagram. To visualize all the data on the same figure we changed the references of the logarithmic axes.

7.1.1 The normalized Schelleng diagram

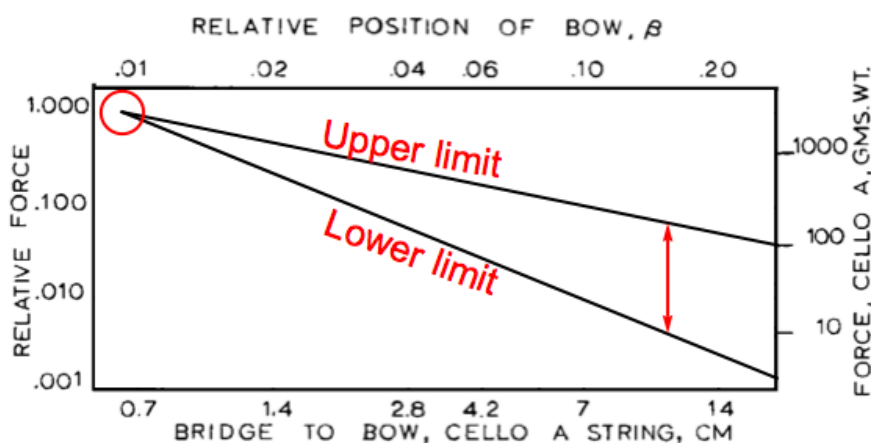


FIGURE 7.1: The standard representation of Schelleng's diagram shows the upper and lower bow force limits on logarithmic force and position axes. The reference for the force is some arbitrary constant force. The reference for the bridge-to-bow distance is the length of the string. The diagram is valid only for a certain bow speed and note frequency as changing either will change the plotted limits.

Force normalization.

In the usual Schelleng diagram, the force axis uses an arbitrary constant as its reference. The line representing the upper bow force limit has slope -1 and is translated upward as the bow speed increases. In the normalized Schelleng diagram (Figure 7.2), we normalize the force to the upper bow force limit, which depends on the bridge-to-bow distance. In this way the diagram is transformed so that the upper bow force limit will always be represented by a horizontal line at $\log(F/F_{max}) = 0$. This gives us a way of comparing bow force and bridge-to-bow distance data measured at different bow speeds.

Bridge-to-bow distance normalization.

In the usual Schelleng diagram, the bridge-to-bow distance axis is normalized to the string length. This allows us to compare strings of different lengths on the same diagram with the naïve assumption that it allows us to compare notes of different pitches (since pitch is usually adjusted by changing the string length). The problem is that the lower bow force limit depends on the frequency-dependent bridge mobility. Even though we are able to compare notes played on strings of different lengths, those strings would likely have different lower bow force limits due to different string admittances or bridge mobilities. In the normalized Schelleng diagram, we normalize the bridge-to-bow distance to the distance between the bridge and the point where the upper and lower bow force limits intersect. Thus we are allowing the dynamics of the system –rather than the geometry– to determine the relevant length scales. With this normalization, the limit intersection point is always found at $\log(\beta/\beta_0) = 0$, independent of the string length, tension, mass, and frequency.

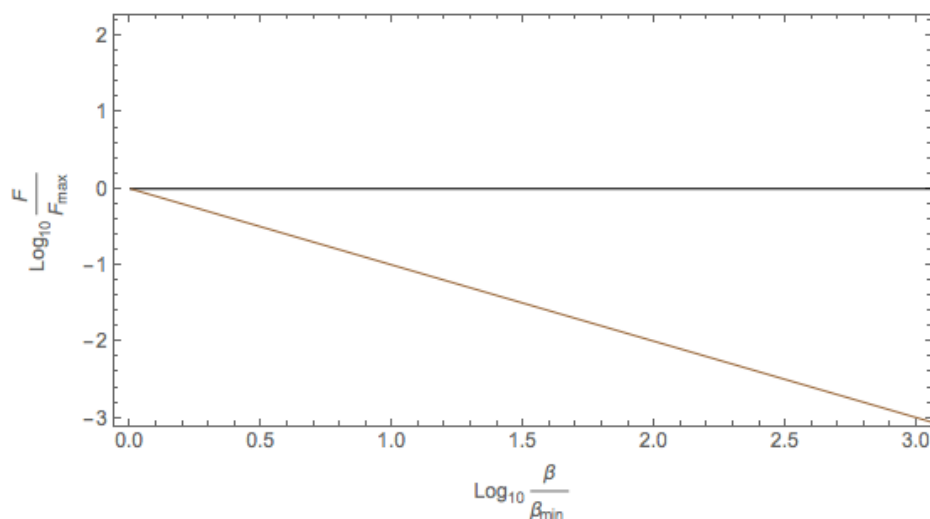


FIGURE 7.2: This normalized representation of Schelleng’s diagram shows force and position on logarithmic axes, but with different references. The force is referenced to the upper bow force limit as a function of position. The position along the string is referenced to the point of intersection of the upper and lower limits. The diagram does not change with bow speed, frequency, or any other control parameter, string property, or bridge mobility.

Interpreting the diagram.

Interpreting the relationship between two nearby points on the normalized Schelleng diagram must be done with care due to the ambiguity introduced by the non-constant references. Moving up on the diagram could be due to a larger applied bow force or a smaller upper bow force limit. A lower bow speed, a larger distance from the bridge, or playing on a string with a smaller admittance all cause upward movement on the normalized Schelleng diagram. Similarly playing closer to the bridge, or anything which increases minimum bow force will show itself as movement toward the left on the normalized Schelleng diagram. If we look at increasing the bow speed, we find that it raises both the upper and lower limits, which is visualized as movement downward and to the left on the normalized Schelleng diagram, clearly increasing the margin from the upper limit and approaching the lower limit.

7.1.2 Results.

For each frame of motion capture data in the database, we calculated the upper and lower bow force limits given the bridge-to-bow distance, bow speed, bridge mobility, vibration frequency and string properties. This allows us to then calculate $\log(F/F_{max})$ and $\log(\beta/\beta_0)$ at each moment and plot the data on the normalized Schelleng diagram (Figure 7.3). That is, each point on the diagram represents 1/120th of a second worth of data. It is immediately obvious that the player nearly always plays with healthy margins from both the upper and lower limits as expected. She never plays near the intersection point and the regions near the upper and lower limits have very few points. In fact, the points in the figure form a semi-transparent point cloud rather than a proper density plot, so the points near the upper and lower limits are over-represented by several orders of magnitude compared to the mass of points in the center. I chose this visualization to emphasize that the musician *does* play in these regions, if only very rarely.

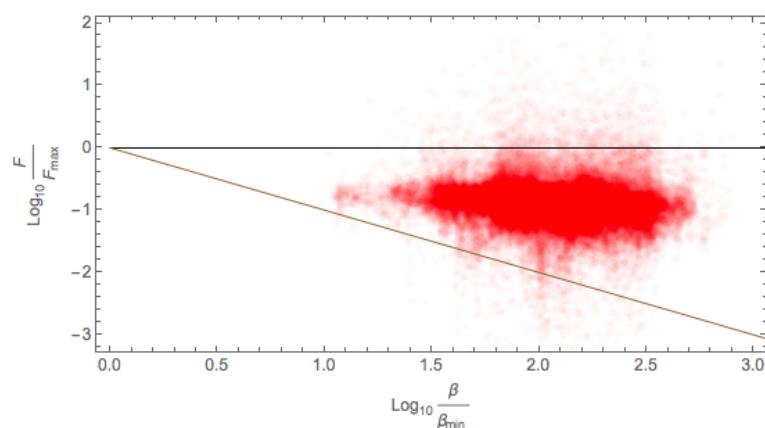


FIGURE 7.3: Data from 1297 notes is plotted on the normalized Schelleng diagram. Each point represents 1/120th of a second. The points are semi-transparent which helps us see overlapping points. The density of points is overrepresented by several orders of magnitude near the limits due to saturation of the semi-transparency in the central region.

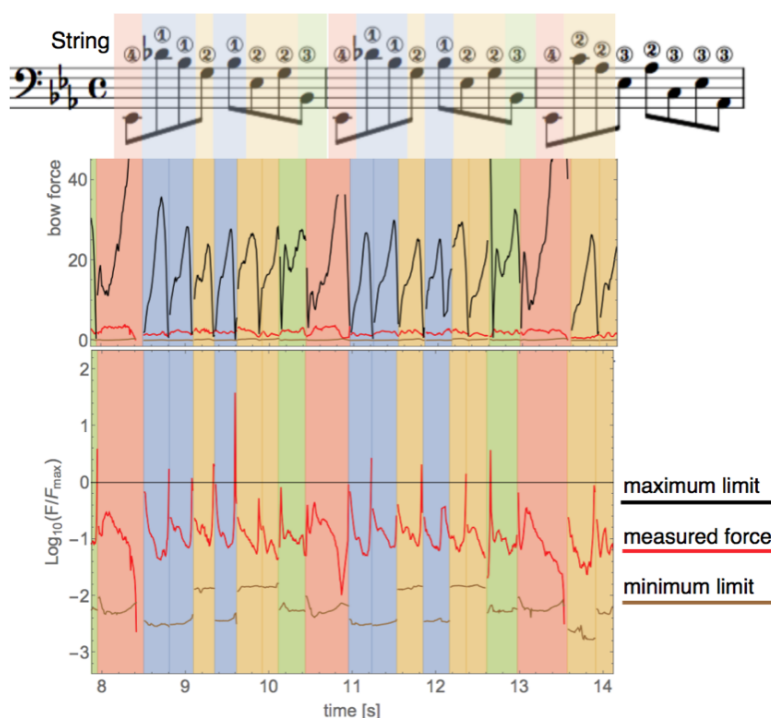


FIGURE 7.4: A typical plot of bow force over time. The plots are highlighted based on the string numbers indicated in the score. Top: the score of an excerpt from Bach, Suite IV, Prelude. Middle: Bow force on a linear scale as a function of time. Bottom: Bow force on a log scale using the upper bow force limit as a reference as a function of time. In each plot the upper curve (black) is the upper bow force limit, the middle curve (red) is the applied bow force, and the lower curve (brown) is the lower bow force limit.

Having answered whether and how often the player plays near the bow force limits, we now examine the circumstances under which she does so. If we plot the applied force and the upper and lower limits on log axes with the upper limit as the reference, we get plots like the one shown at the bottom of Figure 7.4. This diagram clearly indicates that the player may go under the lower limit at the very end of a note, and that she may go over the upper limit during bow changes.

Since the normalization of the force axis creates an ambiguity between changing forces and changing limits, we turn to the plot in the middle of Figure 7.4 in which we plot the force on a linear scale. We can see from this figure that the player does not go over the upper limit by increasing the applied bow force, rather it is the upper limit which falls below the applied force. The reason the upper limit falls is because the bow changes direction at these moments. Whenever the bow speed approaches zero, the upper bow force limit approaches zero, so *any* applied force at this moment will correspond to a point in the raucous region of the Helmholtz diagram. The figure also confirms that the player went underneath the lower limit at the end of the note by lowering the applied force below the limit *as she lifted the bow off the string*.

7.1.3 Interpretation.

Finding the majority of points well within the Helmholtz region was as expected. However, we did expect to see at least some notes played near the limit intersection

point, but the database contains no data points in this region at all. That may be because the recorded data corresponded to musical extracts which apparently did not indicate playing so close to the bridge. But a quick calculation places the intersection point within a few millimeters of the bridge, and a review of the video during the free evaluation phase shows that the player never played very close to the bridge. In fact, during my observations at Violoncelle En Seine and of the other amateur and professional cellists before the experiment, I only observed two cellists playing near the bridge during an evaluation. One had been specifically asked to explore the region near the bridge. The other had generally behaved differently from the other cellists by playing scales and long notes outside of a musical context.¹ It seems that while the region very near the bridge may be worth exploring to a few cellists for their own reasons, the region near the intersection of the upper and lower bow force limits is probably not relevant to classical cellists outside of specialized techniques.

We had imagined that the player would push the limits of the cello, exploring the parameter space near each border and occasionally going outside of the Helmholtz region. That would have been strong evidence to support the hypothesis that the musician perceives these limits. Instead, we see that the areas near the borders are nearly empty. The few data points that we did see in these regions do not correspond to intentionally trying to play near the limits, but to unavoidable technicalities; Lifting the bow off the string cannot be done without reducing the applied force to zero; Changing the bow direction cannot be done without bringing the bow speed to zero. At typical bow speeds and bridge-to-bow distances, the upper limit has values on the order of tens of Newtons, whereas the maximum force that can be applied by the bow is only about 10 Newtons² due to the deformation of the hair and stick. Likewise, at typical bow speeds and bridge-to-bow distances, with the exception of wolf notes, the lower bow force limit is 0.2 Newtons or usually less. To apply such a little force to the string, the player would have to support almost all of the weight of the bow.

7.2 On the interpretation of Guettler diagrams

In Section 2.5, we presented a Guettler diagram (Figure 2.15) showing the duration of initial transients for strings initially at rest with the bow accelerating uniformly from rest with a constant bow force, for various values of the acceleration and force. Its speckled appearance implies that musicians should not be able to reliably achieve short transient durations, which is contrary to our impressions of professional performances. We made two hypotheses to explain this discrepancy. First, our impressions may not be correct since we listen to music rather than trying to count disturbances in the string vibration during initial attacks. Second, the experiment uses a gesture which might not be representative of what the musician actually does.

Available data.

The gesture used to produce the Guettler diagram in Figure 2.15 models an attack in which the bow is pressed against a resting string and then accelerated from rest. There are not many such attacks in our data set because the strings are often vibrating

¹I often wonder whether he was demonstrating what he thought we wanted to see or what he thought musicians should do rather than what he would do if nobody were watching him.

²It is easy to apply forces of up to 15 or 20 Newtons near the frog, but these forces cannot be maintained beyond the initial transient of a bow stroke.

or the bow is moving. However the six repetitions of the Brahms excerpt provide 66 examples of bow changes without string crossings and the seven repetitions of Bach provide another 413 examples. During these bow changes the sawtooth waveform of the first note must change sign to become the sawtooth waveform of the second note, making this gesture arguably more difficult than an initial attack on a string at rest. Figure 7.5 shows the waveform of the string vibrations during a bow change.

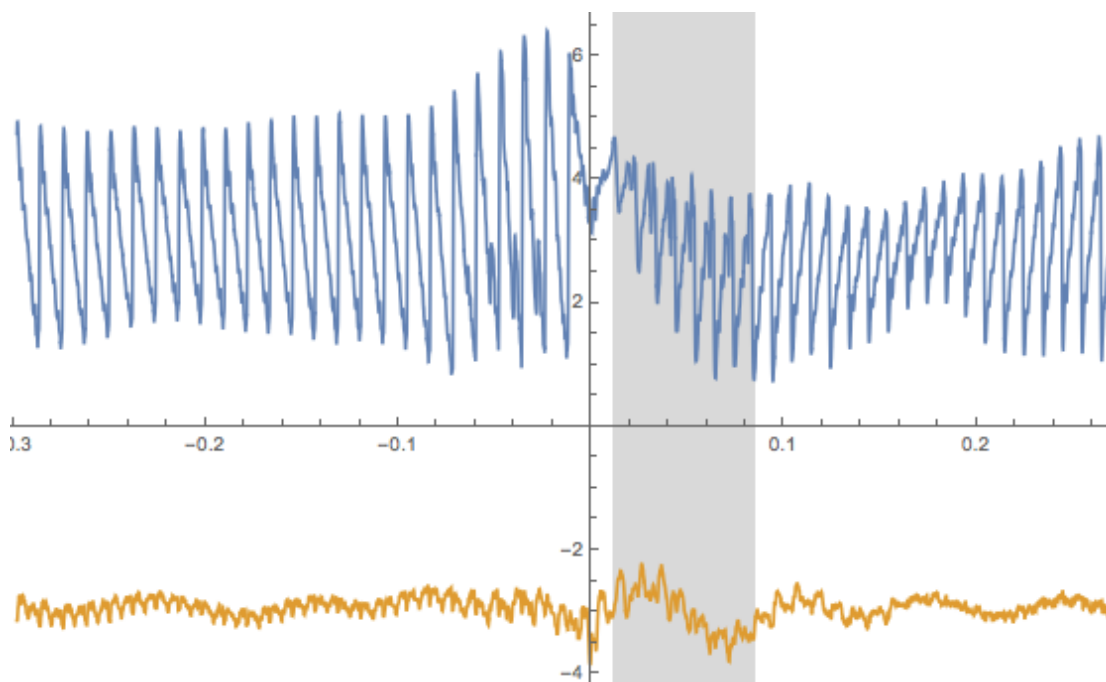


FIGURE 7.5: A typical bridge force signal of a bow change. The upper waveform shows the vibrations in the polarization with maximal amplitude (shifted up by 3 Newtons). The lower waveform is the orthogonal polarization (shifted down by 3 Newtons). The gray highlight shows the 73 millisecond window containing 7 periods of vibrations before a regular string motion is achieved. The synchronization of the motion capture data with the piezo signals is demonstrated here.

Distribution of durations.

Guettler and Askenfelt (1997) found that transient durations shorter than 50 to 90 milliseconds are acceptable in a neutral context (scales). This corresponds to about 6-9 periods in the lower register of the cello. Figure 7.6 shows the distribution of transient durations for 479 bow changes. The durations were determined by manually inspecting each of the waveforms, identifying the first slip after the bow change and the last slip before Helmholtz motion was achieved, and counting the number of periods between them (see for example, Figure, 7.5). We see that about 58% of the bow changes have acceptable durations with about 15% being perfect and about a 15% having very long transient durations (more than 16 periods). About 6% of the bow changes never achieved Helmholtz motion. These figures, played on the cello, are consistent with the distributions of violin transient durations described in (Guettler and Askenfelt, 1997). When comparing the 6 repetitions of each bow change in Brahms and the 7 repetitions

of each bow change in Bach, we find that every bow change had repetitions with acceptably short transients, and most had repetitions with perfect bow changes as well as very long transients.

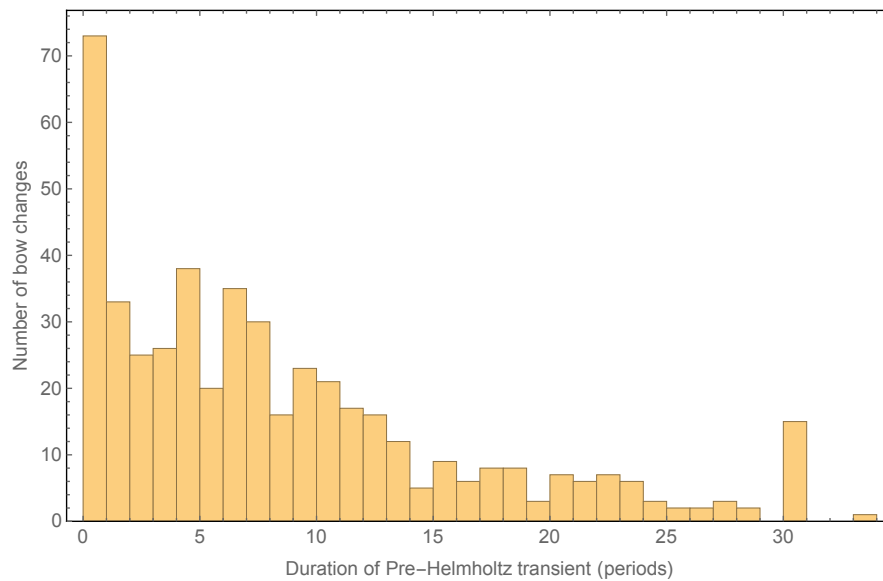


FIGURE 7.6: Histogram of bow change transient durations. An acceptable attack duration is shorter than about 7 periods.

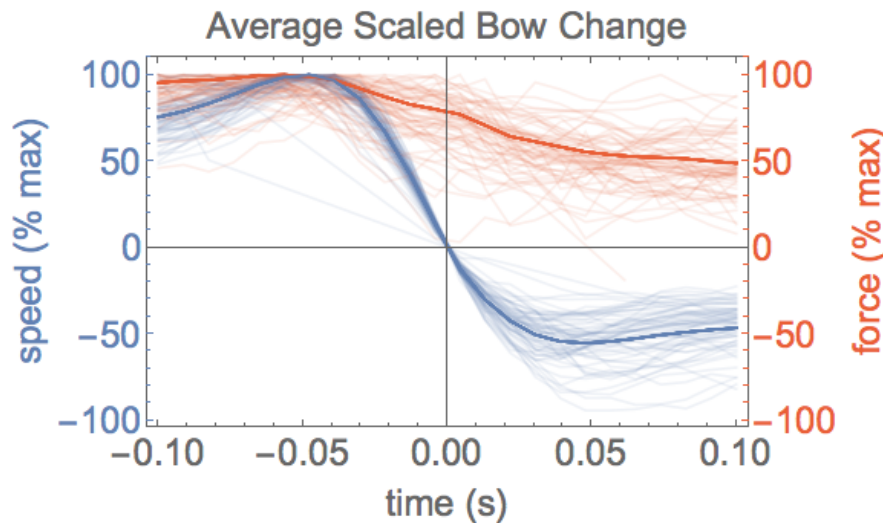


FIGURE 7.7: The speed (blue) and force (red) recordings for 66 bow changes without string crossings from 6 recordings of the Brahms excerpt performed on two cellos by one musician. Changes from down-bow to up-bow and vice versa are both represented. The curves were scaled so that each maximum reached 100%. The average was then calculated and rescaled so that its maximum reached 100%.

Bow change strategy.

One objection to the studies which produced the Guettler diagrams is that the control parameters might not be what musicians actually use. Our data gives us an opportunity to observe actual gestures and possibly revisit those studies. While looking at bow changes on one string, we noted a counterintuitive feature in the control parameter signals. We can reasonably expect the bow speed to slow to a rest before accelerating in the opposite direction during a bow change. However, we noticed that during the tenth of a second before the bow speed changes sign, the cellist increases the bow speed by a factor of 1.3 to 2.0, reaching a maximum about a twentieth of a second before the bow speed changes sign (Figure 7.7). While variations in the details were observed, this general strategy was present for each bow change during the recordings of the Brahms excerpt.

How does it work?

This increase in bow speed causes the amplitude of the string vibrations to increase. We need to reduce the amplitude of the down-bow waveform to zero before initiating the up-bow waveform, so it seems like a bad idea to increase the amplitude of string vibrations just before a bow change. Demoucron (2015) investigated the effects of different deceleration and acceleration rates using many different initial conditions (starting at different moments within the stick-slip cycle). Demoucron explains that waves from the first note remain in the string, but are not large enough to trigger slipping on their own, but help initiate the regular slipping once the bow has reached a certain minimum speed. To minimize the time during which these remaining waves could trigger unwanted slips, the deceleration and acceleration should be sufficiently large. However, the acceleration after the bow change should not be too large, as we would rather convert an existing corner into the Helmholtz corner rather than introducing an additional one.

Why this strategy?

By watching the video of the experiment, we can watch the players movements and see how she uses the kinematic chain from her shoulder, through her elbow, wrist, and fingers to manipulate the bow. What we see is that she leads the bow with her wrist, dragging her hand, fingers, and bow behind it. During the bow change, the wrist quickly straightens as the shoulder and elbow begin to lead the wrist in the opposite direction. I suggest that this straightening of the wrist accounts for the increase in bow speed in the instant before the bow changes direction.

This technique allows the wrist rather than the elbow to make the quick movement necessary for a clean bow change. It requires the wrist to be relaxed so it can whip forward during the bow change. It also reduces the tension in the elbow as well since the elbow is not trying to execute this movement. Among all the strategies which produce acceptable attacks, this one also helps cellists play longer without fatigue or sports injuries (like carpal tunnel or tennis elbow).³ Obviously, if it were not possible to have acceptable attacks using this technique, other strategies would be taught instead.

³Other strategies for changing the bowing direction in different contexts are also taught. See for example, (Guettler, 2010).

Chapter 8

Comparison between cellos

In this chapter we take another look at the statistics of the control parameters, their coordination, and the resulting transient durations, focusing this time on the differences between cellos and strings. We then let the musician's comments guide us to look more closely at some interesting features of the dataset.

8.1 Signs of adaptation

We suspect that cellists might adapt their control parameters in response to perceived differences between instruments, strings on an instrument, or even notes on a string. Furthermore, we suspect that the musician may not always be aware of these adaptations if they are the result of applying the same control method to different instruments. Since musicians may not be able to tell us whether and how adaptations were made, we are interested in trying to identify adaptations without relying on their comments. To this end, we designed the experimental tasks so that the datasets from each cello may be aligned and compared. We shouldn't expect that two repetitions of an excerpt are exactly the same, even if the musician intended to produce identical performances. We are thus presented with the problem of identifying meaningful differences among natural variations. Of course, once we have identified a suspected adaptation, we can review the musician's comments to see if a consistent narrative emerges.

Our strategy is to perform a two-way univariate analysis of variance (ANOVA) on the influence of cello and string on the mean values of each control parameter during a note. The main effects will tell us if the two cellos were played differently overall and if, for example, lower strings are played differently than higher strings, while the interaction effect will tell us whether a string on one cello is played differently (relative to the other strings on the cello) than the corresponding string on the other cello.

8.1.1 Influence of cello and string on force

Tables 8.1 and 8.2 give the data and results of the two-way ANOVA on the influence of cello and string on the mean force during a note. The main effect of cello on force was not significant, [$F(1, 1289) = 0.26, p = 0.6$]. The mean forces on the two cellos (1.8 N and 1.7 N) are not significantly different. The main effect of string on force was significant, [$F(3, 1289) = 11.6, p < 0.001$]. The lower strings were played with larger mean forces (1.9 N and 1.8 N) than the higher strings (1.6 N and 1.7 N). However there is also a significant cello-string interaction effect on force, [$F(3, 1289) = 23, p < 0.001$], suggesting that these main effects may be misleading. Strings I and III had essentially the same mean forces on either cello, while String II was played with less force on Cello A and string IV was played with more force on Cello A.

		I	II	III	IV	Total
A	count	101	257	200	168	726
	mean (N)	1.6	1.5	1.9	2.0	1.8
	st.d. (N)	0.4	0.6	0.5	0.7	0.6
B	count	82	214	170	105	571
	mean (N)	1.6	1.8	1.8	1.5	1.7
	st.d. (N)	0.5	0.7	0.7	0.9	0.7
Total	count	183	471	370	273	1297
	mean (N)	1.6	1.7	1.9	1.8	1.7
	st.d. (N)	0.4	0.7	0.6	0.8	0.7

TABLE 8.1: Summary of mean force data gathered by cello and string.

	DF	SumOfSq	MeanSq	FRatio	PValue
Cello	1	0.11	0.11	0.26	0.6
String	3	14.37	4.79	11.6	< 2e-7
Interaction	3	29.01	9.67	23.5	< 9e-15
Error	1289	530.38	0.41		
Total	1296	573.82			

TABLE 8.2: Summary of two-way ANOVA results describing the influence of cello and string on the mean values of force during a note.

The musician complained that String II on Cello A was "molle" [soft/slack] compared to the other strings on the cello. A natural reaction to such a feeling would be to reduce the amount of force used on this string to avoid accidentally touching the adjacent strings. This is evident in the results of this section. I am not certain why the musician felt that this string felt slack because the two cellos used strings of the same model, with the same nut-to-bridge length, and nearly the same tension (tuned to nearly the same frequency). My best guess is that the musician is responding to slight differences in the bridge curvature.

The results of this section also show that String IV on Cello A was played with a larger force on average. By applying a greater bow force, the Helmholtz corner is sharpened, resulting in a greater contribution of higher harmonics, which is perceived as a richer timbre. Indeed, the musician complained that String IV on Cello A had a poor timbre. The greater average bow force on this string is likely a result of her attempts to find an acceptable timbre.

8.1.2 Influence of cello and string on absolute bow speed

Tables 8.3 and 8.4 give the data and results of the two-way ANOVA on the influence of cello and string on the mean absolute bow speed during a note. The main effect of cello on speed was significant, [$F(1, 1289) = 7.5, p = 0.006$]. Cello A was played with slightly faster bow speeds (345.7 mm/s) than Cello B (331.0 mm/s). The main effect of string on speed was significant, [$F(3, 1289) = 143, p < 0.001$]. A higher bow speed (451.6 mm/s) was used String I than on string II (359.4 mm/s) which was higher than

the bow speeds on strings III and IV (298.4 mm/s and 284.4 mm/s). There was not a significant cello-string interaction effect on speed, [$F(3, 1289) = 3.6, p = 0.014$].

I am not certain why Cello A was played with a slightly faster bow speed. Faster bow speeds give larger amplitude string vibrations and louder sounds, but Cello A was not mentioned to be inherently quieter than Cello B.

We would like to believe that differences between strings are due to the difference in mass, tension, or position of the strings. However, they are likely to be highly dependent on the musical excerpts. For example, slower speeds are associated with quieter notes and very long notes, which may appear more frequently on one string than another.

		I	II	III	IV	Total
A	count	101	257	200	168	726
	mean (mm/s)	460.5	375.1	305.7	279.3	345.7
	st.d. (mm/s)	119.1	92.8	76.4	98.2	111.5
B	count	82	214	170	105	571
	mean (mm/s)	440.6	340.6	289.7	292.6	331.0
	st.d. (mm/s)	113.6	95.0	92.2	100.0	110.0
Total	count	183	471	370	273	1297
	mean (mm/s)	451.6	359.4	298.4	284.4	339.2
	st.d. (mm/s)	116.8	95.3	84.3	98.9	111.0

TABLE 8.3: Summary of mean absolute speed data gathered by cello and string.

	DF	SumOfSq	MeanSq	FRatio	PValue
Cello	1	6.9e5	6.9e5	7.5	0.006
String	3	3.9e6	1.3e6	143	< 2e-80
Interaction	3	9.8e4	3.3e4	3.6	0.014
Error	1289	1.2e7	9.2e3		
Total	1296	1.6e7			

TABLE 8.4: Summary of two-way ANOVA results describing the influence of cello and string on the mean values of absolute speed during a note.

8.1.3 Influence of cello and string on bridge-to-bow distance

Tables 8.5 and 8.6 give the data and results of the two-way ANOVA on the influence of cello and string on the mean bridge-to-bow distance during a note. The main effect of cello on bridge-to-bow distance was significant, [$F(1, 1289) = 25, p < 0.001$]. Cello A was played at 71.0 mm which is about a quarter bow-width further from the bridge than cello B (68.7 mm). The main effect of string on bridge-to-bow distance was significant, [$F(3, 1289) = 51, p < 0.001$]. Strings I and II (70.5 mm and 69.3 mm) were played about a quarter to a third bow-width further from the bridge than string III (66.9 mm) but about a half bow-width closer than string IV (75.0 mm). However there is also a significant cello-string interaction effect on bridge-to-bow distance, [$F(3, 1289) = 4.7,$

$p = 0.003$], suggesting that the main effect of cello may be misleading. Cello A is played further from the bridge than Cello B except on string IV.

While the differences between cellos and between strings are statistically significant, I am not certain they are meaningful since they are less than a bow width. The cellist may have been gradually moving toward the bridge in response to the flatter bridge curvature found on Cellos A and B compared to the cellist's personal cello. That Cello B is played closer to the bridge may just be due to having played Cello B second.

		I	II	III	IV	Total
	count	101	257	200	168	726
A	mean (mm)	72.6	70.4	67.9	74.7	71.0
	st.d. (mm)	7.7	7.4	8.3	7.2	8.0
	count	82	214	170	105	571
B	mean (mm)	67.8	68.0	65.8	75.5	68.7
	st.d. (mm)	8.5	8.3	10.7	7.6	9.6
	count	183	471	370	273	1297
Total	mean (mm)	70.5	69.3	66.9	75.0	70.0
	st.d. (mm)	8.4	7.9	9.6	7.3	8.8

TABLE 8.5: Summary of mean bridge-to-bow distance data gathered by cello and string.

	DF	SumOfSq	MeanSq	FRatio	PValue
Cello	1	1.7e3	1.7e3	25.	< 7e-7
String	3	1.0e4	3.5e3	51.	< 5e-30
Interaction	3	9.6e2	3.2e2	4.7	0.003
Error	1289	8.8e4	69.		
Total	1296	1.0e5			

TABLE 8.6: Summary of two-way ANOVA results describing the influence of cello and string on the mean values of bridge-to-bow distance during a note.

8.1.4 Influence of cello and string on tilt

Tables 8.7 and 8.8 give the data and results of the two-way ANOVA on the influence of cello and string on the mean tilt during a note. The main effect of cello on tilt was not significant, [$F(1, 1289) = 1.8, p = 0.17$]. The mean tilt angles on cello A (34.5°) and cello B (35.0°) are similar. The main effect of string on tilt was significant, [$F(3, 1289) = 182, p < 0.001$]. The cello is played with increasingly tilted bow from string IV (29.9°) to string I (40.6°). The cello-string interaction effect on tilt was not significant, [$F(3, 1289) = 1.6, p = 0.18$].

The increasing tilt angle from low strings to high strings was commonly seen in our informal observations and is sometimes taught as part of bowing technique. The more massive lower strings are sometimes thought to require more contact with the hair to pull them properly while the timbre of the upper strings is favored by using less hair. The tilt angle is generally controlled by rolling the bow between the fingers

and thumb, but it also depends on the angles of the wrist, elbow, and shoulder. The difference in the tilt angle from String IV to String I may also be due to constraints in the coordination of these joint angles.

		I	II	III	IV	Total
A	count	101	257	200	168	726
	mean (°)	40.8	37.5	32.8	28.5	34.6
	st.d. (°)	5.5	6.2	6.1	6.5	7.4
B	count	82	214	170	105	571
	mean (°)	40.5	37.1	32.8	29.9	35.0
	st.d. (°)	5.8	5.8	5.7	6.3	6.8
Total	count	183	471	370	273	1297
	mean (°)	40.6	37.3	32.8	29.0	34.8
	st.d. (°)	5.6	6.0	5.9	6.5	7.2

TABLE 8.7: Summary of mean tilt data gathered by cello and string.

	DF	SumOfSq	MeanSq	FRatio	PValue
Cello	1	65.7	65.7	1.8	0.179
String	3	1.99e4	6.60e3	182	< 5e-98
Interaction	3	177	59.1	1.63	0.181
Error	1289	4.68e4	36.3		
Total	1296	6.67e4			

TABLE 8.8: Summary of two-way ANOVA results describing the influence of cello and string on the mean values of tilt during a note.

8.1.5 Influence of cello and string on absolute skew

Tables 8.9 and 8.10 give the data and results of the two-way ANOVA on the influence of cello and string on the mean absolute skew during a note. The main effect of cello on skew was not significant, [$F(1, 1289) = 0.2, p = 0.6$]. The mean skew angles on cello A (2.8°) and cello B (2.9°) are similar. The main effect of string on skew was significant, [$F(3, 1289) = 4.5, p = 0.004$]. Only the difference in skew angle between the strings with the least and most amount of skew is statistically significant, though at a difference of only 0.4° compared to the range of $\pm 12^\circ$, it is probably not meaningful. The cello-string interaction effect on skew was not significant, [$F(3, 1289) = 1.2, p = 0.3$].

		I	II	III	IV	Total
A	count	101	257	200	168	726
	mean (°)	2.7	2.7	2.9	2.9	2.8
	st.d. (°)	1.7	1.6	1.5	1.4	1.5
B	count	82	214	170	105	571
	mean (°)	2.5	2.8	3.2	2.7	2.9
	st.d. (°)	1.4	1.7	1.7	1.6	1.7
Total	count	183	471	370	273	1297
	mean (°)	2.6	2.7	3.1	2.8	2.8
	st.d. (°)	1.6	1.7	1.6	1.5	1.6

TABLE 8.9: Summary of mean absolute skew data gathered by cello and string.

	DF	SumOfSq	MeanSq	FRatio	PValue
Cello	1	0.62	0.62	0.24	0.6
String	3	34.9	11.6	4.5	0.004
Interaction	3	9.08	3.03	1.2	0.3
Error	1289	3.31e3	2.57		
Total	1296	3.35e3			

TABLE 8.10: Summary of two-way ANOVA results describing the influence of cello and string on the mean values of absolute skew during a note.

8.2 Normalized Schelleng diagrams for both cellos

In Section 8.1, we examined the global differences between the control parameters used on each cello and found that they were similar, but with statistically significant differences. We plot the data from each cello on separate normalized Schelleng diagrams (Figure 8.1) to see if this representation can help us interpret the data and the musician's comments. We have already seen in Section 7.1 that the musician neither approached the apex of the Schelleng diagram nor spent a significant time near Schelleng's maximum and minimum limits on either cello. Figure 8.1 shows that the musician did play closer to the apex on Cello B than on Cello A for at least some notes. Due to the ambiguity of the normalized Schelleng diagram, however, we do not immediately know whether this is because of differences in the musician's control parameters or differences in the properties of the instrument.

To get a better idea of what is pictured in Figure 8.1, we separated each pitch onto its own diagram, some of which are shown in Figure 8.2. The repetitions of each pitch give data points that are clustered around the same region of the Schelleng diagram. While this is expected for repetitions of the same note, we wouldn't necessarily expect this for different notes of the same pitch in different positions within the excerpt or in different excerpts. That the repetitions of different notes of the same pitch all collect in the same region indicates that either the control parameters are not very different, or that the normalized Schelleng diagram is not very sensitive to these kinds of differences.

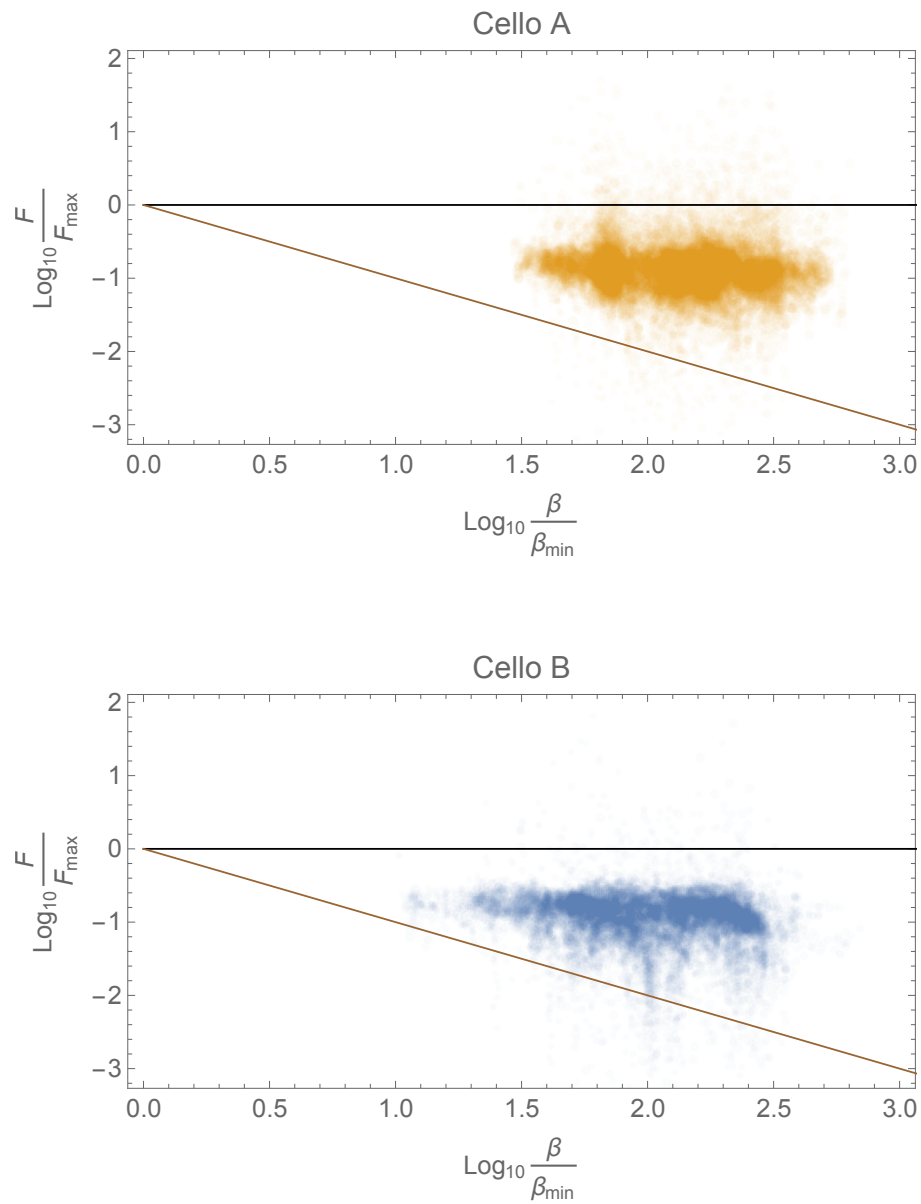


FIGURE 8.1: Normalized Schelleng diagrams for Cello A (top) and B (bottom).

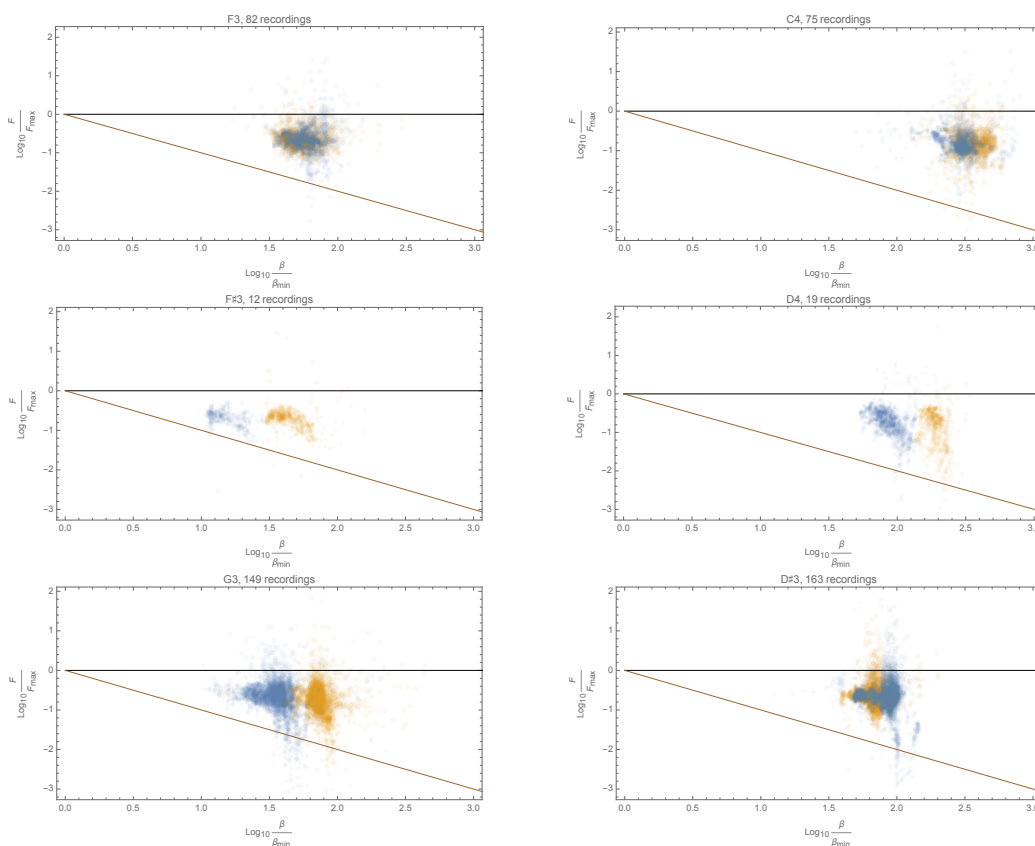


FIGURE 8.2: Normalized Schelleng diagrams for different pitches on Cello A (yellow) and Cello B (blue).

If we compare the cluster of data points for a note on Cello A with that of Cello B, we see that the two clusters have very similar shapes. This is because the datasets represent the same music, played with roughly the same sets of gestures. In some cases, such as with F_3 and C_4 , the two clusters overlap. In other cases, such as $F\sharp_3$, G_3 and D_4 , the Cello B data is shifted to the left of the Cello A data. For a few notes, like $D\sharp_3$, Cello B is shifted to the right of Cello A. The differences in the gestures for these notes is comparable to those found on other notes, so it is a bit surprising to find such a large shift in the figures. The shift is easily explained by looking at the bridge mobility. For notes with nearly equal bridge mobilities, the clusters overlap. For notes with large differences in mobility, we see the large shifts shown here. The cello with the higher bridge mobility (Cello B: $F\sharp_3$, G_3 and D_4 ; Cello A: $D\sharp_3$) has a higher Schelleng's lower limit, so its cluster appears shifted to the left.

8.3 Transients

It is logical to assume that a cello which more consistently gives acceptable transients would be preferable. In Section 7.2, we saw the overall distribution of transient durations found by manually inspecting each bow change. In this section we will compare transient duration statistics between cellos and strings. We would like to know if it was clearly easier to produce acceptable attacks on one cello than on the other.

We will also see if any strings stand out as being much more or less likely to produce acceptable attacks than another.

Figure 8.3 compares the distributions of transient durations between the two cellos. While both cellos have nearly the same percentage of acceptable attacks (A:58%, B:55%), Cello B is both much more likely to have a nearly perfect attack (A:14%, B:26%) and much more likely to have an attack that fails to achieve Helmholtz motion (A:6%, B:16%). The musician commented that Cello B was much easier to play.

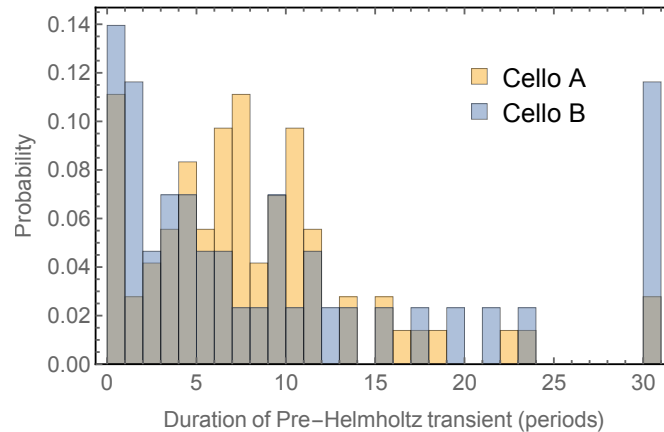


FIGURE 8.3: Comparison of distributions of transient durations for each cello.

Figure 8.4 compares the distributions of transient durations on each string of each cello¹. The white lines indicate the median, the boxes represent the interquartile range, and the whiskers show the minimum and maximum, all of which are calculated after removing the outliers shown as dots. String I on both instruments has many perfect transients but a relatively wide range. It seems that String I is easier to get a perfect transient, but that there is a greater risk of having a longer transient. Meanwhile String IV on Cello A has a slightly narrower interquartile range centered well within the acceptable duration. It seems that it is quite difficult to have a perfect transient on the heavier string, but an acceptable outcome is more likely. String II on Cello A stands out as having one of the highest medians, and the widest interquartile range. It certainly looks like the musician had difficulty playing it.

Referring back to Section 8.1.1, we see that String II on Cello A was played with less force than than the corresponding string on Cello B. I suspect that not using sufficient bow force on this string is what lead to having longer transient durations. Similarly, Section 8.1.1 shows String IV on Cello A was played with more force than the corresponding string on Cello B, explaining the shorter transient durations.

We might have hoped that we could predict something about the perception of strings based on their transient durations; if a string has longer transient durations, it should be perceived poorly. However, Strings II and IV on Cello A were both perceived negatively even though String II had long transient durations and String IV had short transient durations. It seems transient durations have more to do with the control parameters that the musician chooses to apply to the string than the musician's perceptions of the string independent of the control parameters applied to it.

¹See Table 2.1 for alternative names, pitches, and fundamental frequencies of each string.

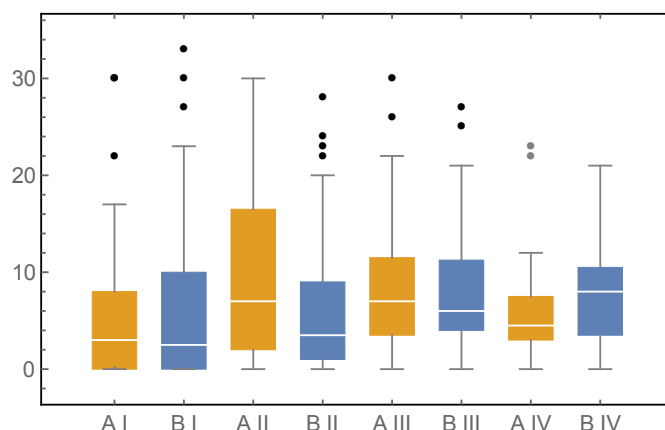


FIGURE 8.4: Comparison of distributions of transient durations (in periods) for each string (I, II, III, IV) of each cello (A, B).

8.4 Perception of bridge curvature

The musician complained of not being able to change the color of the sound and not being able to get the sound that she wanted in the last few measures of the Brahms excerpt while playing cello A. In particular, she struggled with the G_3 in the next-to-last measure, played by stopping string III at the midpoint with a contact point as far from the bridge as possible.

At first, she only identified the sound as being a problem and she associated it with a limitation of the instrument. She began to modify her control parameters accordingly (Figure 8.5). She associated the sound she wanted with playing high over the fingerboard, so her next few attempts showed increasing bridge-to-bow distances and higher bow speeds. As she played further from the bridge, she lowered the bow force to prevent touching the adjacent strings. Then she wanted to use more force, which helped her realize that the problem was not the inherent sound of the instrument, but the height of the strings (which could be adjusted).

Stopping the string lowers the portion of the string between the bridge and the stopping point with respect to the adjacent strings. This effect is greater when the bridge has a larger radius of curvature (i.e. flatter) and as the stopping point moves closer to the bridge, and its impact on playing is greater when the bow is placed further from the bridge. In particular when stopping an inner string near the midpoint and playing with the bow over the fingerboard, it may become difficult to play the string without touching one of the adjacent strings. We verified after the experiment that the musician's personal cello has a bridge with a much smaller radius of curvature than the bridges on our cellos.

Once the problem was properly diagnosed, the musician made a final recording in which she played initially closer to the bridge with a larger force, giving her a larger variation in the bowing parameters during the note as she transitioned into the final portion of the note.

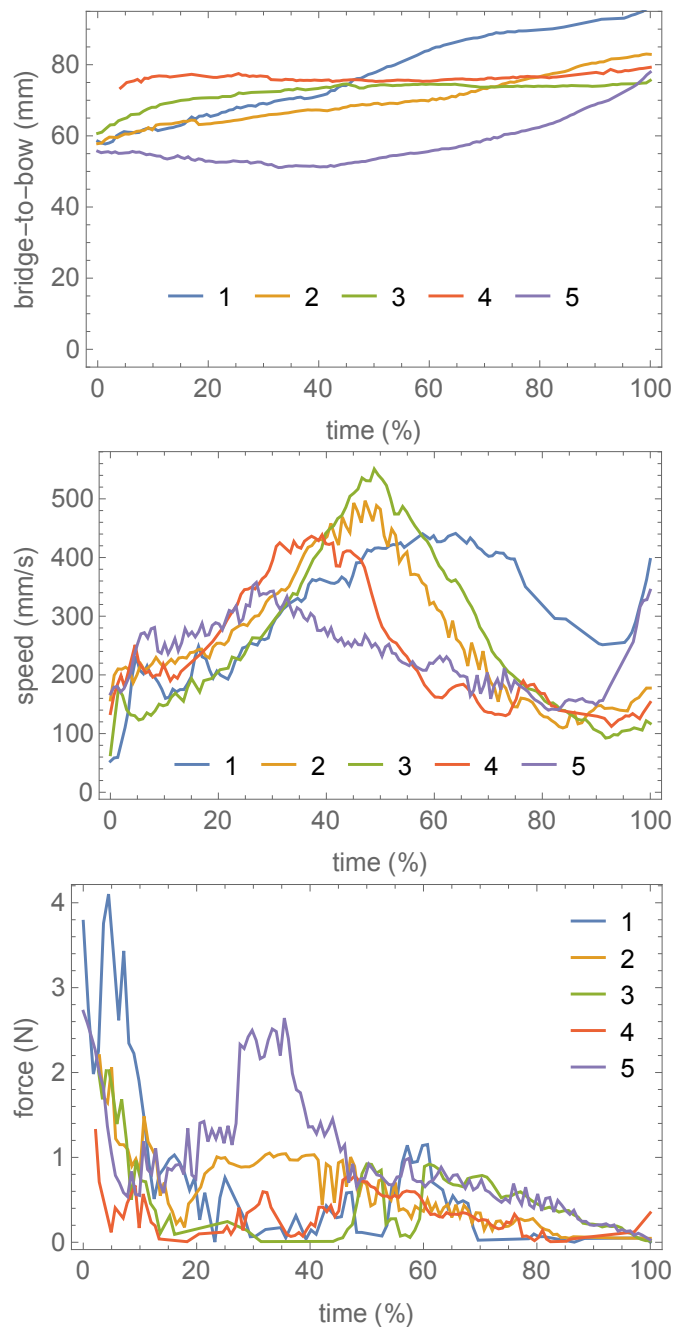


FIGURE 8.5: Control parameters for five attempts at playing the G_3 in the Brahms excerpt satisfactorily.

8.5 Richness comment

The musician thought there was a loss of richness between the first two notes of the Bach excerpt while playing Cello A. This is a two-octave leap from Eb_2 on string IV to Eb_4 on string I. Figure 8.6 shows how the musician changed her control parameters over several repetitions. The bow was brought about 8 mm closer to the bridge for

both notes, the bow speed was reduced for the second note, and the force was held the same.

The harmonic spectral centroid (μ), harmonic spectral deviation (σ), and the tris-timulus ratios ($T_{low}, T_{mid}, T_{high}$) were calculated for each note by Equation 8.1 where f_n is the frequency and w_n is the amplitude of the n^{th} harmonic.

$$\begin{aligned} \mu &= \frac{\sum_{n=1}^{20} f_n w_n}{f_1 \sum_{n=1}^{20} w_n} & T_{low} &= \frac{w_1}{\sum_{n=1}^{20} w_n} \\ \sigma &= \sqrt{\frac{\sum_{n=1}^{20} \left(\frac{f_n}{f_1} - \mu\right)^2 w_n}{\sum_{n=1}^{20} w_n}} & T_{mid} &= \frac{\sum_{n=2}^5 w_n}{\sum_{n=1}^{20} w_n} \\ & & T_{high} &= \frac{\sum_{n=6}^{20} w_n}{\sum_{n=1}^{20} w_n} \end{aligned} \quad (8.1)$$

The harmonic spectral centroid for Eb_4 starts lower than that of Eb_2 in the first repetition, indicating a loss of richness (Table 8.11). The tris-timulus ratios indicate that the energy of the Eb_4 is overly concentrated in the fundamental compared to the distribution of energy in Eb_2 . For the third repetition, the bow is placed closer to the bridge and a larger force is used for the first note, raising the harmonic centroid. The second note continues closer to the bridge with a larger force, but the speed is reduced relative to the previous repetitions. The net effect is that while the centroid of Eb_4 was increased, it was not sufficient to match the increased centroid of the Eb_2 . The last repetition reduces the force during the first note to lower the centroid of the Eb_4 while maintaining the greater force during the second note, with the result that the centroids are matched with energy being redistributed from the fundamental into the upper partials.

		μ	σ	T_{low}	T_{mid}	T_{high}
1	Eb_2	2.83	2.99	0.44	0.45	0.11
	Eb_4	2.42	2.56	0.52	0.39	0.09
2	Eb_2	2.97	3.21	0.45	0.42	0.13
	Eb_4	2.37	2.61	0.55	0.37	0.08
3	Eb_2	3.40	3.62	0.40	0.42	0.18
	Eb_4	2.69	3.07	0.52	0.38	0.11
4	Eb_2	3.09	3.29	0.42	0.44	0.14
	Eb_4	3.05	3.31	0.46	0.40	0.14

TABLE 8.11: Comparison of timbre indicators for the first two notes of the Bach excerpt on Cello A across four repetitions.

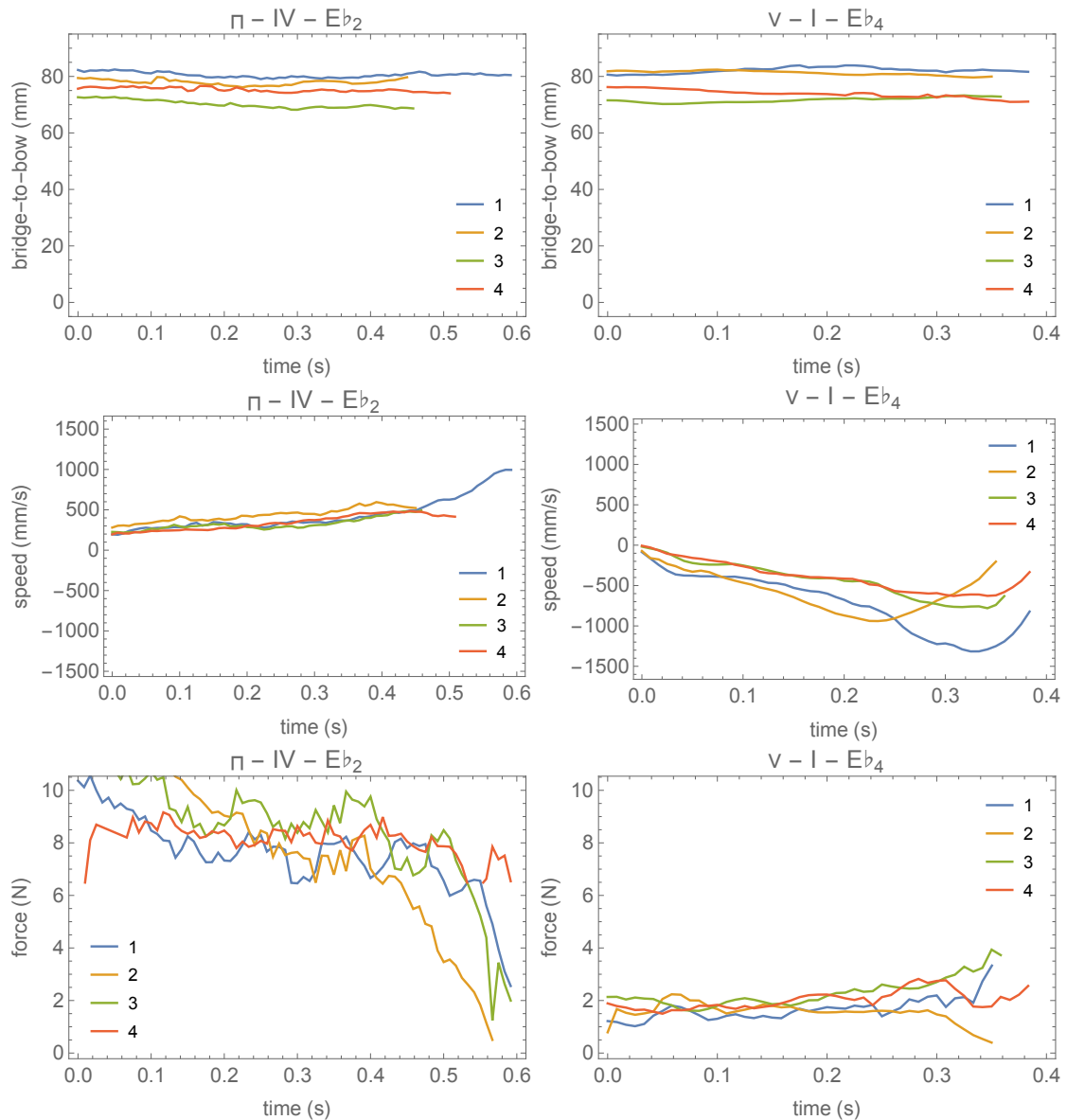


FIGURE 8.6: The evolution of control parameters as the musician seeks a gesture which does not give the perception of a loss of richness from the first note (left) to the second (right).

8.6 Piezo to microphone ratio and radiation

The musician² commented that String IV on Cello B "manque de puissance" [lacks power] and is "un peu plus sourd" [a little more muted] than String IV on Cello A. It is important to note that in each case, the comment was about the cello and not the sound. Whatever the musician is perceiving is attributed to an inherent property of the cello, not the result of applying particular control parameters to the instrument. For this reason we chose to look at ratio of the root mean square amplitude of the microphone

²Several of the musician's who evaluated the cellos made similar comments.

over the duration of a note to that of the string vibrations. Figure 8.7 shows that some notes are systematically louder on one cello than on the other for the same amplitude string motion.

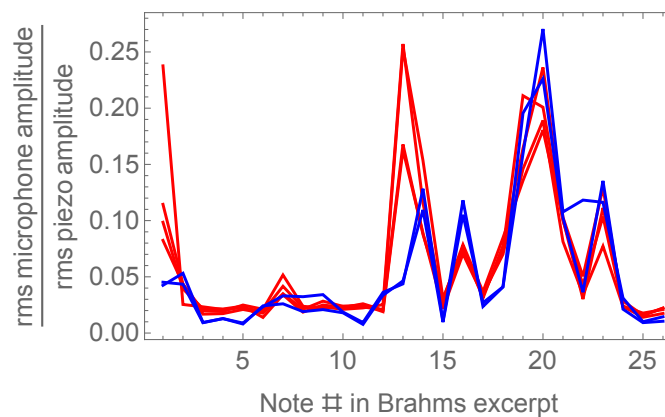


FIGURE 8.7: The ratio of the rms microphone amplitude to the rms piezo amplitude for each note in the Brahms excerpt for Cello A (red) and Cello B (blue).

To investigate this figure further, we collected all instances of each pitch on each cello, calculated the microphone-to-piezo ratios and overlaid the results on the radiativity measurements (Figure 8.8). The dots show the ratios of the rms microphone amplitude to the rms piezo amplitude for Cello A (yellow dots) and Cello B (blue dots). It is difficult to explain why sometimes blue dots are higher than yellow dots (or vice versa) when we look at the radiativity measurements for these cellos (Figure 2.8). But if we recognize that the radiativity measurements were made with the force applied along specific directions (horizontal and vertical), and if we realize that the bow is pulled across the string along the direction indicated by the inclination angle, then we conclude that the relevant radiativity is a linear combination of the horizontal and vertical radiativities. If we vary the inclination angle, then the radiativity creates a band rather than a line as seen in Figure 8.8.

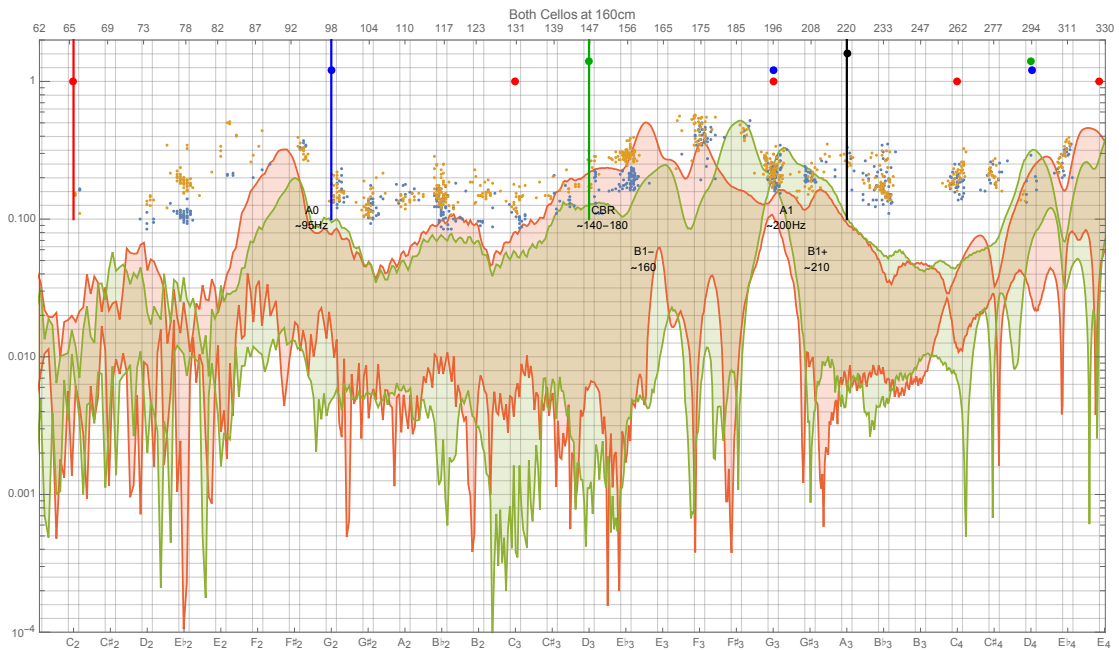


FIGURE 8.8: The ratio of the rms microphone amplitude to the rms piezo amplitude for each note played on Cello A (yellow dots) and Cello B (blue dots). Compare with the range of radiativities for Cello A (red) and Cello B (green).

A reasonable, yet naïve, approach to using the figure above is to use the inclination angle of the bow to determine the direction of the applied force. What we really need is the polarization of the vibrating string; after all, it is the string that is applying the force to the bridge. Figure 8.9 shows the relationship between inclination angle and string polarization. There are four clusters corresponding to the four strings of the cello, indicating that there is a range of preferred inclination angles for each string. It shows that the polarization angle is generally not equal to the inclination angle for any given bow stroke. We find that the entire range of radiativities is covered by the observed range of polarization angles. This is convenient because it means we do not need to measure the range of polarization angles for each string; we can just find the polarization angles for each frequency which maximizes or minimizes the magnitude of the radiativity.

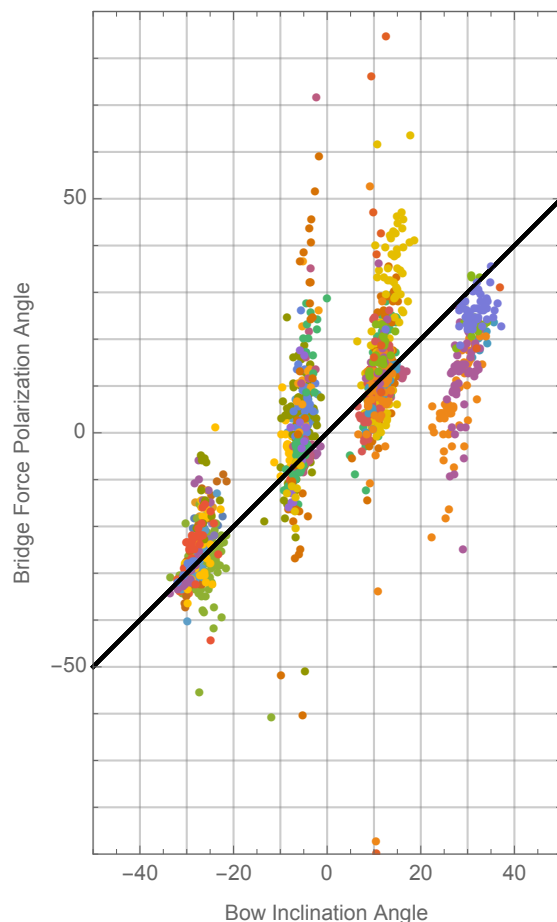


FIGURE 8.9: The mean polarization angle of piezo force signals as a function of the mean bow inclination angle for each note. Colors indicate pitch.

Returning to the musician's comment and Figure 8.8, let's look at the notes of the String IV. For the notes from 65 Hz to 82 Hz, the ranges of the fundamental are about equal, but their second harmonic (from 130 Hz to 164 Hz) show Cello A (red band) to have a higher radiativity at least some of the time. For the note at 87 Hz, both the fundamental and the second harmonic are greater. In each of these cases, the ratios of microphone to piezo for cello A (yellow dots) is greater than that of Cello B (blue dots). At just above 92 Hz, the radiativities at the fundamental are again equal, but the radiativity at the second harmonic of Cello B is greater than that of Cello A. Correspondingly we see that the ratios of microphone to piezo for Cello B are now slightly above those of Cello A. Thus by extending the traditional horizontal / vertical radiativity measurements to maximum / minimum radiativity measurements and looking at weighted sums of harmonic contributions, we may be able to explain the trends in the perceived difference in loudness between two cellos.

Chapter 9

Conclusion

This thesis concerns the relationship between the physical properties of an instrument and its perceived properties as a *musical* instrument. In particular, we focus on the relationship between the physical properties of a cello and its perceived playability.

Previous research has focused on the role of bridge mobility and has produced the Schelleng and Guettler diagrams. Discussions of playability using these diagrams depend on two assumptions which, before this thesis, had not yet been validated: that the musician perceives differences in the diagrams, and that the differences are relevant to the musician's perception of playability.

Our first goal was to validate whether these assumptions are true. Our second goal was to try to identify other physical measures that affect the perception of playability. Finally, we tried to find out how a particular change in cello set-up affects the perception of playability. To accomplish these goals, we bought two nearly identical cellos, and changed the soundposts so that one would be more tightly fit than the other. Additionally, we placed sensors in the bridge to measure the string vibrations, as well as passive markers on the cellos and bow to capture their motions. We hired a professional musician to evaluate and compare the two instruments. We used the musician's comments to help us interpret the physical measurements recorded during the experiment.

Section 9.1 describes our main contributions in the experiment design. Section 9.2 summarizes the data that we contribute to the discussion about the relationship between the physical properties of a cello and its perceived playability. Sections 9.3 and 9.4 discuss some of the implications of our data. Finally, Section 9.5 discusses the limitations of our work and suggests future lines of research.

9.1 Contributions in experiment design

We built a system for measuring control parameters and string vibrations which will be useful for future studies. The system consists of a commercial motion capture system, a cello bridge equipped with piezo sensors, commercial software for synchronizing signals, a bow force estimation model, a force transducer for calibrating the bridge sensor and the bow force estimation model, and a pipeline for extracting useful information (control parameters, pitch tracking, and string vibrations along different polarization axes) from the raw data.

In Section 4.3 we provided a thorough review of the principles of camera-based motion capture technique. In particular, we explored different methods of minimizing systematic errors when locating landmarks from the positions of passive markers. These methods include choosing appropriate camera and marker positions, enforcing rigid body constraints, using temporary markers, and using optimization procedures (plane fitting, cylinder fitting) to average out random position measurement errors.

In Section 4.2, we described our modification of an existing sensor design to improve its mechanical robustness. A pair of piezoelectric elements are placed underneath each string, held in place by plastic supports. The wires connecting the piezoelectric elements to the circuit pass through the bridge which minimizes the stresses on the electrical connections at the ends of the wires. This prevents the electrical connections from breaking due to movements of the wires during handling of the cello. In addition, we interpret the calibration coefficients of the bridge sensor in terms of the gains of the piezos and their orientations (Equation 4.11). Having piezos under each string reveals events on individual strings which cannot be separated using a single contact microphone (Figure 6.3). Using two piezos under each string enables us to separate the horizontal and vertical polarizations of the string vibrations, which is useful for, among other things, distinguishing hammer-downs of a left-hand finger from bow strokes.

In Section 3.3, we extended an existing method of estimating the bow force from motion capture data so that it takes into account the compliance of the string. We established that the limiting factor in the accuracy of this technique is the spatial resolution of the motion capture system, which cannot be overcome through processing of the noisy data.

In Section 6.1, we provided a complete list of steps in the pipeline for pre-processing data from our system. The pipeline includes steps for calibrations, error corrections, estimation of the control parameters (bow force, bow speed, bow position, bow angles, and string length), pitch tracking, and calculating Schelleng's maximum and minimum bow force limits. Since many calculations depend on other calculations and measurements, it is helpful to have them all listed in an order which ensures that the necessary dependencies are available.

In Section 5.5, we suggested three excerpts which are useful for evaluating cellos based on prior observations of cellists evaluating instruments at Violoncelle En Seine (Paris, 2014). We also discussed framing the experiment and constructing questions to elicit a natural performance and honest responses, potentially leading to unexpected insights into how cellos are evaluated.

9.2 Summary of results

In Section 7.1, we normalized the Schelleng diagram, so that we can compare notes with different bow speeds and frequencies. We found that the gestures used by the musician to play our excerpts leave a healthy margin from Schelleng's maximum and minimum bow force limits. Therefore, slight changes in these limits are not likely to affect the cellist's evaluation of the instrument.

In Section 8.2, we found that the Schelleng diagram is not appropriate for comparing similar gestures because the log scales minimize the visual impact of differences which are smaller than an order of magnitude. We also found that visual differences in the normalized Schelleng diagram are dominated by differences in the bridge mobility.

In Section 7.2, we presented data which confirms that transient durations by a human professional cello player follow a distribution similar to what was seen in previous studies of the violin. In particular, while many bow changes are considered perfect and roughly half of the bow changes are considered acceptable, the other half would be considered unacceptable, and many bow changes didn't even achieve Helmholtz motion within the observation window. However, the musician didn't complain about

the overly-long transients suggesting that there may be more important considerations than transient length when evaluating the quality of bow changes.

A bow change strategy was presented in Section 7.2 which is useful for simulation studies. In Section 6.3, we provide typical and extreme values of each control parameter for cellists. These measurements will be useful when designing systems to measure control parameters, when deciding the ranges of values to use in simulation studies, and when considering the implications of the results of simulation studies.

In Section 8.1, an ANOVA analysis of the control parameters was performed which indicates adaptation of the musician to the properties of individual strings on each cello. In particular, the musician said that the D string felt "molle" [soft/slack] on a cello set-up to be "souple" [flexible]. She ended up using less bow force on the string which lead to longer transients during bow changes, as seen in Section 8.3. The perception that the string feels slack is likely a comment on the perceived compliance of the string. Since the string make and model, length, and tension are all the same as on the other cello, we suspect that the difference in perception is due to slight differences in the geometry of the bridge.

Whereas we would like to think that perceived differences in sound are due to differences in vibrational behavior of the instrument, we have seen further evidence that such perceptions might sometimes actually be due to differences in geometry, e.g., bridge curvature. Section 8.4 describes the evolution of gestures based on unsatisfactory responses of the cello. Once the musician realized that the cause of the problem was the relative heights of the adjacent strings near the bowing point, she was able to immediately adapt her gestures to achieve a satisfactory sound.

In Section 8.5, we presented evidence that the perceived richness may be related to the harmonic spectral centroid and tristimulus ratios. We also demonstrate how the control parameters may be changed in order to balance the richness of two notes.

In Section 8.6, we explored measuring the radiativity of the cello using a microphone and the string vibrations of real playing. We found that when interpreting the radiativity measured with an impulse hammer and a microphone at a point, we should look at the range (or possibly just the maximum) of radiativities over all force polarization angles. Then we should include not just the fundamental but also the contributions from higher harmonics. This study was motivated by the musician's perception that the C string on one cello was louder than the other. We conclude that the comment is not necessarily based on the absolute loudness of the notes played (which depend on the control parameters used), but on the inherent properties of the instrument as measured by the radiativity.

9.3 Schelleng's limits

The common strategy in classical cello playing is to use typical range of bow forces in the range of 1-2.5 Newtons and bow speeds of 200-500 millimeters per second at bridge-to-bow distances between 0.09 and 0.12 times the string length. Bow speed and bow position work together to determine the amplitude of the sound (within the Helmholtz region) while the force is varied to change the timbre of the sound. These three main control parameters are coordinated: as the musician plays closer to the bridge, she tends to use more force and less bow speed. If the musician would like to maintain large margins from the upper and lower limits, she is well served by adopting the common strategy.

If the musician ever deviates far from the common strategy, she will encounter odd sounds and perceive the upper and lower limits. Moving the bow toward the bridge while increasing the bow speed raises the lower bow force limit allowing the musician to play in the multiple-slip region of Schelleng's diagram. Likewise, moving the bow away from the bridge while lowering the bow speed lowers the upper bow force limit allowing the musician to play in the raucous region of Schelleng's diagram.

The range of expression available using the common strategy is sufficient for classical music so classical cellists rarely encounter these limits while evaluating a cello. Therefore any variations in the upper and lower limits between notes or between cellos are not likely to be a factor in the evaluation of a cello.

Wolf note An exception to the previous paragraph are wolf notes, which occur when the lower bow force limit is sufficiently large. While our cellos did not have severe wolf notes, we noticed that cellists don't always comment on the wolf note and may not even notice it. Our hypothesis is that the players have sufficient experience to work around the wolf note. Luthiers may try to shift a wolf note to a frequency between the notes of the chromatic scale. Some have suggested that the player might deal with a wolf note by playing slightly out of tune, the musician's equivalent to the luthier's actions. Wolf notes are usually found when playing softly quite far from the bridge where the string is more compliant. In this case, a large bow force is likely to cause the string to displace enough for the bow to accidentally stroke adjacent strings. To prevent this from happening the player reduces the bow force and inadvertently approaches the lower bow force limit. If the player moves closer to the bridge and uses a slower bow speed, the string will not be displaced as much and the player will be encouraged to apply a force greater than the lower bow force limit. Professional cellists are probably accustomed to playing closer to the bridge with more force and thus avoid wolf notes entirely, explaining the lack of comments.

An informal experiment. The Schelleng diagram indicates a monotonically *increasing* range of log-forces as the musician plays further from the bridge (Figure 9.1). If musicians perceive bow force on a logarithmic scale, they should perceive an increasing range of forces as they move away from the bridge.

The range of forces (on a linear scale) will reach a maximum at twice the distance from the bridge as the point where the upper and lower limits are equal (Figure 9.2). This point is still very close to the bridge, so the region of interest (where musicians usually play) shows a monotonically *decreasing* range of forces as the musician plays further from the bridge. If musicians perceive bow force on a linear scale, they should perceive a decreasing range of forces as they move away from the bridge.

I asked a violinist and a cellist who were unfamiliar with the Schelleng diagram to describe their perceptions of the range of forces available at each position, indicating where the range of forces is largest and where it is smallest. The experiment failed because the musicians would change bow speed along with the bow position and force. They recognized the need for greater forces near the bridge, but they were incapable of comparing the range of large forces near the bridge to the range of smaller forces over the fingerboard. I rephrased the question in terms of timbre, but they were unsure of how to quantify differences in timbre.

I now suspect that by changing the bow speed at nearly any distance from the bridge, they are able to increase the upper bow force limit above the limit imposed by the deformation of the bow and to decrease the lower limit below the threshold for perceiving differences in the force.

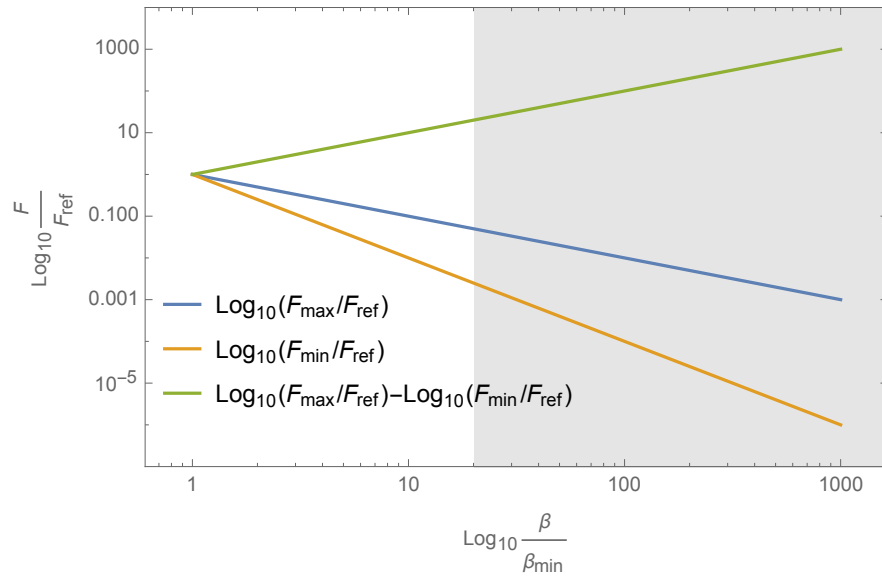


FIGURE 9.1: If bow forces are perceived logarithmically, then the perceived range between Schelleng's minimum and maximum forces should increase as the musician plays further from the bridge. The gray region is where a musician is likely to play.

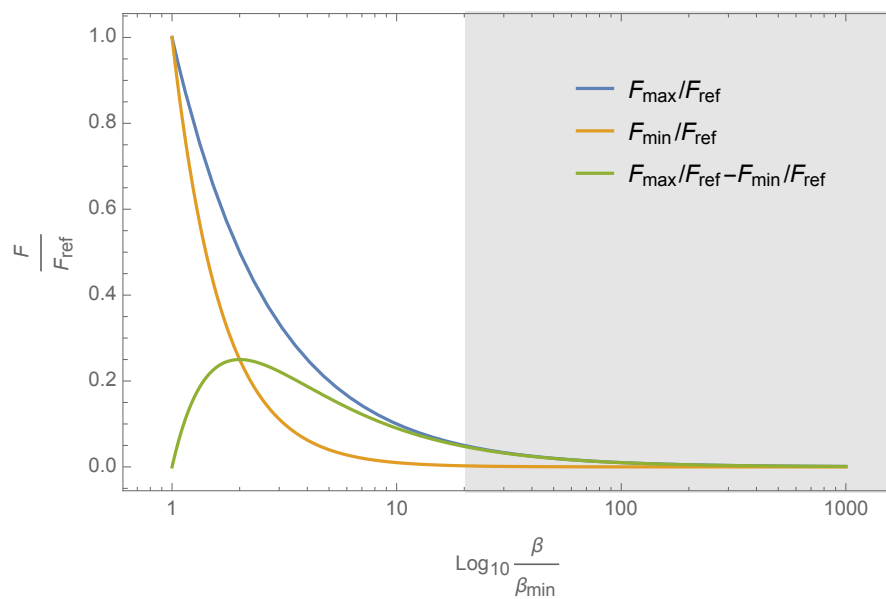


FIGURE 9.2: If bow forces are perceived linearly, then the perceived range between Schelleng's minimum and maximum forces should decrease as the musician plays further from the bridge. The gray region is where a musician is likely to play.

9.4 Guettler's diagram

Research strategy. Transient duration times are sensitive to initial conditions and slight variations in gestures. Rather than using a single initial condition and simulating its deterministic outcome for various gestures, it may be more useful to simulate each gesture starting from several initial conditions and interpret the results probabilistically as in Demoucron, 2015. Using this approach, useful predictions about the physical behavior of bowed strings can be generated even when using simplified models. However, we must be careful when using these results to infer conclusions about the player's perception of transients.

Measuring transients. Often, transient durations are measured by examining the time-domain waveform of the string vibrations. The perception of the transient not only depends on its nature (prolonged sticking vs multiple slipping) as discussed by Guettler and Askenfelt (1997), but also on growth rates (rise times), and the timbre of the subsequent steady-state motion. While we have been using a thumb-rule of 70 ms or 7 periods to threshold the acceptability of a transient, we should remind ourselves often that this threshold comes from a particular musical context (neutral scales) and that the acceptable durations of transients are dependent on the musical context. First steps in studying this effect would be to characterize the effect of rise times and post-transient timbres using listening tests.

Acceptability definition. It is an open question whether the acceptability thresholds for cello and bass attacks are the same as for violin. In particular, should we be concerned with the absolute duration (milliseconds) or the relative duration (vibration periods). We observed transient duration distributions on the cello which are similar to those on the violin. But a larger sample including a wider range of musical contexts and a dedicated perceptual study is still needed for the larger instruments. Note, our musician did not complain about the longer transients, and in fact seemed quite happy with the longest ones given the musical context.

Player strategies. It has been suggested that musicians have heightened senses, fine motor control, and reaction times and that these above-average capabilities allow the musician to control their instrument. However, the best human reaction times are roughly twice the duration of acceptable transients. The musician simply does not have time to sense the instrument response, understand it, devise an appropriate reaction, and execute it in time to ensure an acceptable transient. Any successful strategy must be one that is determined before the gesture is executed. In Section 7.2 we described one such gesture observed on the cello.

9.5 Limitations and Perspectives

While the experiment has produced interesting results, some of our conclusions are necessarily qualified by the limitations of the experiment.

We were only able to get a somewhat complete set of data from one professional musician. The data from the experiment represents her perceptions and her techniques. We feel that it is safe to generalize our rather tame conclusions to other musicians based on informal observations, but a formal study to validate the generalization would be welcome.

Having only one musician also limits the amount of data available to analyze, especially comments. An easy solution to this problem is to repeat the experiment with other musicians. Another approach to eliciting more comments would be to give

the cellists more to comment on. While the sound-post adjustments were apparently enough to make the instruments distinguishable, I think that we could have made the instruments even more different. Our luthier gave us two variations on what his customers tend to like. A second luthier may have made a very different adjustment corresponding to the preferences of her customers. I think that having larger differences might have led to a larger number of useful comments during the experiment.

Due to time constraints during recording, we were only able to examine three short musical excerpts. While we tried to cover ranges of dynamics, tempo, and expressivity versus technique, the chosen excerpts still represent a rather limited range of bowing techniques and musical styles. Knowing that the musician would have only a short time to familiarize herself with the bow, we avoided bowing techniques which strongly depend on the physical characteristics of the bow (e.g., *sautillé*, *spiccato*). The excerpts also didn't call for any specialized techniques (*pizzicato*, *col legno*, etc.), some of which would have changed the range of bridge-to-bow distances (*sul tasto*, *ponticello*) or the importance of the accuracy of estimating string crossing boundaries (*double-stops*).

Time constraints also prevented us from making many recordings of the same gestures. We compared average values of control parameters over several notes to find signs of adaptation. If we had more repetitions of each note, then we could begin to look at the variations in the time-series of the control parameters during the note. The goal would be to identify specific changes in the gestures (such as the attacks) which result in desired changes in the sound, both during the evolution of the note and between repetitions of the note. One strategy for increasing the number of repetitions is to use series exercises in which a pattern of intervals is played starting on different pitches. We could argue that notes in the same position of the pattern are equivalent except in as much as the particular pitch affects the result. An analysis of variance would indicate whether the pitch of a note in the pattern requires adaptation by the musician.

One of the reasons we only had data for one musician is due to problems with the piezo sensor/circuit. The discharge rate of the capacitors in the circuit was too slow for the application. The circuit needed to be reset occasionally to prevent the circuit from becoming saturated. Even after realizing the need to reset the circuit, the signals were sometimes noisier than we would have liked. This problem was made worse by the data acquisition card imposed upon us by the synchronization system which appeared to leak signals, contaminating the microphone signal with the noise of the piezos. Given that the synchronization software was not particularly convenient, I would recommend developing another system using multiple data acquisition devices and a common synchronization signal.

We claim that Schelleng's minimum bow force limit is probably not relevant to the evaluation of the cello based on the observation that there weren't data approaching that limit except when lifting the bow off the string. Part of this is because the lower limit is extremely small at many frequencies. But even when the lower limit is reasonably high, it is usually smaller than the estimated accuracy of our bow force estimation. This means that if the bow force were very near the limit, then it would not be significantly different from zero given the measurement accuracy. Measurement error is then more likely to falsely indicate zero force and discard the data. To further validate the claim that Schelleng's minimum bow force limit is probably not relevant to the evaluation of the cello, a force estimation system with better accuracy should be used.

Several musicians stated that they would require their own bow to give an accurate evaluation of a cello. Nonetheless, none of the three professional musicians who evaluated our instruments complained about using our bow. The musician studied in this thesis even praised the performance of our bow. Given the comments, I suggest that

we continue to look for non-invasive ways to accurately measure control parameters using the musician's personal bow, but I also wouldn't discredit any research based on the use of a common bow if the musicians do not complain about it.

Beyond shoring up the results of this thesis, I think that further progress in relating physical properties of instruments to their perceived quality may be found through listening tests in which musicians are asked to describe subtle variations in Helmholtz motion to better understand how a group of musicians describes various sounds. Simulation studies could then relate the combinations of control parameters which lead to these different named timbres. Musicians could also be asked to describe variations in attack transients with the same goals: find the vocabulary used to talk about transients and identify meaningful attributes of transients beyond their durations. In particular I would look at the effect of rise times and post-transient timbres.

Appendix A

Circuit for bridge sensors

Appendix B

Skew Projection

We have used skew projection to approach two problems in this thesis: when calculating the bow position control parameters (Section 3.2.2), and when calculating the piezo calibration coefficients (Section 4.2.2). In this appendix we'll explain how skew projection is performed and how it is related to the more commonly known orthogonal projection.

Given an n -dimensional vector space, we can choose any n linearly independent vectors as a basis. We often work with vector spaces which have an inner product which allows us to talk about the angle between two vectors. In this case we usually choose an orthonormal basis. The inner products between horizontal H and vertical V basis vectors of the piezo calibration problem satisfy the orthogonal and normalization conditions.

$$\begin{aligned}
 \vec{e}_H \cdot \vec{e}_V &= 0 && \text{orthogonal} \\
 \vec{e}_H \cdot \vec{e}_H &= 1 && \text{normalized} \\
 \vec{e}_V \cdot \vec{e}_V &= 1 && \text{normalized}
 \end{aligned} \tag{B.1}$$

While orthonormal bases make certain calculations easy, they are not always the most convenient or natural bases to work with. In Section 4.2.2 the orientations of the piezos in the bridge sensor provided natural directions. While we aimed to have the piezos orthogonal to each other, this was not guaranteed. Choosing to keep the basis vectors to be normalized while allowing them to be skewed gives us the following relations between the inner products. The treble T and bass B basis vectors of the piezo calibration problem demonstrate the general case.

$$\begin{aligned}
 \vec{e}_T \cdot \vec{e}_B &= m_{TB} = (m_{TT}m_{BB})^{1/2} \cos(\theta_{TB}) && \neq 0 \\
 &&& \text{skew} \\
 \vec{e}_T \cdot \vec{e}_T &= m_{TT} && = 1 \\
 &&& \text{normalized} \\
 \vec{e}_B \cdot \vec{e}_B &= m_{BB} && = 1 \\
 &&& \text{normalized}
 \end{aligned} \tag{B.2}$$

Any vector within a vector space can be written as a linear combination of basis vectors. The force vector from the piezo calibration problem can be written as a linear combination of either the HV-basis or the TB-basis.

$$\begin{aligned}
 \vec{F} &= F^H \vec{e}_H + F^V \vec{e}_V \\
 \vec{F} &= F^T \vec{e}_T + F^B \vec{e}_B
 \end{aligned} \tag{B.3}$$

The only difficulty is in determining the coefficients. In an orthonormal basis, we can use the familiar orthonormal projection relations shown here with proofs.

$$\begin{aligned}
F^H &= \vec{F} \cdot \vec{e}_H & F^V &= \vec{F} \cdot \vec{e}_V \\
\vec{F} \cdot \vec{e}_H &= (F^H \vec{e}_H + F^V \vec{e}_V) \cdot \vec{e}_H & \vec{F} \cdot \vec{e}_V &= (F^H \vec{e}_H + F^V \vec{e}_V) \cdot \vec{e}_V \\
&= F^H \vec{e}_H \cdot \vec{e}_H + F^V \vec{e}_V \cdot \vec{e}_H & &= F^H \vec{e}_H \cdot \vec{e}_V + F^V \vec{e}_V \cdot \vec{e}_V \\
&= F^H(1) + F^V(0) & &= F^H(0) + F^V(1) \\
&= F^H & &= F^V
\end{aligned} \tag{B.4}$$

However these relations do not hold if the basis vectors are not normalized or are not orthogonal.

$$\begin{aligned}
F^T &\neq \vec{F} \cdot \vec{e}_T & F^B &\neq \vec{F} \cdot \vec{e}_B \\
\vec{F} \cdot \vec{e}_T &= (F^T \vec{e}_T + F^B \vec{e}_B) \cdot \vec{e}_T & \vec{F} \cdot \vec{e}_B &= (F^T \vec{e}_T + F^B \vec{e}_B) \cdot \vec{e}_B \\
&= F^T \vec{e}_T \cdot \vec{e}_T + F^B \vec{e}_B \cdot \vec{e}_T & &= F^T \vec{e}_T \cdot \vec{e}_B + F^B \vec{e}_B \cdot \vec{e}_B \\
&= F^T(m_{TT}) + F^B(m_{TB}) & &= F^T(m_{TB}) + F^B(m_{BB}) \\
&\neq F^T & &\neq F^B
\end{aligned} \tag{B.5}$$

The previous calculation shows us that orthonormal projection is a special case of the more general skew projection. It was very convenient to have the inner products reduce to zeros and ones in the orthonormal calculation. To get a similar convenience in the general case we introduce the dual bases for each of our bases. The dual basis (\vec{e}^H, \vec{e}^V) is dual to the direct basis (\vec{e}_H, \vec{e}_V) . The dual basis (\vec{e}^T, \vec{e}^B) is dual to the direct basis (\vec{e}_T, \vec{e}_B) . The inner products between the direct and dual basis vectors satisfy the duality relations, which look a lot like the orthonormal conditions that we found so convenient before.

$$\begin{aligned}
\vec{e}^H \cdot \vec{e}_V &= 0 & \vec{e}^T \cdot \vec{e}_B &= 0 \\
\vec{e}^V \cdot \vec{e}_H &= 0 & \vec{e}^B \cdot \vec{e}_T &= 0 \\
\vec{e}^H \cdot \vec{e}_H &= 1 & \vec{e}^T \cdot \vec{e}_T &= 1 \\
\vec{e}^V \cdot \vec{e}_V &= 1 & \vec{e}^B \cdot \vec{e}_B &= 1
\end{aligned} \tag{B.6}$$

We can write the dual basis vectors as linear combinations of the direct basis vectors by using the duality relations which define them. The resulting expressions can be verified to satisfy the duality relations and to be linearly independent of each other.

$$\begin{aligned}
\vec{e}^H &= \vec{e}_H & \vec{e}^T &= \frac{(\vec{e}_B \cdot \vec{e}_B) \vec{e}_T - (\vec{e}_B \cdot \vec{e}_T) \vec{e}_B}{(\vec{e}_B \cdot \vec{e}_B)(\vec{e}_T \cdot \vec{e}_T) - (\vec{e}_B \cdot \vec{e}_T)(\vec{e}_B \cdot \vec{e}_T)} \\
\vec{e}^V &= \vec{e}_V & \vec{e}^B &= \frac{(\vec{e}_T \cdot \vec{e}_T) \vec{e}_B - (\vec{e}_B \cdot \vec{e}_T) \vec{e}_T}{(\vec{e}_T \cdot \vec{e}_T)(\vec{e}_B \cdot \vec{e}_B) - (\vec{e}_B \cdot \vec{e}_T)(\vec{e}_B \cdot \vec{e}_T)}
\end{aligned} \tag{B.7}$$

The inner product of a vector \vec{F} with the dual basis vectors (\vec{e}^T, \vec{e}^B) gives us the coefficients (F^T, F^B) of that vector with respect to the direct basis vectors (\vec{e}_T, \vec{e}_B) . By

using the dual basis to calculate the projection coefficients, we can treat both orthonormal and skewed projections in exactly the same way.

$$\begin{aligned}
F^H &= \vec{F} \cdot \vec{e}^H & F^T &= \vec{F} \cdot \vec{e}^T \\
\vec{F} \cdot \vec{e}^H &= (F^H \vec{e}_H + F^V \vec{e}_V) \cdot \vec{e}^H & \vec{F} \cdot \vec{e}^T &= (F^T \vec{e}_T + F^B \vec{e}_B) \cdot \vec{e}^T \\
&= F^H \vec{e}_H \cdot \vec{e}^H + F^V \vec{e}_V \cdot \vec{e}^H & &= F^T \vec{e}_T \cdot \vec{e}^T + F^B \vec{e}_B \cdot \vec{e}^T \\
&= F^H(1) + F^V(0) & &= F^T(1) + F^B(0) \\
&= F^H & &= F^T \\
F^V &= \vec{F} \cdot \vec{e}^V & F^B &= \vec{F} \cdot \vec{e}^B \\
\vec{F} \cdot \vec{e}^V &= (F^H \vec{e}_H + F^V \vec{e}_V) \cdot \vec{e}^V & \vec{F} \cdot \vec{e}^B &= (F^T \vec{e}_T + F^B \vec{e}_B) \cdot \vec{e}^B \\
&= F^H \vec{e}_H \cdot \vec{e}^V + F^V \vec{e}_V \cdot \vec{e}^V & &= F^T \vec{e}_T \cdot \vec{e}^B + F^B \vec{e}_B \cdot \vec{e}^B \\
&= F^H(0) + F^V(1) & &= F^T(0) + F^B(1) \\
&= F^V & &= F^B
\end{aligned} \tag{B.8}$$

We are now in position to derive Equation 4.5 in which \vec{e}_T and \vec{e}_B are normalized but not necessarily orthogonal.

$$\begin{aligned}
F^T &= \vec{F} \cdot \vec{e}^T \\
&= \vec{F} \cdot \frac{(\vec{e}_B \cdot \vec{e}_B) \vec{e}_T - (\vec{e}_B \cdot \vec{e}_T) \vec{e}_B}{(\vec{e}_B \cdot \vec{e}_B)(\vec{e}_T \cdot \vec{e}_T) - (\vec{e}_B \cdot \vec{e}_T)(\vec{e}_B \cdot \vec{e}_T)} \\
&= \frac{(\vec{e}_B \cdot \vec{e}_B)(\vec{F} \cdot \vec{e}_T) - (\vec{e}_B \cdot \vec{e}_T)(\vec{F} \cdot \vec{e}_B)}{(\vec{e}_B \cdot \vec{e}_B)(\vec{e}_T \cdot \vec{e}_T) - (\vec{e}_B \cdot \vec{e}_T)(\vec{e}_B \cdot \vec{e}_T)} \\
&= \frac{(1)(\vec{F} \cdot \vec{e}_T) - (\vec{e}_T \cdot \vec{e}_B)(\vec{F} \cdot \vec{e}_B)}{(1)(1) - (\vec{e}_T \cdot \vec{e}_B)(\vec{e}_T \cdot \vec{e}_B)} \\
F^B &= \vec{F} \cdot \vec{e}^B \\
&= \vec{F} \cdot \frac{(\vec{e}_T \cdot \vec{e}_T) \vec{e}_B - (\vec{e}_B \cdot \vec{e}_T) \vec{e}_T}{(\vec{e}_T \cdot \vec{e}_T)(\vec{e}_B \cdot \vec{e}_B) - (\vec{e}_B \cdot \vec{e}_T)(\vec{e}_B \cdot \vec{e}_T)} \\
&= \frac{(\vec{e}_T \cdot \vec{e}_T)(\vec{F} \cdot \vec{e}_B) - (\vec{e}_B \cdot \vec{e}_T)(\vec{F} \cdot \vec{e}_T)}{(\vec{e}_T \cdot \vec{e}_T)(\vec{e}_B \cdot \vec{e}_B) - (\vec{e}_B \cdot \vec{e}_T)(\vec{e}_B \cdot \vec{e}_T)} \\
&= \frac{(1)(\vec{F} \cdot \vec{e}_B) - (\vec{e}_T \cdot \vec{e}_B)(\vec{F} \cdot \vec{e}_T)}{(1)(1) - (\vec{e}_T \cdot \vec{e}_B)(\vec{e}_T \cdot \vec{e}_B)}
\end{aligned} \tag{B.9}$$

In Section 3.2.2 we used skew projection in three-dimensions. The direct basis was $(\hat{x}_H, \hat{y}_S, \hat{z}_{HS} = \frac{\hat{x}_H \times \hat{y}_S}{\|\hat{x}_H \times \hat{y}_S\|})$ with the following inner products.

$$\begin{aligned}
\hat{x}_H \cdot \hat{x}_H &= 1 & \hat{x}_H \cdot \hat{y}_S &= \sin(\theta_S) \\
\hat{y}_S \cdot \hat{y}_S &= 1 & \hat{y}_S \cdot \hat{z}_{HS} &= 0 \\
\hat{z}_{HS} \cdot \hat{z}_{HS} &= 1 & \hat{x}_H \cdot \hat{z}_{HS} &= 0
\end{aligned} \tag{B.10}$$

The corresponding dual basis is given by

$$\begin{aligned}
\vec{x}^H &= \frac{(\hat{y}_S \cdot \hat{y}_S) \hat{x}_H - (\hat{x}_H \cdot \hat{y}_S) \hat{y}_S}{(\hat{y}_S \cdot \hat{y}_S)(\hat{x}_H \cdot \hat{x}_H) - (\hat{x}_H \cdot \hat{y}_S)(\hat{y}_S \cdot \hat{x}_H)} \\
&= \frac{(1) \hat{x}_H - (\hat{x}_H \cdot \hat{y}_S) \hat{y}_S}{(1)(1) - (\hat{x}_H \cdot \hat{y}_S)^2} \\
\vec{y}^S &= \frac{(\hat{x}_H \cdot \hat{x}_H) \hat{y}_S - (\hat{x}_H \cdot \hat{y}_S) \hat{x}_H}{(\hat{y}_S \cdot \hat{y}_S)(\hat{x}_H \cdot \hat{x}_H) - (\hat{x}_H \cdot \hat{y}_S)(\hat{y}_S \cdot \hat{x}_H)} \\
&= \frac{(1) \hat{y}_S - (\hat{x}_H \cdot \hat{y}_S) \hat{x}_H}{(1)(1) - (\hat{x}_H \cdot \hat{y}_S)^2} \\
\vec{z}^{HS} &= \hat{z}_{HS} = \frac{\hat{x}_H \times \hat{y}_S}{\|\hat{x}_H \times \hat{y}_S\|}
\end{aligned} \tag{B.11}$$

Appendix C

Bridge Sensor Calibration Coefficients

The piezo calibration coefficients allow us to calculate the horizontal F^x and vertical F^z force components of the string against the bridge given the measured potentials from the treble V^T and bass V^B piezos according to the matrix equation

$$\begin{pmatrix} F^x \\ F^z \end{pmatrix} = \begin{pmatrix} C_T^x & C_B^x \\ C_T^z & C_B^z \end{pmatrix} \begin{pmatrix} V^T \\ V^B \end{pmatrix}.$$

The calibration coefficients were measured and calculated as described in Section 4.2.2. The values are reported in the table below.

	Cello A	Cello B
String I (A_3, La)	$\begin{pmatrix} 1.22192 & -3.84013 \\ 4.51239 & 1.96915 \end{pmatrix}$	$\begin{pmatrix} 0.763116 & -3.22863 \\ 3.27689 & 1.78093 \end{pmatrix}$
String II (D_3, Re)	$\begin{pmatrix} 1.61237 & -2.29604 \\ 2.38739 & 2.27941 \end{pmatrix}$	$\begin{pmatrix} 1.48214 & -2.6127 \\ 2.45718 & 2.61037 \end{pmatrix}$
String III (G_2, Sol)	$\begin{pmatrix} 3.12035 & -1.68679 \\ 2.07961 & 3.68318 \end{pmatrix}$	$\begin{pmatrix} 2.51916 & -1.76809 \\ 2.0122 & 3.2196 \end{pmatrix}$
String IV (C_2, Do)	$\begin{pmatrix} 2.75696 & -0.248084 \\ 0.331221 & 3.65458 \end{pmatrix}$	$\begin{pmatrix} 3.51625 & -0.31179 \\ 1.14915 & 3.36772 \end{pmatrix}$

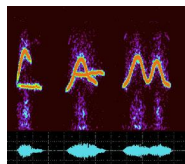
Appendix D

Recording session outline

1. Musician is given the bow, excerpts, and instructions at least one day before the experiment.
2. Before the musician arrives on the day of the experiment
 - (a) Microphone, load cell, and piezo signals are connected to DAQ board.
 - (b) Motion capture cameras are calibrated
 - (c) Marker placements on the cello are verified.
 - (d) Rigid bodies are defined for the cellos and load cell.
 - (e) Cellos are tuned
3. Once the musician arrives
 - (a) Musician warms up on her own cello.
 - (b) Musician completes demographic questionnaire
 - (c) Frog and Tip rigid bodies are defined
 - (d) Setup data logging program
4.
 - (a) Musician tunes and freely evaluates the first cello.
 - (b) Musician performs the requested excerpts.
 - (c) Musician describes the cello.
5. Calibrate bow while musician takes a break.
6.
 - (a) Musician tunes and freely evaluates the second cello.
 - (b) Musician performs the requested excerpts.
 - (c) Musician describes the cello.
7. Musician records an excerpt for a repeatability analysis.
8. Musician compares the two cellos.
9. Calibrate bow again.

Appendix E

Texts, questions, and sheet music presented to the musician



Lutheries – Acoustique Musique
Institut Jean le Rond d'Alembert
Université Pierre et Marie Curie
Paris, France



Merci d'accepter de participer à notre étude. Un compositeur en résidence dans un conservatoire régional nous a demandé d'équiper une paire de violoncelles avec des capteurs qui permettent au violoncelliste d'interagir en temps réel avec un ordinateur durant l'interprétation de sa pièce. Ces violoncelles vont être utilisés par un groupe d'étudiants pour leur examen de fin d'année. Nous aimerions que quelques musiciens professionnels évaluent ces deux instruments et enregistrent quelques extraits courts (que nous pourrions leur transmettre), afin que nous puissions décider avec eux si des ajustements par un luthier sont nécessaires avant que nous leur envoyons les violoncelles. Nous vous demandons donc aujourd'hui d'évaluer ces deux violoncelles, de discuter leurs qualités et défauts, et d'enregistrer quelques extraits.

Nous profitons de cette opportunité pour étudier le comportement d'un violoncelle en situation réelle de jeu. En plus d'enregistrer le mouvement des cordes grâce aux capteurs mentionnés ci-dessus, nous allons enregistrer les mouvements relatifs de l'archet et du violoncelle grâce à un système de capture du mouvement (consistant en 10 caméras infrarouges) et filmer avec un caméscope. Nous vous poserons donc aussi quelques questions qui nous permettront d'interpréter les données enregistrées.

Nous estimons la durée de votre participation à environ 2h30.

Timothy Wofford (wofford.timothy@gmail.com) et Claudia Fritz (claudia.fritz@upmc.fr)

Formulaire de consentement

J'ai été informé du but de l'étude et des méthodes et outils utilisés dans ce projet, et je les accepte. Je suis conscient que ma participation est volontaire et que j'ai le droit de me retirer de l'étude à tout moment, sans donner de raison et sans encourir aucune responsabilité. J'ai également été informé que les réponses aux questions ont un caractère facultatif et le défaut de réponse n'aura aucune conséquence pour moi, et que les informations me concernant seront conservées et traitées de manière anonyme et confidentielle.

Date _____

Nom _____

Signature

After each repetition

- Etes-vous satisfait de cet enregistrement ?
- Que voudriez-vous améliorer ?

After each excerpt

- Quelles propriétés (qualités et défauts) de l'instrument ont pu être montrées dans cet enregistrement ?

After all excerpts on each cello

- Pourriez-vous décrire ce violoncelle ?
- Que pensez-vous de ce violoncelle ?
- Qu'est-ce que vous appréciez particulièrement ?
- Pensez-vous que ce violoncelle aurait besoin d'être modifié ; en particulier, à supposer qu'un luthier puisse ajuster le violoncelle si vous lui expliquez ce que vous aimeriez, que lui demanderiez-vous ?

During the comparison

- Qu'avez-vous perçu comme différences ?
- Parmi elles, quelles sont celles qui vous semblent être mises en lumière de manière évidente dans quels extraits (parmi les 3) que vous avez enregistrés ?
- Comment ces différences ont-elles affecté votre manière de jouer les extraits correspondants ?
- Pourriez-vous proposer d'autres extraits qui mettent davantage en valeur les différences entre les 2 instruments ?

Bibliography

- Ablitzer, Frédéric (2011). “Influence des paramètres mécaniques et géométriques sur le comportement statique de l’archet de violon en situation de jeu”. PhD thesis. Université du Maine (cit. on pp. 9, 46).
- Aitchison, Robin (2016). *Selected cello string tensions 1922 – 2016*. URL: <https://www.aitchisoncellos.com/publications/cello-and-bow-articles/string-and-case-reviews/string-tension-charts/> (visited on 01/02/2019) (cit. on p. 37).
- Al-Sharadqah, Ali, Nikolai Chernov, et al. (2009). “Error analysis for circle fitting algorithms”. In: *Electronic Journal of Statistics* 3, pp. 886–911 (cit. on p. 73).
- Arun, K Somani, Thomas S Huang, and Steven D Blostein (1987). “Least-squares fitting of two 3-D point sets”. In: *IEEE Transactions on pattern analysis and machine intelligence* 5, pp. 698–700 (cit. on p. 69).
- Askenfelt, A (1983). “A simple device for the simultaneous registration of bow motion and bow force”. In: *Proceedings of the Stockholm Music Acoustics Conference*. Citeseer (cit. on pp. 26, 31).
- Askenfelt, A and K Guettler (1998). “The bouncing bow: An experimental study”. In: *Catgut Acoust. Soc. J* 3.6, pp. 3–8 (cit. on p. 44).
- Askenfelt, Anders (1986). “Measurement of bow motion and bow force in violin playing”. In: *The Journal of the Acoustical Society of America* 80.4, pp. 1007–1015 (cit. on pp. 26, 31).
- (1988). “Measurement of the bowing parameters in violin playing”. In: *Journal of the Acoustical Society of America* 29.1, pp. 1–30 (cit. on pp. 26, 31).
- Baez, Raquel (2013). “Using infrared motion capture data to measure the bow pressing force in bowed string instruments”. MA thesis. Barcelona: Universitat Pompeu Fabra (cit. on pp. 32, 49).
- Baillet, Yohan, L Davis, and J Rolland (2001). “A survey of tracking technology for virtual environments”. In: *Fundamentals of wearable computers and augmented reality*, p. 67 (cit. on p. 30).
- Bancroft, Jared B and Gérard Lachapelle (2012). “Estimating MEMS gyroscope g-sensitivity errors in foot mounted navigation”. In: *Ubiquitous Positioning, Indoor Navigation, and Location Based Service (UPINLBS), 2012*. IEEE, pp. 1–6 (cit. on p. 28).
- Bissinger, George (2008). “Structural acoustics of good and bad violins”. In: *The Journal of the Acoustical Society of America* 124.3, pp. 1764–1773 (cit. on p. 11).
- Caussé, R et al. (2001). “Study of violin bow quality”. In: *International Symposium on Musical Acoustics, Perugia, Italy (September 10–14 2001)*, pp. 1–6 (cit. on p. 9).
- Chen, Jessie et al. (2008). “Pitch and space maps of skilled cellists: accuracy, variability, and error correction”. In: *Experimental brain research* 188.4, pp. 493–503 (cit. on pp. 25, 26).
- Cheveigné, Alain de and Hideki Kawahara (2001). “Comparative evaluation of F0 estimation algorithms”. In: *Seventh European Conference on Speech Communication and Technology* (cit. on p. 33).

- Curtin, Joseph (2018). *Introducing the Impulse Measurement Rig, Model 2.0*. URL: <https://josephcurtinstudios.com/research/measurement-rig/> (visited on 09/28/2018) (cit. on p. 11).
- De Cheveigné, Alain and Hideki Kawahara (2002). “YIN, a fundamental frequency estimator for speech and music”. In: *The Journal of the Acoustical Society of America* 111.4, pp. 1917–1930 (cit. on p. 33).
- Demoucron, Matthias (2015). “The performance of bow changes: some mechanical aspects”. In: *Acta Acustica united with Acustica* 101, pp. 331–346 (cit. on pp. 2, 23, 24, 94, 110, 132).
- Demoucron, Matthias, Anders Askenfelt, and René Causse (2009). “Measuring bow force in bowed string performance: Theory and implementation of a bow force sensor”. In: *Acta Acustica united with Acustica* 95.4, pp. 718–732 (cit. on p. 31).
- Desvages, Charlotte and Stefan Bilbao (2016). “Two-polarisation physical model of bowed strings with nonlinear contact and friction forces, and application to gesture-based sound synthesis”. In: *Applied Sciences* 6.5, p. 135 (cit. on p. 10).
- Donnarumma, Marco, Baptiste Caramiaux, Atsu Tanaka, et al. (2013). “Muscular Interactions Combining EMG and MMG sensing for musical practice”. In: (cit. on p. 34).
- Draper, Norman R and Harry Smith (2014). *Applied regression analysis*. John Wiley & Sons (cit. on p. 62).
- Freed, Adrian (2009). “Novel and Forgotten Current-steering Techniques for Resistive Multitouch, Duotouch, and Polytouch Position Sensing with Pressure.” In: *NIME*, pp. 230–235 (cit. on p. 34).
- Galluzzo, Paul M (2004). “On the playability of stringed instruments”. PhD thesis. University of Cambridge (cit. on pp. 22, 23).
- Gershenfeld, Neil A (1993). *Method and apparatus for electromagnetic non-contact position measurement with respect to one or more axes*. US Patent 5,247,261 (cit. on p. 27).
- Goudeseune, Camille (2001). “Composing with parameters for synthetic instruments”. PhD thesis. University of Illinois at Urbana-Champaign (cit. on p. 26).
- Gough, Colin E (2012). “Violin bow vibrations”. In: *The Journal of the Acoustical Society of America* 131.5, pp. 4152–4163 (cit. on p. 9).
- Grosshauser, Tobias, Sebastian Feese, and Gerhard Tröster (2013). “Capacitive left hand finger and bow sensors for synchronization and rhythmical regularity analysis in string ensembles”. In: *Proceedings of the Stockholm Music Acoustics Conference 2013*. Logos-Verl. (cit. on p. 34).
- Grosshauser, Tobias, Ulf Großekathöfer, and Thomas Hermann (2010). “New sensors and pattern recognition techniques for string instruments”. In: *Proceedings of the 2010 Conference on New Interfaces for Musical Expression++ (NIME 2010), Sydney, Australia* (cit. on p. 34).
- Guaus, Enric et al. (2007). “Measuring the bow pressing force in a real violin performance”. In: *Proceedings of International Symposium on Musical Acoustics* (cit. on pp. 26, 31).
- Guaus, Enric et al. (2009). “Calibration method to measure accurate bow force for real violin performances”. In: *ICMC* (cit. on p. 31).
- Guettler, Knut (2002). “On the creation of the Helmholtz motion in bowed strings”. In: *Acta Acustica united with Acustica* 88.6, pp. 970–985 (cit. on pp. 2, 22).
- (2010). “Bowing gesture analysis: For whom, why, and how”. In: *Proceedings of the Second Vienna Talk, University of Music and Performing Arts, Vienna, Austria* (cit. on p. 110).

- Guettler, Knut and Anders Askenfelt (1997). "Acceptance limits for the duration of pre-Helmholtz transients in bowed string attacks". In: *The Journal of the Acoustical Society of America* 101.5, pp. 2903–2913 (cit. on pp. 24, 108, 132).
- Helmholtz, Hermann (1954). "On the sensations of tone". In: *Trans. AJ Ellis, Dover, New York*, pp. 390–394 (cit. on p. 13).
- Hsu, Ling-Chi et al. (2014). "Detection of Motor Changes in Violin Playing by EMG Signals." In: *ISMIR*, pp. 495–500 (cit. on p. 34).
- Issanchou, Clara et al. (2017). "A modal-based approach to the nonlinear vibration of strings against a unilateral obstacle: Simulations and experiments in the pointwise case". In: *Journal of Sound and Vibration* 393, pp. 229–251 (cit. on p. 10).
- Kapur, Ajay et al. (2004). "The electronic sitar controller". In: *Proceedings of the 2004 conference on New interfaces for musical expression*. National University of Singapore, pp. 7–12 (cit. on p. 34).
- Le Carrou, J-L et al. (2014). "A low-cost high-precision measurement method of string motion". In: *Journal of Sound and Vibration* 333.17, pp. 3881–3888 (cit. on p. 19).
- Llimona, Quiml (2014). *Bowing the violin - a case study for auditory-motor pattern modeling in the context of music performance*. Barcelona (cit. on pp. 32, 76).
- Luna. *ODiSI* (cit. on p. 33).
- Machover, Tod (1992). *Hyperinstruments: A Progress Report, 1987-1991*. MIT Media Laboratory (cit. on pp. 26, 27, 30, 31).
- Maestre, Esteban et al. (2007). "Acquisition of violin instrumental gestures using a commercial EMF tracking device". In: *Proceedings of the 2007 International Computer Music Conference (ICMC07)*. Vol. 1, pp. 386–393 (cit. on pp. 30, 32, 40, 44, 94).
- Mansour, Hossein, Jim Woodhouse, and Gary P Scavone (2017). "On Minimum Bow Force for Bowed Strings". In: *Acta Acustica united with Acustica* 103.2, pp. 317–330 (cit. on p. 21).
- Marchini, Marco et al. (2011). "A Hair Ribbon Deflection Model for Low-intrusiveness Measurement of Bow Force in Violin Performance." In: *NIME*. Citeseer, pp. 481–486 (cit. on pp. 32, 75, 76).
- McMillen, Keith A (2008). "Stage-Worthy Sensor Bows for Stringed Instruments." In: *NIME*. Citeseer, pp. 347–348 (cit. on p. 27).
- Medina, Carlos, José Carlos Segura, and Angel De la Torre (2013). "Ultrasound indoor positioning system based on a low-power wireless sensor network providing sub-centimeter accuracy". In: *Sensors* 13.3, pp. 3501–3526 (cit. on p. 30).
- Monti, G. and M. Sandler (2002). "Pitch-Locking Monophonic Music Analysis". In: *Proc. of the AES 112th Convention, Munich, Germany* (cit. on pp. 33, 91).
- Mores, Robert (2016). "Maximum bow force revisited". In: *The Journal of the Acoustical Society of America* 140.2, pp. 1162–1171 (cit. on p. 94).
- Nichols, Charles (2002). "The vBow: development of a virtual violin bow haptic human-computer interface". In: *Proceedings of the 2002 conference on New interfaces for musical expression*. National University of Singapore, pp. 1–4 (cit. on p. 30).
- Overholt, Daniel (2011). "The overtone fiddle: an actuated acoustic instrument". In: *New Interfaces for Musical Expression*, pp. 4–7 (cit. on p. 26).
- Paradiso, Joseph A (1997). "Electronic music: new ways to play". In: *IEEE spectrum* 34.12, pp. 18–30 (cit. on pp. 26, 27).
- Paradiso, Joseph A and Neil Gershenfeld (1997). "Musical applications of electric field sensing". In: *Computer music journal* 21.2, pp. 69–89 (cit. on pp. 26, 27, 34).
- Pardue, Laurel and Andrew McPherson (2013). "Near-Field Optical Reflective Sensing for Bow Tracking." In: *NIME*, pp. 363–368 (cit. on p. 32).

- Pardue, Laurel S, Christopher Harte, and Andrew P McPherson (2015). "A Low-Cost Real-Time Tracking System for Violin". In: *Journal of New Music Research* 44.4, pp. 305–323 (cit. on pp. 32, 34).
- Pérez Carrillo, Alfonso Antonio (2006). *Gesture based synthesis of bowed string instruments* (cit. on p. 28).
- Pickering, Norman C (1986). "Elasticity of violin strings". In: *Journal of Catgut Acoustical Society* 46.2, p. 3 (cit. on pp. 36, 37).
- Pitteroff, R and J Woodhouse (1994). "Influence of a bow of finite width on bowed string motion: numerical modelling and experimental evidence". In: *Le Journal de Physique IV* 4.C5, pp. C5–605 (cit. on p. 9).
- Raman, Chandrasekhara V (1918). "On the mechanical theory of the vibrations of bowed strings and of musical instruments of the violin family, with experimental verification of the results". In: *Indian Assoc. Cultivation Sci. Bull* 15, pp. 1–158 (cit. on pp. 21, 26).
- Raman, CV (1920). "Experiments with mechanically-played violins". In: (cit. on p. 26).
- Rasamimanana, Nicolas (2004). "Gesture analysis of bow strokes using an augmented violin". In: *Memoire de stage de DEA ATIAM, Tech. Rep* (cit. on pp. 29, 31).
- Reinicke, Friedrich Ludwig Walter (1973). "Die Übertragungseigenschaften des Streichinstrumentensteges". PhD thesis (cit. on p. 56).
- Rossing, T et al. (2010). *The science of string instruments*. Springer New York (cit. on p. 6).
- Saitis, Charalampos et al. (2012). "Bridge admittance measurements of 10 preference-rated violins". In: *Acoustics 2012* (cit. on p. 11).
- Sarlo, Rodrigo, David Ehrlich, and Pablo A Tarazaga (2016). "Measuring Violin Bow Force During Performance". In: *Sensors and Instrumentation, Volume 5*. Springer, pp. 37–46 (cit. on p. 33).
- Schelleng, John C (1973). "The bowed string and the player". In: *The Journal of the Acoustical Society of America* 53.1, pp. 26–41 (cit. on pp. 2, 19–21).
- Schönemann, Peter H (1966). "A generalized solution of the orthogonal Procrustes problem". In: *Psychometrika* 31.1, pp. 1–10 (cit. on p. 69).
- Schoonderwaldt, Erwin and Matthias Demoucron (2009). "Extraction of bowing parameters from violin performance combining motion capture and sensors". In: *The Journal of the Acoustical Society of America* 126.5, pp. 2695–2708 (cit. on pp. 26, 29, 30, 40, 94).
- Schoonderwaldt, Erwin, Knut Guettler, and Anders Askenfelt (2008). "An empirical investigation of bow-force limits in the Schelleng diagram". In: *Acta Acustica united with Acustica* 94.4, pp. 604–622 (cit. on p. 20).
- Schoonderwaldt, Erwin, Nicolas Rasamimanana, and Frédéric Bevilacqua (2006). "Combining accelerometer and video camera: Reconstruction of bow velocity profiles". In: *Proceedings of the 2006 conference on New interfaces for musical expression*. IRCAM—Centre Pompidou, pp. 200–203 (cit. on p. 29).
- Smith, Joshua R. (1996). "Field mice: Extracting hand geometry from electric field measurements". In: *IBM systems journal* 35.3.4, pp. 587–608 (cit. on p. 27).
- Smith, Joshua Reynolds (1995). "Toward electric field tomography". PhD thesis. Massachusetts Institute of Technology (cit. on p. 27).
- "The Augmented Violin Project". "The Augmented Violin Project: Research, Composition and Performance Report". In: *Proceedings of the International Conference on New Interfaces for Musical Expression*. URL: http://www.nime.org/proceedings/2006/nime2006_402.pdf (cit. on pp. 26, 27).
- Trueman, Dan and Perry Cook (2000). "BoSSA: The deconstructed violin reconstructed". In: *Journal of New Music Research* 29.2, pp. 121–130 (cit. on pp. 26, 29, 32).

- Woodhouse, J (1994). "On the stability of bowed string motion". In: *Acta Acustica united with Acustica* 80.1, pp. 58–72 (cit. on p. 2).
- Woodhouse, James (1993). "On the playability of violins. Part I: Reflection functions". In: *Acta Acustica united with Acustica* 78.3, pp. 125–136 (cit. on p. 21).
- Young, Diana (2002). "The hyperbow controller: Real-time dynamics measurement of violin performance". In: *Proceedings of the 2002 conference on New interfaces for musical expression*. National University of Singapore, pp. 1–6 (cit. on pp. 26, 27, 31).
- (2003). "Wireless sensor system for measurement of violin bowing parameters". In: *Stockholm Music Acoustics Conference*, pp. 111–114 (cit. on p. 31).
- Young, Diana S (2001). "New frontiers of expression through real-time dynamics measurement of violin bows". PhD thesis. Massachusetts Institute of Technology (cit. on p. 31).
- Young, Diana Santos (2007). "A methodology for investigation of bowed string performance through measurement of violin bowing technique". PhD thesis. Citeseer (cit. on pp. 26, 29, 31).
- Zhang, A and J Woodhouse (2014a). "On the playability of wolf note". In: *Proceedings of the International Conference on Noise and Vibration Energy 2014*, pp. 31–37 (cit. on p. 25).
- Zhang, Ailin (2015). "Playability of bowed string instruments". PhD thesis. University of Cambridge (cit. on pp. 19, 21, 56, 57, 59, 62, 94).
- Zhang, Ailin and Jim Woodhouse (2014b). "Reliability of the input admittance of bowed-string instruments measured by the hammer method". In: *The Journal of the Acoustical Society of America* 136.6, pp. 3371–3381 (cit. on p. 12).
- Zhang, Ailin, Jim Woodhouse, and George Stoppani (2016). "Motion of the cello bridge". In: *The Journal of the Acoustical Society of America* 140.4, pp. 2636–2645 (cit. on p. 13).